IDENTIFYING STRUCTURE-PROPERTY-PROCESSING RELATIONSHIPS OF TYROSOL-DERIVED POLYARYLATES FOR THE EFFICIENT DESIGN OF BIODEGRADABLE MEDICAL DEVICES

By

JARROD PAUL COHEN

A dissertation submitted to the

Graduate School-New Brunswick

Rutgers, the State University of New Jersey

In partial fulfillment of the requirements

For the degree of

Doctor of Philosophy

Graduate Program in Chemistry and Chemical Biology

Written under the direction of

Joachim Kohn

And approved by

_____

_____

_____

_____

New Brunswick, New Jersey

January 2021

ABSTRACT OF THE DISSERTATION

Identifying structure property-processing relationships of tyrosol-derived polyarylates for the efficient design of biodegradable medical devices

By JARROD PAUL COHEN

Dissertation Director:

Joachim Kohn

Polymeric biomaterials have revolutionized the medical sector, but acidic degradation byproducts, limited tunability, and non-degradability of those used in commercial products, has led to an unmet need for new, improved libraries of polymers. Specifically, the design of new materials with defined structure-property relationships will enable faster, and more efficient material selection for application specific research. Biomedical research intertwines itself between many scientific disciplines including chemistry, materials science, biology, engineering and medicine. Due to the complexity in designing new biomaterials, many research groups focus on incremental chemical or physical modifications to existing materials such as composites of metal alloys or synthetic polymers like poly(lactic acid) (PLA). To address limitations polymeric biomaterials, several laboratories have focused their efforts on developing new libraries based on amino acids for their improved biocompatibility and tunability. Tyrosine has had great

translational success from the Kohn group into the clinic due to the structurally rigid aromatic ring and biocompatibility of the amino acid. Tyrosine has been successfully used by the Kohn lab to generate polycarbonates and polyarylates, which exhibit excellent biocompatibility and tunability. Slight modifications to these polymers including incorporation of hydrophilic oligomers of PEG or free acid groups led to a library of materials with predictable tunability. One major limitation of tyrosine-based polymers is the mismatch between degradation and resorption due to the presence of amide linkages, the degradation of which is limited to enzymatic modes. We hypothesize that to overcome this limitation, replacing the amide bond in the tyrosine diphenol with an ester derived from tyrosol will promote resorption while maintaining biocompatibility and tunability.

Tyrosol is a naturally derived anti-oxidant commonly found in olive oil. A small subset of the library described in this dissertation have been previously used in 3D printing applications. However, the design of such polymers for broader biomedical applications has not been explored. Establishing structure property relationships within a library of tyrosol-derived polymers was a main thrust of this dissertation. We hypothesize that establishing these correlations will enable the more efficient design of polymers for specific application. Synthetic optimization of novel tyrosol diphenols and subsequent polymers followed by an intensive examination of polymer properties was carried out to identify the great potential of this library. Tyrosol derived poly(ester-arylate)s were explored with three major structural comparisons: (i) diphenol symmetry, (ii) diacid carbon chain length, and (iii) diacid bond rigidity. Resulting polymers were then characterized for their chemical, degradative, thermal, mechanical, and biological properties. Structure-property relationships were established to better guide material design.

A wide range of material parameters were obtained and implications in polymer design identified. These design parameters were extended to specific processing techniques including additive manufacturing. Methods for improving bioinks used in additive manufacturing were explored through the use of click chemistry to further expand on the polymer properties of printed constructs using fused deposition modeling. Correlations between polymer molecular weight, printing parameters, and post printing curing times were identified.

Additionally, these polymers were investigated for their use as drug eluting devices. A subset of the developed polymer library was chosen, and chemical modifications were made to the polymers in order to provide improved drug delivery for both hydrophobic and hydrophilic APIs. Extruded implantable devices loaded with drug were designed for applications including implantable birth control and treatments for HIV. Poor patient compliance is often a hurdle in improving clinical outcomes, and therefore, long acting implants can improve treatment effectiveness.

Guided rationale based upon the known chemical properties of monomers was used to design an expanded library of poly(ester-arylate)s for a range of biomedical applications. Tunability of thermal, mechanical, and processing properties enables selection of a material for specific physiological applications, as different pathologies require materials to match their properties. This library has established a platform for developing versatile polymeric materials by biomolecular tethering to improve device properties, incorporation of peptides for improved biologically responsive degradation, and new resorbable nerve conduits.

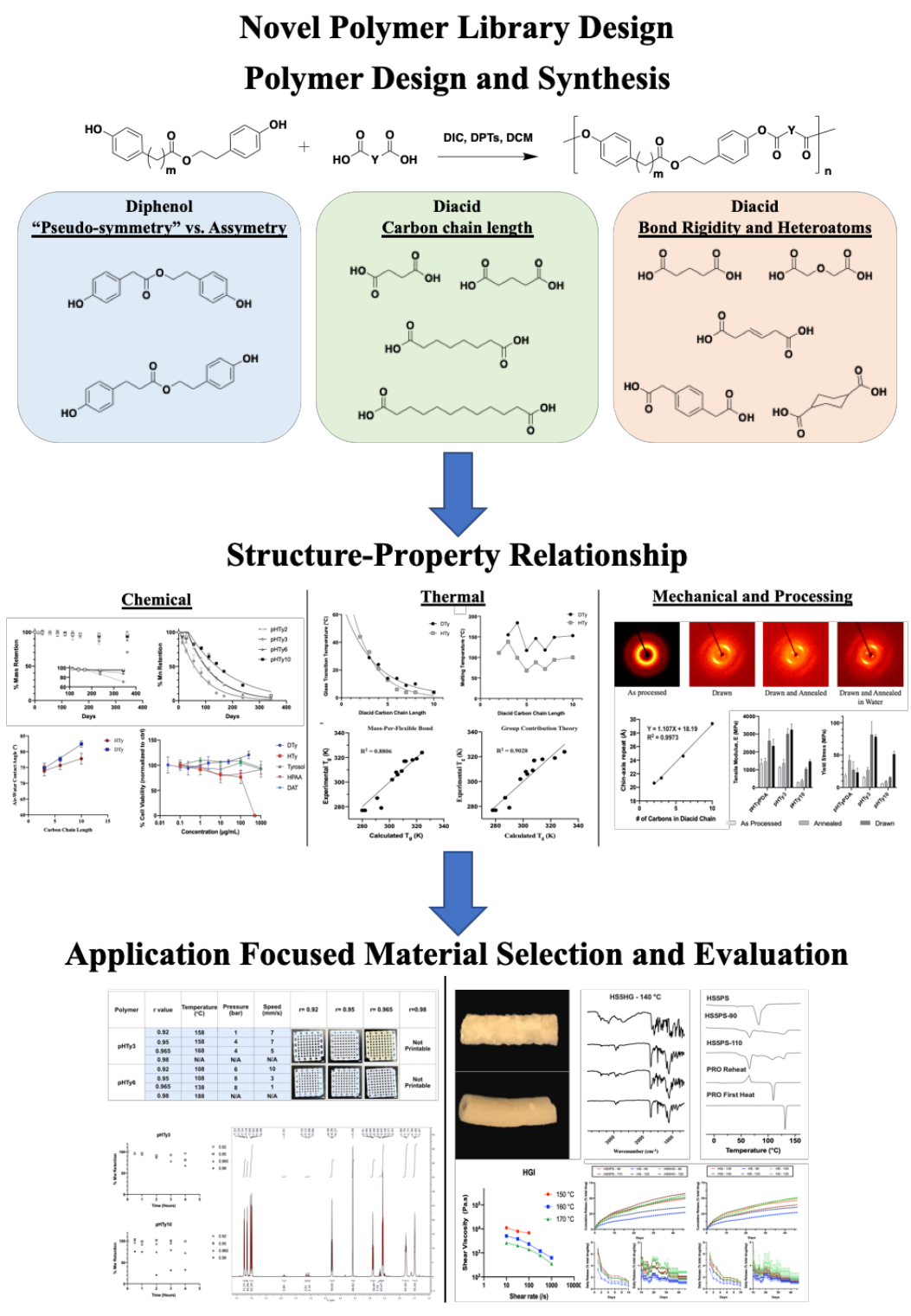

Figure i. Graphical abstract of the dissertation.

ACKNOWLEDGEMENT

I would like to acknowledge the following people for their support and advice throughout my studies at Rutgers:

Committee Members Dr. Joachim Kohn, Dr. Spencer Knapp, Dr. Ralf Warmuth, Dr. Adam Gormley, and Dr. John Brennan for their guidance and mentorship throughout my doctoral research career.

A special thanks to Dr. Yong Mao, Dr. Kim-Phuong Le, Dr. N. Sanjeeva Murthy, and Dr. Fatima Buevich who enabled me to finish my research and helped mentor and prepare me for industry.

I would also like to thank all of my fellow graduate students over the years including: Dr. Koustubh Dube, Dr. Joseph Molde, Dr. Xiohuan Wu, Stephanie Fung, Mariana Reis Nogueira de Lima, and Nityananda Pal who all helped during the difficult times and celebrated the successes.

I also would like to especially thank Christine Gwin and Andrew Mullaghy who both contributed immensely to the work presented in this thesis and whose help was crucial to my success.

I would like to thank postdoctoral researches in the lab who collaborated with me on both federal and industrial projects including Dr. Robert Shultz, Dr. Cemile Bektas, Dr. Daniel Chakhalian, and Dr. Mario Perera.

Previous lab members often go forgotten but without them I would not be where I am today. I would like to thank Dr. Murat Guvendiren, Dr. Vinod Damodaran, Carmine Iovine,

Dr. Hilton Kaplan, Dr. Julian Chesterman, Dr. Divya Bhatnagar, Dr. Ritu Goyal, Dr. Tommy Pashuck, Dr. Joseph Steele, Dr. Maziar Shah Mohammadi.

I would also like to recognize the administrative staff at NJCBM including Dr. Sangya Varma, Mindy Drake, Carol Lenardson, Carmen Castro, Louli Kourkounakis, Carole Kantor, John Watkins, Sasha Hutnick, Nnadilim Okafor, and Dana Downer for all of their help with tasks no matter how large or small.

I would like to thank, my parents Louis Cohen and Judith Cohen for supporting me along my path to graduate and my brother Seth Cohen for being the comical relief in a stressful environment and always rooting for me. My in-laws Victor Sarro Sr. and Joan Sarro for their complete support and my brother-in-law Victor Sarro Jr. who always has my back no matter the circumstance. I would also like to thank my grandparents Stanley Shaw, Gloria Shaw, Henry Cohen and Doris Cohen who have always believed in me and have been my biggest cheerleaders throughout my life. I would also not be forgiven if I didn't thank my canine companion Winnie who has brought so much joy to me and my family and made stressful writing days bearable.

Last but most important I would like to thank my wife Christina who has made this experience exponentially more enjoyable and has been my rock through ups and downs. Without her I would be lost and I cannot thank her enough for her guidance and support of my career and academic journey. Research can be tough but it's a whole lot easier with you by my side Christina.

TABLE OF CONTENTS

LIST OF TABLES

LIST OF ILLUSTRATIONS

LIST OF ABBREVIATIONS

%	percent
°C	degrees Celsius
~	approximately
±	plus or minus
^{1}H NMR	proton nuclear magnetic resonance
^{13}C NMR	carbon nuclear magnetic resonance
3D	three dimensional
ACN	acetonitrile
ACY	acyclovir
alt	alternating
an	annealed
aq	aqueous
ASTM	American Society for Testing and Materials
ATR	attenuated total resonance
AUC	area under the curve
AWCA	air-water contact angle
b	broad
$CDCl_3$	deuterated chloroform
CHD	cyclohexanedioate
cm	centimeter
DAT	desaminotyrosine
Da	dalton
DCC	*N,N'*-dicyclohexyl carbodiimide
DCE	dichloroethane
DCM	dichloromethane
d	doublet
dd	doublet of doublets
DG	Diglycolate
DI	deionized
DIC	*N,N'*-diisopropylcarbodiimide
dir	directional
DIW	direct ink writing
DMAP	*N,N'*-dimethylaminopyridine
DMF	*N,N'*-dimethylformamide
DMSO-d6	deuterated-dimethylsulfoxide
DP	degree of polymerization
DPTS	4-(Dimethylamino)pyridinium 4-toluenesulfonate
dr	drawn

DSC	differential scanning calorimetry
DT	desaminotyrosyl-tyrosine
dt	doublet of triplets
DTE	desaminotyrosyl-tyrosine ethyl ester
DTy	tyrosyl 4-hydroxyphenylpropanoate
E	Young's modulus
E1001(1k)	poly(DTE-co-10%DT-co-1% PEG_{1K} carbonate)
ε_y	strain at yield
equiv	equivalent
EtOAc	ethyl acetate
FDA	Food and Drug Administration
FDM	fused deposition modeling
FTIR	Fourier transform infrared spectroscopy
g	gram
GCT	group contribution theory
GPa	gigapascal
GPC	gel permeation chromatography
GRAS	Generally regarded as safe
GSD	glycinesuccinamide diacid
h	hour
H	hydrogen
HCl	hydrochloric acid
HDF	human dermal fibroblasts
hMSC	human mesenchymal stem cells
HO-f	human osteoblasts – femoral
HPAA	(4-hydroxyphenyl)acetic acid
HPLC	high performance liquid chromatography
HSC	human Schwann cells
HTy	tyrosyl 4-hydroxyphenylacetate
Hz	hertz
IC_{50}	half-maximal inhibitory concentration
IPA	isopropanol
IVIVC	*in vitro-in vivo* correlations
K	Kelvin
kDa	kilodaltons
lbs	pounds
m	multiplet
M/f	mass-per-flexible bond
MeOH	methanol

mg	milligram
MHz	megahertz
min	minute
mL	milliliter
mm	millimeter
mmol	millimole
mol	mole
M_n	number average molecular weight
MPa	megapascal
MPF	mass-per-flexible bond theory
MTS	mechanical testing system
M_w	weight average molecular weight
µg	microgram
µL	microliter
µm	micrometer
N	Newton
$NaHCO_3$	sodium bicarbonate
NaOH	sodium hydroxide
NIH	National Institute of Health
nm	nanometer
Pa	Pascal
PBS	phosphate buffered saline
PCL	polycaprolactone
PDA	phenylenediacetate
PDI	polydispersity index
PDLLA	poly(DL-lactide)
PEG	poly(ethylene glycol)
PETMP	Pentaerythritol tetrakis(3-mercaptopropionate)
PGA	polyglycolide or poly(glycolic acid)
PLA	polylactide or poly(lactic acid)
PLGA	poly(lactide-co-glycolide)
PLLA	poly(L-lactide)
ppm	parts per million
PRO	progesterone
PS	polystyrene
PTMC	poly(trimethylene carbonate)
PTSA	p-toluene sulfonic acid
QSPR	quantitative structure property relationship
s	singlet
s^{-1}	per second
SAXS	small angle x-ray scattering
scr	scrambled
SDS	sodium dodecyl sulfate

sec	second
σ_y	stress at yield
SLS	sodium lauryl sulfate
SPR	structure-property relationship
t	time
t-Hexe	trans-hexenedioate
T_c	crystallization temperature
TCPS	tissue-culture polystyrene
T_d	Decomposition temperature
TFA	trifluoroacetic acid
T_g	glass transition temperature
TGA	thermogravimetric analysis
THF	tetrahydrofuran
T_m	melting temperature
T_p	printing temperature
w/v	weight by volume
w/w	weight by weight
λ	wavelength
WAXS	wide-angle x-ray scattering
XRD	X-ray diffraction

CHAPTER 1: INTRODUCTION

The National Institute of Health (NIH) originally defined a biomaterial in 1982, as "any substance or combination of substances, other than drugs, synthetic or natural in origin, which can be used for any period of time, which augments or replaces partially or totally any tissue, organ or function of the body, in order to maintain or improve the quality of life of the individual."[1] As the average life expectancy increases and new medical problems arise, the need for new materials and treatments arise.[2, 3] One key indicator of the current need is the market value of biomaterials, which has grown exponentially over the last decade. Most recent approximate valuation of the field was in 2019 at 106.5 billion dollars and expects to reach 348.4 billion dollars by 2027.[4] Polymers, specifically have dominated the market accounting for over 40% of the total market share in 2019.[4]

Biomaterial use began back during the middle ages when Egyptians used sutures to mend wounds. Throughout time, wood, metals, and natural materials have been used to treat damaged and diseased tissues.[5-7] Recently, the focus has expanded past treatments alone to improving quality of life.[5] The field's growth has led to a broadened definition incorporating many new areas of medicine. A more modern definition indicates that "biomaterials may be natural or synthetic and are used in medical applications to support, enhance, or replace damaged tissue or a biological function". Due to the broad scope of the definition, biomaterial's applications can stretch from contact lenses to coronary stents, each requiring extremely different properties (Figure 1.1).[8-16]

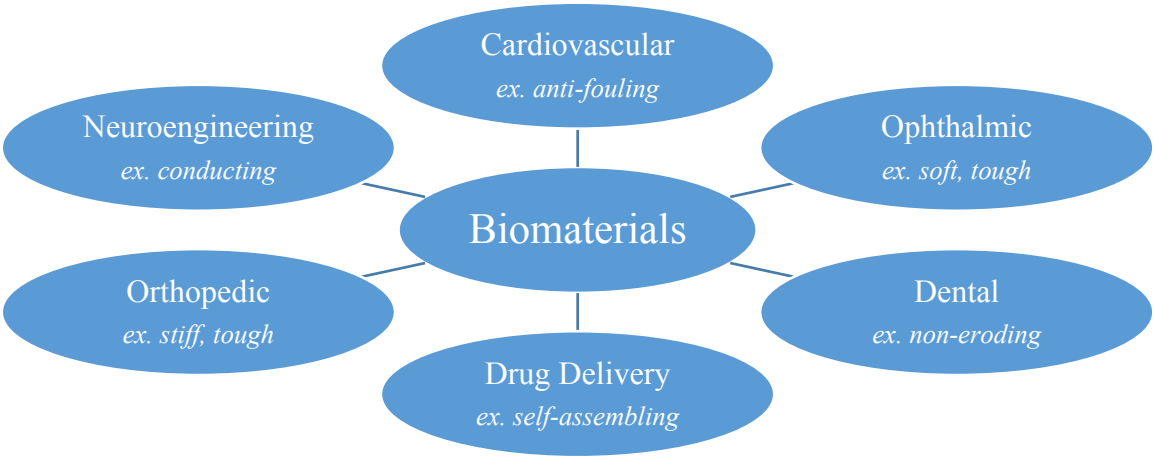

Figure 1.1. Classes of biomaterials applications.

1.1 Types of Biomaterials

Due to the vast amount of applications using biomaterials, the need for materials exhibiting a large range of properties is required. Four major classes of materials have been studied for their use in medical applications: metals, ceramics, synthetic polymers, and natural polymers (Figure 1.2). Each class of materials has their own benefits and deficits towards use in biomedical applications. Availability, cost, reproducibility, strength, tunability, and biocompatibility all play a role in material selection.[17] While early biomaterials research used natural polymers , shifts towards synthetic materials have further advanced the field. Material selection depends on the property of the materials, the biocompatibility of the implant, and the heath of the patient. The first two factors will be investigated in this thesis as key contributors to the success of a new material.

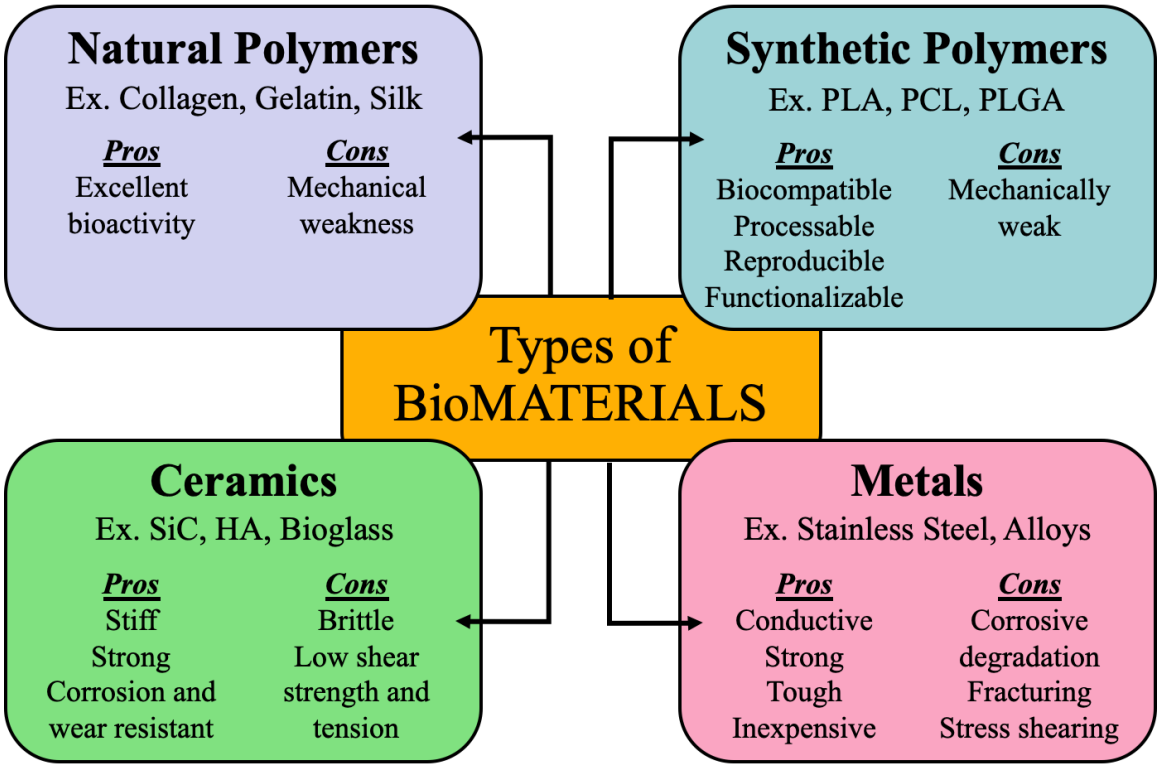

Figure 1.2. Types of biomaterials with their advantages and disadvantages.

Two of the largest differences in material type are degradability and mechanical properties. The latter requirement is dictated by the targeted regenerating tissue type. When comparing the properties of biological tissue, they can be split into hard and soft tissues. Hard tissues include bone and enamel while soft tissues include cartilage, ligaments, and skin.[7] Depending on the tissue type, moduli can range from 17 Pa for fat tissue up to 18 GPa for bone. Tensile strength is also important and can range from 2 MPa to 133 MPa. These differences highlight the need for large amounts of materials that can match these properties (Table 1).[7, 18]

Table 1.1. Mechanical properties of biological tissue types[7, 18]

Tissue	Modulus (MPa)	Tensile Strength (MPa)	Tissue	Modulus (MPa)	Tensile Strength (MPa)
Cortical bone	17700	133	**Tendon**	401.5	46.5
Cancellous bone	400	7.4	**Articular cartilage**	10.5	27.5
Enamel	84300	10	**Ligament**	303.0	29.5
Dentine	11000	39.3	**Skin**	0.1-0.2	7.6

Material degradability or lack thereof also plays a role in material selection. Some tissue types are slow or non-regenerating and as such, require materials that are non-degradable. This includes applications such as meniscus repair or cardiac leads for a pacemaker. On the other hand, many tissues can rebuild themselves in the weeks to months post injury. Ideally, an implantable biomaterial will provide support during the early stages of healing and then slowly transfer the mechanical load to the newly formed tissue. When non-degradable devices are used for these applications, a second surgery is required for removal but recent advances have led to degradable materials that eliminate this need. Tissue types have varying regenerative timelines.[19] For tendon and bone repair, the timeline for healing is approximately 4-8 weeks. Comparatively cartilage and ligaments can take 10-12 weeks. Nerve regeneration is dependent on the size of the defect gap and can take 4 weeks up to 24 weeks.

Metals have the advantage of superior strength and toughness compared to other materials. Joint replacements, dental implants, and orthopedic fixation devices have all benefitted from the toughness of metals. One key deficit to these materials is that they often overpower the mechanical environment they are placed into, causing stress shielding.[20, 21]

Stress shielding occurs when the material doesn't transfer mechanical load to the regenerating tissue. This results in a weakened tissue and additional complications. Another problem is that they can also corrode in the body resulting in fracturing of the metal.[20, 22, 23] More recently, metal alloys have been tested as a way to improve on these properties but they have only been moderately improved. Ceramics are stiff, strong and corrosion resistant but can be very brittle and can be difficult to process.[24, 25] Limited bioactivity has also been a concern although the introduction of bioactive ceramics has partially addressed this issue.[26] Natural polymers have showed promise due to their excellent bioactivity but often do not possess the proper mechanical requirements needed for most applications.[27, 28] Biopolymers also have a reproducibility problem as a result of the impact of material source and processing.[29]

These insufficiencies have led to growing interest in synthetic polymers, which are promising due to their biocompatibility, processability, reproducibility, and functionalizability.[9, 30-34] Specifically, synthetic polymers can be processed to possess the proper macro-, micro-, and meso-porosity seen in natural tissue.[35, 36] Increased attention to functionalization of synthetic materials with naturally derived peptides, and proteins have led to improved bioactivity of these typically bioinert polymers.[37-39] Polymers can be separated into two classes of materials: (i) non-degradable and (ii) degradable. Pacemaker leads and dialysis tubing are examples of applications requiring non-degradable polymeric biomaterials, while drug-loaded microspheres and resorbable sutures require biodegradability and excretion from the body. The kinetics of degradation can be tailored to the application, eliminating the need for future removal of the device or implant. This reduces the risk for infection and complications from additional surgeries.[40] In addition,

they have the ability to slowly transfer the mechanical load to the regenerating tissues eliminating the possibility of stress shielding.[41] Herein, this thesis will focus on the design of biodegradable polymers for a variety of applications.

1.2 Development of New Biomaterials

Designing a new biomaterial requires attention to a combination of chemical, biological, and physical science. The interdisciplinary nature of the field requires constant cycles of material design, response, evaluation, and redesign. When a foreign substance enters the body, it will cause an immune response.[42] This can often lead to inflammation and rejection of the material. Polymers, monomers, and degradation byproducts must be non-cytotoxic and have minimal to no inflammatory response.[43] In addition, biodegradable materials must produce degradation products that are easily metabolized and excreted *in vivo*.[44] Degradation rates also need to match the desired application's healing or regenerative process. As a material degrades, the mechanical load the material can handle decreases. As such, scaffolds for bone regeneration that degrade and resorb after one week will ultimately lead to device failure and cause additional complications for a patient.[45]

A polymeric scaffold should also maintain the proper mechanical properties to support regeneration and integration into the native tissue. Lastly, since these materials are degradable, their long-term stability post-processing is important to their translatability to market. Aging after fabrication should be minimized post-fabrication to ensure quality and safety of the product is reproducible.[41] One of the most common ways to ensure a polymer meets the biological requirements of the implant site with minimal immune response is to

derive the material from molecules commonly expressed in the body such as those involved in metabolism.

Commercial polymers with use in FDA-approved medical devices include polylactic acid (PLA), polyglycolic acid (PGA) and polycaprolactone (PCL). The polymers have excellent tunability and meet many of the requirements to designing a polymeric biomaterial. For PLA and PGA, a looming disadvantage is their acidic degradation byproducts, lactic acid and glycolic acid, respectively (Scheme 1.3). Local drops in pH at the implant site have local acidosis of the tissue in later stages of degradation.[46] PCL's degradation byproduct, 6-hydroxyhexanoic acid, is less acidic and less soluble, but increased hydrophobicity leads to slow hydrolytic degradation.[47] An alternative approach, and one that has been explored extensively in the Kohn laboratory is to design polymers based on known amino acids.

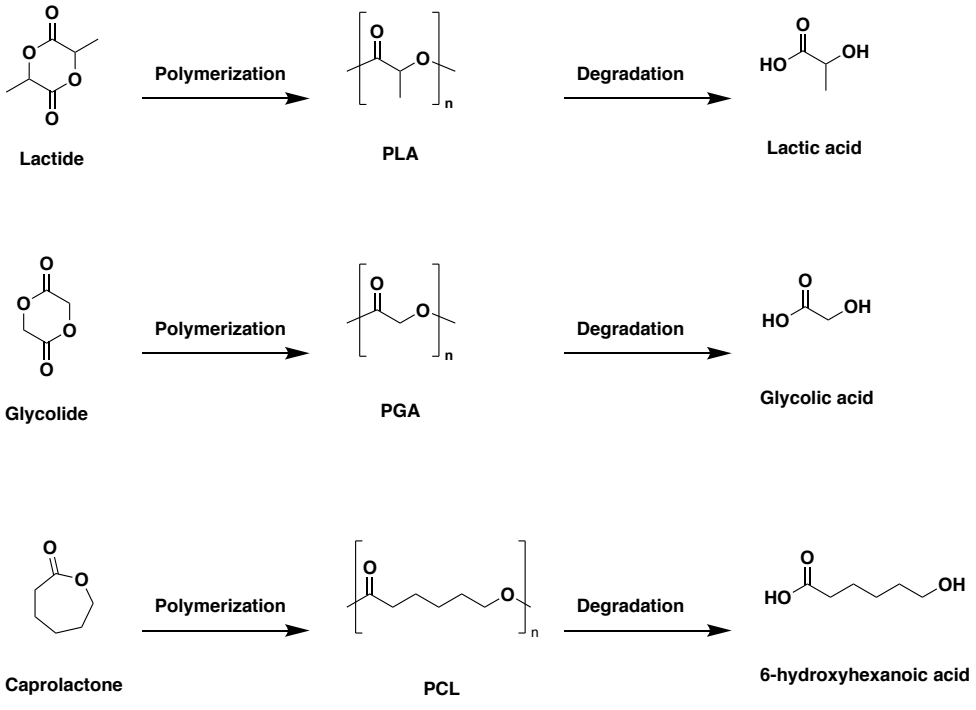

Scheme 1.3. Schematics for the synthesis and degradation of PLA, PGA, and PCL.

1.3 Amino-acid Derived Polymers

Amino acid building blocks in polymeric biomaterials is a way to ensure minimal cytotoxic response upon implantation and during degradation. This approach has led to success by many researchers including Joachim Kohn, Abraham Domb, and Matthew Becker to name a few. While the fundamental polymer design may be varied, the overall goal of a new library of polymers with unique function and good biocompatibility is one that many labs have embraced. Within the Kohn lab, extensive work on tyrosine-derived polycarbonates[48-51] and polyarylates[52-54] has been reported. A library of tunable polymers based on a polycarbonate terpolymer comprised of desaminotyrosyl-tyrosine ethyl ester, desaminotyrosyl-tyrosine, and poly(ethylene glycol) was generated and has shown huge promise in bone regeneration[51, 55, 56], delivery of hydrophobic and hydrophilic APIs[50, 57, 58], and nerve regeneration[59-61].

Abraham (Avi) Domb has also led extensive research in the field of amino acid-based poly(ester-anhydride)s and poly(amide-anhydride)s.[62-64] These polymers exhibit surface erosion and are fast degrading polymers with minimal inflammatory response. Domb also reports benefits of functionalizability, tunability and biological activity with amino acid derived polyanhydrides.[65] Additionally, his work expanded to make polyesters of amino acids through conversion of amino acids to alpha-hydroxy acids and then polymerize them. These polymers have many advantages over commercial polymers including better biological properties, biodegradability, and improved mechanical properties. Tunability occurs from the R-group of the amino acid with varied hydrophobicity, and rigidity.[65]

Matthew Becker's lab has also completed substantial work on poly(ester-urea)s based on several amino acids. These polymers are easily synthesized by making a diamine and then polymerizing with triphosgene. Polymers derived from phenylalanine exhibit superior mechanical properties similar to poly(lactic acid) and have limited acidic byproducts due to buffering effects of the polymer's urea functionality.[66-68] Becker's work also illustrates the vastly improved biological properties through additional conjugation of peptides, catechol groups, and selective crosslinking.[69-73] These labs illustrate a small part of an ever-growing group of research that highlights biocompatible, biodegradable, synthetic polymers.

1.4 Degradation of Polymers

Degradation, or loss of molecular weight, and resorption, or loss of mass, provide ways for a material to be removed and excreted from the body without additional surgical procedures that can cause patient discomfort or complications. While this can be a major advantage, the degradation pathway and rates should be defined to prevent late stage rejection of devices or degradation products. The two major paths for the degradation of polymers are either hydrolytic or enzymatic. Enzymatic degradation is minimally explored in the literature and even less so in regards to biomaterials due to the lack translation of results *in vivo.* Local concentrations and activities of enzymes in the body are often not reported and hard to predict. Instead, hydrolytic degradation has been a main focus of degradation characterization in the field. Understand the aqueous driven process *in vitro* has found correlations to *in vivo* results. Hydrolysis is impacted by chemical bond type, pH, molecular composition, and water uptake by the polymer.[74]

Chemically, hydrolysis can occur at an appreciable rate for esters, carbonates, and anhydrides. Amides, on the other hand, are extremely slow degrading hydrolytically and typically require amidase enzymes to be hydrolyzed.[75] This has been realized by previously designed tyrosine-derived polycarbonates and polyarylates that degrade but resorb at much slower rates. Work within the Kohn laboratory has identified the amide-bond as the limiting factor in the ability of these polymers to resorb.[76-79]

Rates of degradation can also dictate the erosion process for a polymeric device. Ideally, a device will surface erode as it's being degraded in the body.[80] This occurs when a polymers degradation is much slower than the resorption of the degradation products. In this case, diffusion of water into the scaffold is typically very slow allowing for the surface to hydrate, degrade, and resorb prior to deeper layers of the scaffold being impacted. The main advantage of this pattern of degradation is the retention of mechanical properties throughout the duration of the device's lifetime in the body. More commonly, polymers erode in the bulk. The rate of polymer chain degradation and monomer resorption is much slower that the diffusion of water into the volume of the device, thus resulting in a mismatch between hydrolysis of the polymer backbone and clearance of the degradation products. This ultimately leads to a loss in mechanical properties and rapid resorption late in the device's lifetime. While this is not ideal, if the polymer retains mechanical properties long enough to transfer mechanical load to the healing tissue, then the device can still serve its regenerative purpose. Understanding the chemical impact on resorption rates, helps dictate potential applications a polymer can be used for. Degradation and resorption are main thrusts of this thesis will be further explored in Chapters 3 and 4.

1.4 Structure Property Relationships (SPR)

"Structure determines property" is a concept widely accepted by chemists and applied scientists.[81] Due to the fact that biomaterials require a wide range of properties, understanding the correlation between chemical structure and material behavior allows for more efficient design of medical devices. Biomaterials design requires precise modulation of thermal, mechanical, and biological properties and it is often difficult to decouple them from each other.[82] Finding ways to alter polymer properties independently and in a predictable fashion based on chemical design is a very appealing aspect to material development. When needing to design a new polymer library, addressing multiple properties, SPR has proven to be effective.

Previously in our lab Brocchini et al. used the structure property approach to develop a library of tyrosine-derived pol(ester-arylate)s.[83] By varying the backbone chain length in the diacid along with the pendent chain length in the diphenol, a library of over 110 polymers was synthesized and evaluated for property trends. Some trends were found to be more nonspecific - for example, increasing chain length, regardless if it was pendant or part of the backbone, resulted in an increased T_g. On the other hand, hydrophobicity was more sensitive to the pendant chain of the polymer compared to the backbone. The incorporation of heteroatoms led to an increase in hydrophilicity and glass transition temperature of the polymer. Mechanical and biological properties were also evaluated, drawing conclusions that incorporation of heteroatoms improved proliferation rates of cells and increasing chain lengths in both the backbone and pendant chain lowered the material stiffness. This work highlights the power that a combinatorial approach to material design can have. Resulting from this pivotal work were two medical device products that have

saved thousands of lives.[84, 85] The fundamental correlations drawn by Brocchini et al, have accelerated application-driven polymer development for use in medical devices.

1.5 Functionalization Through Click Chemistry

A major advantage to synthetic polymers is the ability to tune their properties through chemical and physical modifications. An increasingly popular area of research is the use of click chemistries. Originally employed in bioconjugation methods for protein and peptide modifications, these quantitative synthetic processes under mild conditions and with limited byproducts are a unique and effective way to change the bulk or surface properties of a polymer.[86] Two of the most commonly used click chemistries are ultraviolet light mediated thiol-alkene chemistry[87] to form thioethers and copper mediated azide-alkyne[88] reactions. More recent approaches have looked at strained alkynes for improved reaction kinetics without the use of toxic copper catalysts.[89] These reactions can be used to tether bioactive molecules or induce crosslinking/chain extension with peptides and other oligomers.[90]

1.6 Thesis Design and Organization

The main goal of this thesis was to design, synthesize, and characterize a library of novel polymers with enhanced resorption over tyrosine-derived polymers and better tunability than commercially available libraries. It was hypothesized that establishing structure-property relationships of these polymers would accelerate lead polymer candidate decisions for application specific research in the lab. The work in thesis takes you through the steps of developing a biomaterial from the design phase through to the application

phase. These polymers possess novelty in the field by exhibiting tunability over a wide range of polymer properties including non-acidic degradation and resorption which many materials are lacking.

Polymer design can be accomplished with two approaches. The first, and more common, approach is to use the properties of a desired application and try to match them based on previous experimentation and synthetic knowledge. The other approach is to build a large library with a range of tunable properties and screen them for potential hits. This library can also be used to understand which chemical features correlate to specific properties. This becomes a basis for a larger range of applications and projects. This thesis will use the latter approach to develop a library of polymers that can be used in additive manufacturing for complex scaffold design, drug delivery with tunable release, and nerve regenerative conduits for critical sized defects. In order to meet the desired goal of this research project, the parameters investigated include biocompatibility, degradation and resorption, processability, and thermal properties. In addition, basic modeling was used to demonstrate predictability of polymer properties based on chemical structure. Another major appeal to synthetic polymers is their ability to be scaled in a reproducible fashion. All polymers presented in this research were scaled above 20 grams with some reaching a 150-gram scale. This also allowed us to investigate commonly applied commercial polymer extrusion techniques for devices requiring larger amounts of polymer. Considerations that needed to be accounted for in the synthesis of these monomers and polymers include workup procedures which could not include techniques such as columns due to limited translation commercially. To circumvent these limitations, extractions,

precipitations, and recrystallizations were completed in order to ensure purity of the final products on hundred-gram scales.

Herein this thesis, we present research developing a library of poly(ester-arylate)s comprised of tyrosol-derived diphenols. Tyrosol is a natural phenolic antioxidant commonly found in olive oil and wine, therefore already introduced in many of our diets.[91] It has been reported to have an advantageous antioxidative effect *in vivo*, potentially being cardioprotective, as well as preventing cells from oxidative injury.[91] Tyrosol has increased solubility compared to tyrosine, and when reacted with 2-(4-hydroxyphenyl)acetic acid or 3-(4-hydroxyphenyl)propionic acid, forms an ester bond which is hydrolytically degradable compared to the previously reported amide containing diphenols. It was hypothesized through the design of these polymers that replacing the non-hydrolytically degrading amide with an ester would result in increased resorption. Ideally, many of the favorable properties of tyrosine-based polymers would translate over to tyrosol-based polymers due to structural similarities. Polyarylate design was then separated into three investigative trends: (i) asymmetric versus "pseudosymmetric" diphenols, (ii) linear aliphatic diacid chain length, and (iii) diacid rigidity (Figure 1.4). The design and synthesis of this work including structural investigations through analytical methods such as NMR and FTIR are reported in **Chapter 3.**

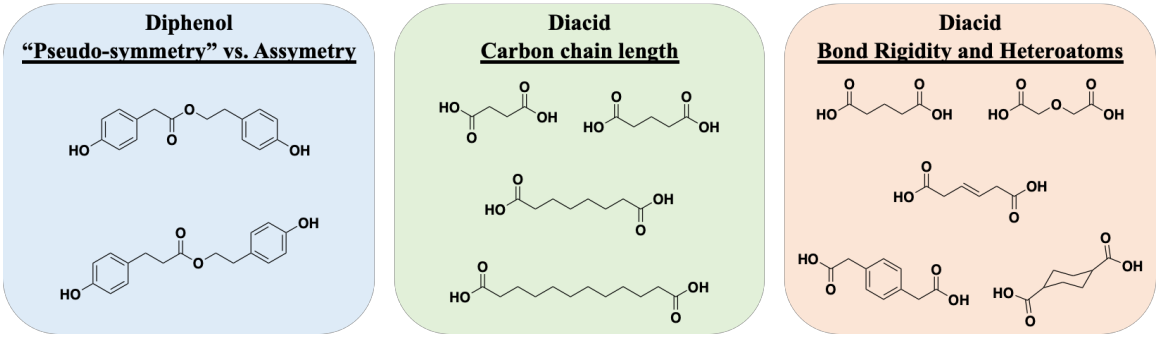

Figure 1.4. Structure trends investigated in this thesis.

Once the polymer's synthesis was defined structure-property relationships needed to be established. This work used both experimental and predictive approaches and are evaluated in **Chapter 4.** Increasing degradation and resorption rates compared to tyrosine-derived polymers is a main objective of this thesis. It is hypothesized that the diphenols containing ester bonds would not only be more soluble as is, but also be able to further degrade into their original starting materials which have higher solubilities. Hydrophobicity and logP calculations were used to better understand ways in which we can manipulate degradation and resorption kinetics can be manipulated while maintaining tunability in other property areas. Hydrolytic degradation was the only mechanism explored in this research. While enzymatic processes will take place in polyesters due to the presence of lipases and esterases in the body, hydrolytic rates are easier to identify and typically occur at much faster rates.

Thermal properties of polymer are also important due to implications on the processability and material behavior in physiological conditions. The presence of water and higher temperatures in the body can vastly affect polymer properties *in vivo* and therefore need to be characterized. Additionally, the mechanical properties can be

evaluated to determine the potential applications for which these polymers can be used. Specifically, tensile properties of thermally processed films can indicate the form and inherent strength of the polymer primarily in an amorphous state. Once these structure property trends were established a case study was performed for polymer candidate selection in nerve guidance conduits. Investigating polymer processing impact on mechanical properties and crystallinity as well as biocompatibility of human Schwann cells on the polymer surface help in the decision-making process. When the data was compiled, 2 lead candidates were identified for further *in vivo* studies.

Bioactivity of polymers was not a major focus of the work presented in this thesis. Preliminary *in vitro* work evaluating the ability for cells to adhere and proliferate on the surface of new polymers. Polymers that are too hydrophilic in nature don't allow serum proteins to adsorb and therefore are poorer cell substrates. Polymers discussed in this thesis are based on tyrosol, an aromatic-containing compound, which exhibits more hydrophobicity than other commonly investigated amino-acid based polymers. Adhesion and proliferation of multiple primary cell types was completed and presented in **Appendix 1**.

With all the knowledge of interactions between polymer properties and their correlation to chemical structure, additive manufacturing was investigated as a way to process polymers with complex architectures in **Chapter 5**. Exploration into the limits of polymer printability was completed and the molecular weight impact on polymer viscosity and printing parameters was defined. Chemical modifications were completed to improve mechanical properties of printed constructs using click chemistry. Polymer properties were tuned based on printed constructs alone in addition to incorporation of UV initiated chain

extension and/or crosslinking. This work has the potential to further expand by attaching bioactive molecules to the polymer for improved bioactivity.

Chapter 6 presents the utility of tyrosol-derived polyarylates as drug delivery matrixes for both hydrophobic and hydrophilic APIs. Long acting polymer-drug complexes that can locally release small amounts of drug over several months are of interest in the pharmaceutical sector. Convenience and improved patient compliance are two driving factors influencing the desire for longer acting implants. These implants have been considered for long term birth control solutions, delivery of immunosuppression agents for vascularized composite allotransplantation, and treatment of defects where cancerous tissue was removed.

The main objectives and hypotheses of this thesis are:

1. To improve the degradability, resorption and acidity of commercially available polymers. We hypothesize this can occur through an incremental change from an amide in tyrosine-derived polymers to an ester in tyrosol-derived polymers.
2. To establish structure property relationships of new polymers to accelerate lead candidate decision making for specific applications. We hypothesize that by tuning chemical structure, incorporating aliphatic carbon chains, aromatic rings, double bonds, and heteroatoms we can obtain a large range of properties. We predict longer aliphatic diacids to have longer degradation and resorption times, as well as decrease glass transition temperatures and polymer stiffness. We also anticipate the increased hydrophobicity which should elicit better overall cell adhesion.

Conversely, we expect shorter chain diacids to have higher stiffness, faster degradation and higher glass transition temperatures.

3. To design a new library of 3D printable inks with defined processing parameters and improved mechanical properties through chemical modifications. We hypothesize that molecular weight has the largest impact on limited mechanical strength. Low molecular weights are easier to print but have the weakest polymer properties. As such, we hypothesize post print curing to increase molecular weight will result in improved mechanical strength.
4. To understand chemical implications on drug release in long acting implantable devices and introduce structural modifications to improve release profiles. We hypothesize that the thermal processability of tyrosol polymers will impact the release profiles of both hydrophobic and hydrophilic drugs. Hydrophobic polymers can trap hydrophobic drug while burst release hydrophilic ones. We hypothesize that through incorporating hydrophilic polymer blocks or hydrogen bonding sources, we can address these limitations for hydrophobic and hydrophilic drugs, respectively.

Overall, the key contribution of this thesis resides in the legacy of these materials over the next several decades. This work aims to establish the fundamental library design to advance their use in application specific research by those within the lab and in the scientific community.

CHAPTER 2: MATERIALS AND METHODS

This chapter contains information about the general solvents, reagents and experimental protocols used throughout the research presented in this thesis. Additional specific conditions and protocols will be further described in more detail within the specific chapter they apply to.

2.1 Materials

2-(4-hydroxyphenyl)acetic acid, 3-(4-hydroxyphenyl)propionic acid, 2-(4-hydroxyphenyl)ethanol, were purchased from TCI America (Portland, OH). All diacids as well as phosphoric acid were purchased from either TCI America (Portland, OH) or Sigma Aldrich (St. Louis, MO). All additional chemicals and reagents including solvents were purchased from VWR (Radnor, PA) or Fisher Scientific (Waltham, MA).

2.2 Methods

2.2.1 General Procedures for Monomer Characterization

Chemical structure was confirmed *via* proton nuclear magnetic resonance spectroscopy (^{1}H NMR, Varian 500 MHz) in DMSO-*d*6. HPLC analysis was used to confirm the presence of any trace impurities. In short, using an Agilent Infinity Instrument equipped with an ultraviolet light absorbance detector and a Kinetex 5 μm C18 Column (150 x 4.6 mm, 100Å), a 19 min gradient from 95:5 A:B to 5:95 A:B was used where A is water + 0.1% trifluoroacetic acid, and B is acetonitrile + 0.1% trifluoroacetic acid. Melting points of the monomers were determined using the thermogram produced by differential scanning calorimetry (DSC 2520, Mettler Toledo) with a heating rate of 10 °C/min.

2.2.2 General Procedures for Polymer Characterization

Chemical composition was determined using proton nuclear magnetic resonance (^{1}H NMR, Varian 500 MHz) in $CDCl_3$. Number average molecular weights (M_n), and weight average molecular weight (M_w) were determined using gel permeation chromatography (GPC, Waters 717) equipped with a differential refractometer (Waters 410). Two Agilent PLGel 5 μm columns (7.5 x 300 mm) with pore sizes of 10^5 and 10^3 Å in tandem were used for optimal separation of molecular weights in chloroform + 0.1% trifluoroacetic acid as a solvent. All results were relative to polystyrene standards in a range of 580 to 920,000 Daltons. Thermal properties of polymers were measured using differential scanning calorimetry (DSC2520, Mettler Toledo) and thermogravimetric analysis (TGA, TA 550). DSC was used to evaluate melting temperatures (T_m), glass transition temperatures (T_g), and crystallization temperatures (T_c) for monomers and/or polymers. Briefly, samples were run in a 5-step program that includes heating from 25 °C to 250 °C at a rate of 10 °C/min, followed by a hold at 250 °C for 2 min, cooling to -50 °C at 10°C/min, a hold a -50 °C for 2 min, and then heating to 250 °C at 10 °C/min. T_g and T_m are reported on the last heat unless otherwise noted. TGA was used to measure percent volatiles and decomposition temperature (T_d). Volatiles were calculated by the step transition between 50 °C and 150 °C, while T_d was calculated by the step transition from the plateau regions prior to and after mass loss.

2.2.3 Compression Molding

Polymer thin films were made using a Carver press compression molder at T_g + 50 °C or T_m + 30 °C. In order to fabricate the films, approximately 0.3 g of polymer that had been pre-dried in a vacuum oven at 60 °C overnight was placed on a metal plate equipped with metal shims at the desired thickness between 60 μm and 250 μm. Kapton® polyimide film was used on both sides to prevent sticking to the metal plates. The polymer was heated to temperature without force for 3 minutes and then pressed at 3000 lbs of force for 3 minutes. Polymer films were ambient cooled or quenched in liquid nitrogen for 1 minute and kept in the freezer to maintain a temperature below T_g.

2.2.4 Mechanical Testing

Specimens with 100 – 300 μm thickness were cut into 3 mm x 40 mm rectangles. Mechanical properties of polymers were collected on an MTS Systems Tester with a 100 N load cell and a 10 mm/min displacement rate. The Young's modulus was calculated from the slope of the tangent drawn at the linear portion of the stress-strain curve (typically between 0 % and 2 %). Strain was calculated based on the displacement between the grips from the initial position. All measurements were collected and averaged for a minimum of 3 specimens per sample.

2.2.5 Spin Coating of Polymer Thin Films

Polymer films were prepared by solution-based spin coating technique using 2 % w/v solutions. 80 μL of solution was added to a 15 mm diameter glass cover slip for air-water contact studies, 12 mm diameter glass cover slip for biological studies. Cover slips/crystals were spun at 3000 rpm for 30 s in order to get even coating. Polymer films were dried in a vacuum oven for at least 12 h of drying.

2.2.6 Polymer UV Sterilization for Cell Culture

Polymer films and devices were sterilized for *in vitro* studies using UV exposure. Samples were placed in a biosafety cabinet with the blower off and UV light on for 30 min intervals. Samples were flipped to ensure complete surface exposure and proper sterility for cell studies.

CHAPTER 3: DESIGN AND SYNTHESIS OF BIORESORBABLE TYROSOL-DERIVED POLY(ESTER-ARYLATE)S

3.1 Abstract

Commercially used polymers such as PLA and PLGA are tunable but upon degradation cause a local drop in pH and as a result, an inflammatory response. PCL and tyrosine-derived polymers on the other hand are slow degrading and resorbing, respectively. A library of tyrosol-derived poly(ester-arylate)s was developed as an alternative to these polymers, both degrading and resorbing at tunable rates without the acidic degradation byproducts. Diphenols, tyrosyl 4-hydroxyphenylacetate (HTy) and tyrosyl 4-hydroxyphenylpropanoate (DTy), were synthesized using Fischer esterification. Solubilities of the monomers were measured at 1.76 mg/mL and 0.6 mg/mL respectively in phosphate buffered saline (PBS) solution. Comparatively, these monomers were more soluble than previously developed desaminotyrosyl-tyrosine ethyl ester (DTE), which is soluble at 0.03 mg/mL. Design of these monomers allows for further hydrolysis into either 4-hydroxyphenylacetic acid (HPAA) or desaminotyrosine (DAT) to further increase solubility. Biocompatibility of predicted degradation products including monomers indicates that all byproducts are nontoxic at concentration > 0.25 mg/mL. Subsequent polymerization was performed using standard carbodiimide chemistry. Diacids were chosen to identify structural impacts of carbon chain length and bond rigidity. Polymerization kinetics were measured and with the exception of poly(DTy succinate) and both diglycolate-containing polymers, molecular weights greater than 150 kDa were obtained. Future work aims to identify structure-property relationships.

3.2 Introduction

Synthetic polymers have found utility as biomaterials due to their ability to degrade and resorb in the body. This eliminates the need for additional surgical procedures which can cause patient discomfort and risk of infection.[92] The ability to design polymers into predictable degradation products results in tailored resorption based on degradation component's solubilities. During the design process, incorporating hydrolytically labile bonds facilitates this process. Specifically, esters, carbonates, and anhydrides hydrolyze at an appreciable rate compared to urethanes, amides, and ethers. As a result, the latter rely on enzymatic processes *in vivo.*[75] One major drawback to enzymatically degradable polymers is difficulty establishing *in vitro-in vivo* correlations (IVIVC). Enzymes present in the body have increased activity and less predictable concentrations which are dependent of the location. Due to the unpredictable nature of enzymatic degradation, hydrolytic degradation will be investigated in this chapter.

Hydrolytic degradation is facilitated by diffusion of water into the polymer matrix, leading to hydrolysis of labile bonds. This is then proceeded by formation of oligomers and monomer units which can be resorbed by solubilization or removal from immune cells such as macrophages.[93] Tunability in degradation and resorption rates aids in the prediction of an erosion profile. Erosion is a balance between the water uptake, degradation, and resorption rates of a polymer. If resorption occurs much faster than degradation and the rate of water uptake, the polymer will be surface eroding. Inversely, if the polymer absorbs water and degrades faster than the rate of resorption, the polymer will undergo bulk erosion (Figure 3.1).[94] Bulk erosion is a more commonly observed pathway for polymers. Surface

erosion is typically only seen with the presence of enzymes or extremely hydrophobic polymers and is more difficult to characterize.

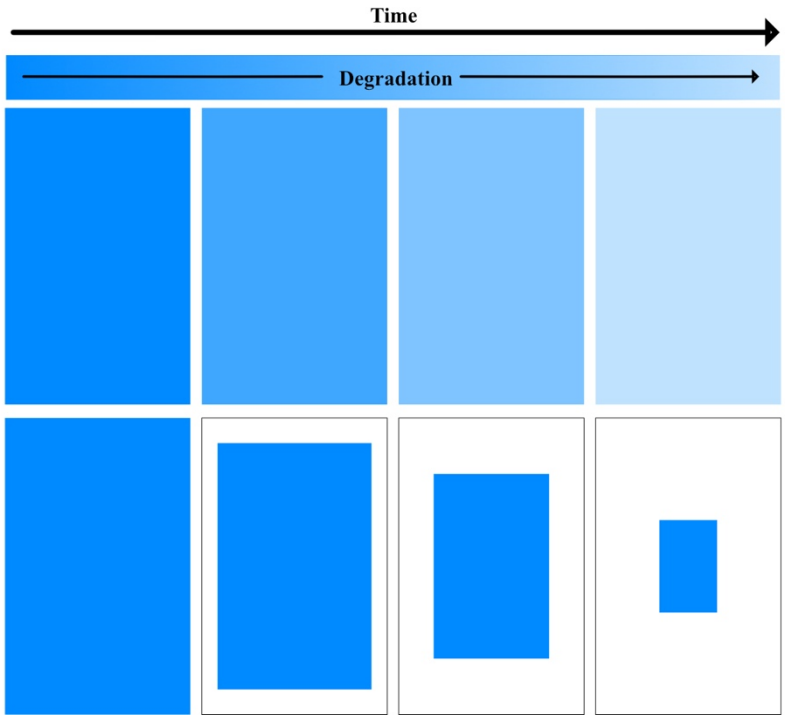

Figure 3.1. Schematic of erosion profiles for bulk eroding (top) and surface eroding (bottom) polymers with respect to time and degradation.

Polymers that are known to undergo surface erosion include PTMC[95] and poly(*alt*-tyrosol carbonate).[78] Surface erosion is ideal due to a retention in mechanical properties throughout the duration of the polymer device lifetime, while bulk eroding polymer's loss of mechanical properties over time and rapid resorption during later stages of degradation is observed.[75] As such, it is important to ensure that the byproducts of the polymer are non-cytotoxic and won't cause late stage complications. Polyesters and polyamides degrade into carboxylic acids and either alcohols or amides, respectively. The presence of free acids

can cause a local drop in pH at the device site. Commonly used polyesters containing lactide (PLA), glycolide (PGA), or copolymers thereof (PLGA), degrade into lactic acid and glycolic acid, respectively, both of which are considered acidic. Devices containing these polymers have reported late stage tissue acidosis and inflammatory responses, resulting in complications.[96] Ideally, matching the tunability of the PLGA polymer library while minimizing acidic degradation byproducts will provide the ideal polymer library.

Previous work within our lab addressed the acidic degradation byproducts through the design of tyrosine-based polymers. Tyrosine derived polymers have shown success in drug delivery and regenerative medicine. Specifically, tyrosine's aromatic ring provides chemical stability and structural rigidity. Unfortunately, these polymers contain an amide linkage which is not hydrolytically labile, leading to slow resorption times and in some cases, device failure.[97] It is hypothesized that by switching out the amide linkage with a more hydrolytically labile ester bond, resorption of the monomer and as a result polymer will increase. 2-(4-hydroxyphenyl)ethanol (tyrosol), is structurally similar to tyrosine, containing an aromatic ring with both a phenol and aliphatic alcohol. Commonly found in olive oil and wine, tyrosol has reported cardioprotective and antioxidant properties.[91] Novel diphenols were synthesized through the esterification of tyrosol, and either 2-(4-hydroxyphenyl)acetic acid (HPAA) or 3-(4-hydroxyphenyl)propionic acid (DAT). Measured solubilities and calculated acidities indicate improved resorption compared to tyrosine diphenols while maintaining their non-acidic properties. Additionally, the incorporation of aliphatic esters can lead to further degradation and therefore faster resorption. These diphenols were then subsequently polymerized with diacids to form arylate bonds. Tyrosol-derived poly(ester-arylate)s have been minimally explored for their

use in 3D printable inks.[98] This chapter aims to investigate a more wholistic approach to polymer library design, identifying trends between chemical structure and material property.

3.3 Materials and Methods

3.3.1 Materials

All chemicals were purchased from TCI America (Portland, OH), Sigma Aldrich (St. Louis, MO), VWR (Radnor, PA) or Fisher Scientific (Waltham, MA) as previously described. Human lung fibroblasts (MRC-5, #CCL-171) and culture medium were purchased from ATCC. Tissue culture treated polystyrene (TCP) flask, multi-well plates were purchased from VWR.

3.3.2 Monomer Synthesis

3.3.2.1 Synthesis of 2-(4-hydroxyphenyl)ethyl 2-(4-hydroxyphenyl)acetate (HTy).

Tyrosol (275.1 g, 1.99 mol, 1.01 equiv.) was added to 2-(4-hydroxyphenyl)acetic acid (300.00 g, 1.97 mol, 1.00 equiv.) and toluene (650 mL, 0.33 L/mol HPAA) in a 5000 mL round bottom flask. The flask was equipped with a dean stark apparatus, water-cooled reflux condenser, thermometer adapter, overhead stirrer with Teflon paddle, and heating mantle. 85% phosphoric acid aqueous solution (22.75 mL, 0.197 mol, 0.10 equiv.) was added and the reaction was heated to reflux. Once the collection of water subsided, the reaction was allowed to reflux for one additional hour to minimize the percentage of phenolic esters present in the reaction. The reaction was then allowed to cool to room temperature and a gummy oil formed. Excess toluene was decanted and the solid was

precipitated in hexanes. The solid was filtered, dried, dissolved in ethyl acetate, washed 3 times with 5% $NaHCO_3$, 2 times with DI water, and once with brine. The resulting oil was concentrated *in vacuo* until concentrated and then the solid was precipitated in hexanes. The white solid was collected by filtration and then dried in the vacuum oven at 50 °C to dry. Yield: 84.6%. Melting point = 94.5 °C. ^{1}H NMR (500 MHz, DMSO-d_6) δ 9.26 (s, 2H), 7.01(d, J = 8.4 Hz, 2H), 6.97 (d, J = 8.4 Hz, 2H), 6.71 (d, J = 8.4 Hz, 2H), 6.69 (d, J = 8.4 Hz, 2H), 4.14 (t, J = 6.9 Hz, 2H), 3.49 (s, 2H), 2.74 (t, J = 6.9 Hz, 2H).

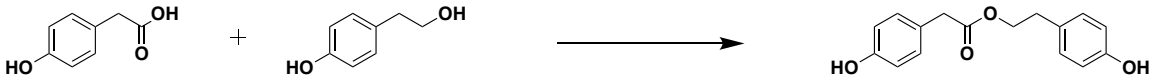

Scheme 3.2. Reaction schematic for the synthesis of 2-(4-hydroxyphenyl)ethyl 2-(4-hydroxyphenyl)acetate.

3.3.2.2 Synthesis of 2-(4-hydroxyphenyl)ethyl 3-(4-hydroxyphenyl)propanoate (DTy).

Tyrosol (167.1 g, 1.21 mol, 1.005 equiv.) was added to 3-(4-hydroxyphenyl)propionic acid (200.0 g, 1.20 mol, 1.00 equiv.) and toluene (410 mL, 0.33 L/mol HPAA) in a 3000 mL round bottom flask. The flask was equipped with a dean stark apparatus, water-cooled reflux condenser, thermometer adapter, overhead stirrer with Teflon paddle, and heating mantle. 85% phosphoric acid aqueous solution (13.87 mL, 0.120 mol, 0.10 equiv.) was added and the reaction was heated to reflux. Once the collection of water subsided, the reaction was allowed to reflux for one additional hour to minimize the percentage of phenolic esters present in the product. The reaction was then allowed to cool to room temperature and a white solid precipitated out of solution. The solid was filtered to remove toluene, followed by 3 washes with 5% $NaHCO_3$, 2 washes

with DI water, and one wash with hexanes. The solid was dried in the vacuum oven at 50 °C overnight. Yield: 96.0%. Melting point = 127.7 °C. ^{1}H NMR (500 MHz, DMSO-d_6) δ 9.18 (s, 2H), 7.02 – 6.97 (m, 2H), 6.97 – 6.92 (m, 2H), 6.69 – 6.66 (m, 2H), 4.11 (t, J = 7.0 Hz, 2H), 2.71 (dt, J = 14.6, 7.2 Hz, 4H), 2.50 (t, J = 7 Hz, 2H).

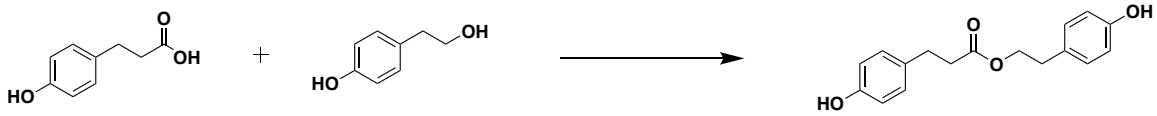

Scheme 3.3. Reaction schematic for the synthesis of 2-(4-hydroxyphenyl)ethyl 3-(4-hydroxyphenyl)propanoate.

3.3.3 Monomer Solubility Analysis *via* HPLC

HTy, tyrosol, HPAA, and DAT were dissolved in a concentration of 1.0 mg/mL in phosphate buffered saline (PBS) solution (pH 7.4). DTy was less soluble and therefore dissolved at 0.125 mg/mL in PBS solution (pH 7.4). The solutions were then serially diluted down 2-fold to 61 ng/mL. Standards were run on an Agilent HPLC equipped with an UV absorbance detector at 220 nm wavelength and a Phenomenex Kinetex C18 5µm 100 Å 4.6 mm x 150 mm column. The following gradient system was used: 95:5:0 A:B:C to 50:50:0 A:B:C over 10 minutes, 50:50:0 A:B:C to 15:75:10 A:B:C over 12 minutes, return to 95:5:0 A:B:C over 2 minutes, for a 24 minute run time; where, Solvent A: Water + 0.1% TFA, Solvent B: Acetonitrile + 0.1% TFA, and Solvent C: Methanol + 0.1% TFA.

3.3.4 *In-Vitro* Leachables Cytotoxicity.

MRC-5 cells were seeded at $1x10^4$/well in 96-well plates and cultured for overnight at 37°C with 5% CO_2 and 95% humidity. Monomeric components including HTy, DTy, tyrosol, HPAA, DAT, and diacids were prepared at 1 mg/mL in cell culture medium. A serial dilution at 1:10 for each component was prepared using culture medium. After overnight incubation, culture medium was removed from cells and medium containing serially diluted monomeric components were added to cells. After incubation at 37°C for 24 h, medium was removed from cells and 0.1 mL of medium containing 10% alamarBlue (Bio-Rad BUF012B) was added to each well. After incubated at 37°C for 45 min, the fluorescent intensity was read using TECAN Spark plate reader with E_x/E_m=540 nm/590 nm.

3.3.5 Polymer Synthesis

3.3.5.1 General Synthetic Procedure for Polyarylates

Diphenol (1 equiv) and diacid (0.98 – 0.99 equiv) were added with 4-(dimethylamino)pyridinium p-toluenesulfonate (DPTS, 0.5 equiv) in dichloromethane (0.3M diphenol in solvent). Once homogenous, diisopropylcarbodiimide (DIC, 2.3 equiv) was added. Reactions were monitored *via* chloroform GPC and stopped once the M_w reached 150 – 200 kDa relative to polystyrene standards. Polymers were precipitated 3 times from methylene chloride in isopropanol and then blended once in DI water. The resulting polymer was then lyophilized for 24 hours and dried in a vacuum oven at 40 °C overnight to remove residual solvent and water.

3.3.5.2 Synthesis of poly(HTy succinate) (pHTy2).

GPC (Chloroform + 0.1% TFA): M_n = 95.0 kDa, M_w = 175.4 kDa, PDI = 1.85. ^{1}H NMR (500 MHz, Chloroform-*d*) δ 7.23 (d, *J* = 7.6 Hz, 2H), 7.13 (d, *J* = 7.9 Hz, 2H), 7.04 (d, *J* = 7.7 Hz, 2H), 7.00 (d, *J* = 7.8 Hz, 2H), 4.28 (t, *J* = 6.9 Hz, 2H), 3.57 (s, 2H), 2.97 (s, 4H), 2.89 (t, *J* = 6.8 Hz, 2H).

Scheme 3.4. Reaction schematic for the synthesis of poly(HTy succinate).

3.3.5.3 Synthesis of poly(HTy glutarate) (pHTy3).

GPC (Chloroform + 0.1% TFA): M_n = 90.9 kDa, M_w = 157.6 kDa, PDI = 1.73. ^{1}H NMR (500 MHz, Chloroform-*d*) δ 7.25 (d, *J* = 8.5 Hz, 2H), 7.15 (d, *J* = 8.5 Hz, 2H), 7.04 (d, *J* = 8.5 Hz, 2H), 7.00 (d, *J* = 8.5 Hz, 2H), 4.29 (t, *J* = 6.9 Hz, 2H), 3.58 (s, 2H), 2.90 (t, *J* = 6.9 Hz, 2H), 2.71 (t, *J* = 7.3 Hz, 4H), 2.18 (p, *J* = 7.3 Hz, 2H).

Scheme 3.5. Reaction schematic for the synthesis of poly(HTy glutarate).

3.3.5.4 Synthesis of poly(HTy adipate) (pHTy4).

GPC (Chloroform + 0.1% TFA): M_n = 105.7 kDa, M_w = 183.6 kDa, PDI = 1.74. ^{1}H NMR (500 MHz, Chloroform-*d*) δ 7.25 (d, *J* = 8.6 Hz, 2H), 7.15 (d, *J* = 8.5 Hz, 2H), 7.04 (d, *J* = 8.6 Hz, 2H), 7.00 (d, *J* = 8.5 Hz, 2H), 4.28 (t, *J* = 6.9 Hz, 2H), 3.58 (s, 2H), 2.90 (t, *J* = 6.9 Hz, 2H), 2.63 (m, 4H), 1.88 (m, 4H).

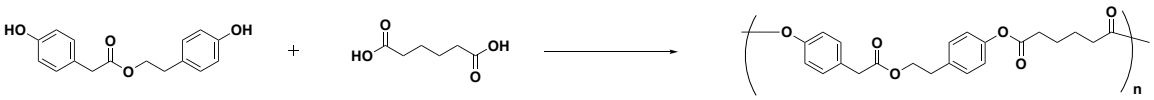

Scheme 3.6 Reaction schematic for the synthesis of poly(HTy adipate).

3.3.5.5 Synthesis of poly(HTy pimelate) (pHTy5).

GPC (Chloroform + 0.1% TFA): M_n = 107.5 kDa, M_w = 192.8 kDa, PDI = 1.79. ^{1}H NMR (500 MHz, Chloroform-*d*) δ 7.24 (d, *J* = 8.4 Hz, 2H), 7.15 (d, *J* = 8.4 Hz, 2H), 7.03 (d, *J* = 8.2 Hz, 2H), 6.99 (d, *J* = 8.2 Hz, 2H), 4.29 (t, *J* = 6.9 Hz, 2H), 3.58 (s, 2H), 2.90 (t, *J* = 6.9 Hz, 2H), 2.59 (t, *J* = 7.4 Hz, 4H), 1.82 (p, *J* = 7.5 Hz, 4H), 1.55 (p, *J* = 7.7, 7.2 Hz, 2H).

Scheme 3.7. Reaction schematic for the synthesis of poly(HTy pimelate).

3.3.5.6 Synthesis of poly(HTy suberate) (pHTy6).

GPC (Chloroform + 0.1% TFA): M_n = 85.4 kDa, M_w = 152.0 kDa, PDI = 1.78. ^{1}H NMR (500 MHz, Chloroform-*d*) δ 7.25 (d, *J* = 8.6 Hz, 2H), 7.15 (d, *J* = 8.6 Hz, 2H), 7.03 (d, *J* = 8.6 Hz, 2H), 6.99 (d, *J* = 8.5 Hz, 2H), 4.29 (t, *J* = 6.9 Hz, 2H), 3.58 (s, 2H), 2.90 (t, *J* = 6.9 Hz, 2H), 2.57 (t, *J* = 7.4 Hz, 4H), 1.84 – 1.73 (m, 4H), 1.50-1.47 (m, 4H).

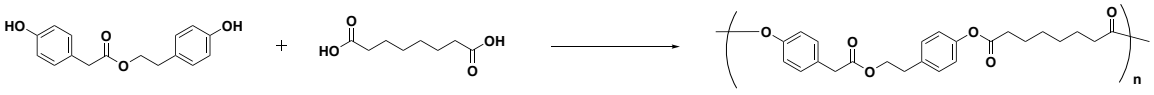

Scheme 3.8. Reaction schematic for the synthesis of poly(HTy suberate).

3.3.5.7 Synthesis of poly(HTy azelate) (pHTy7).

GPC (Chloroform + 0.1% TFA): M_n = 83.6 kDa, M_w = 172.6 kDa, PDI = 2.06.

Scheme 3.9. Reaction schematic for the synthesis of poly(HTy azelate).

3.3.5.8 Synthesis of poly(HTy sebacate) (pHTy8).

GPC (Chloroform + 0.1% TFA): M_n = 117.2 kDa, M_w = 229.6 kDa, PDI = 1.96. ^{1}H NMR (500 MHz, Chloroform-*d*) δ 7.24 (d, *J* = 7.3 Hz, 2H), 7.15 (d, *J* = 7.3 Hz, 2H), 7.03 (d, *J* = 7.0 Hz, 2H), 6.99 (d, *J* = 7.0 Hz, 2H), 4.28 (t, *J* = 6.5 Hz, 2H), 3.58 (s, 2H), 2.90 (t, *J* = 6.9 Hz, 2H), 2.55 (t, *J* = 7.5 Hz, 4H), 1.76 (p, *J* = 7.2 Hz, 4H), 1.48 – 1.33 (m, 8H).

Scheme 3.10. Reaction schematic for the synthesis of poly(HTy sebacate)

3.3.5.9 Synthesis of poly(HTy dodecanedioate) (pHTy10).

GPC (Chloroform + 0.1% TFA): M_n = 104.9 kDa, M_w = 191.0 kDa, PDI = 1.82. ^{1}H NMR (500 MHz, Chloroform-*d*) δ 7.24 (d, *J* = 8.5 Hz, 2H), 7.15 (d, *J* = 8.5 Hz, 2H), 7.03 (d, *J* = 8.5 Hz, 2H), 6.99 (d, *J* = 8.5 Hz, 2H), 4.28 (t, *J* = 7.0 Hz, 2H), 3.58 (s, 2H), 2.90 (t, *J* = 7.0 Hz, 2H), 2.54 (t, *J* = 7.5 Hz, 4H), 1.75 (p, *J* = 7.5 Hz, 4H), 1.45 – 1.30 (m, 12H).

Scheme 3.11. Reaction schematic for the synthesis of poly(HTy dodecanedioate).

3.3.5.10 Synthesis of poly(DTy glutarate) (pDTy3).

GPC (Chloroform + 0.1% TFA): M_n = 84.6 kDa, M_w = 153.5 kDa, PDI = 1.81. ^{1}H NMR (500 MHz, Chloroform-*d*) δ 7.19 (t, *J* = 8.3 Hz, 4H), 7.03 (d, *J* = 8.5 Hz, 2H), 6.99 (d, *J* = 8.5 Hz, 2H), 4.27 (t, *J* = 7.0 Hz, 2H), 2.91 (q, *J* = 7.0 Hz, 4H), 2.71 (t, *J* = 6.0 Hz, 4H), 2.60 (t, *J* = 7.8 Hz, 2H), 2.18 (p, *J* = 7.2 Hz, 2H).

Scheme 3.12. Reaction schematic for the synthesis of poly(DTy glutarate).

3.3.5.11 Synthesis of poly(DTy adipate) (pDTy4).

GPC (Chloroform + 0.1% TFA): M_n = 100.8 kDa, M_w = 194.8 kDa, PDI = 1.93. ^{1}H NMR (500 MHz, Chloroform-*d*) δ 7.19 (t, *J* = 8.3 Hz, 4H), 7.02 (d, *J* = 8.5 Hz, 2H), 6.98 (d, *J* = 8.5 Hz, 2H), 4.27 (t, *J* = 7.1 Hz, 2H), 2.91 (q, *J* = 7.1 Hz, 4H), 2.64 – 2.58 (m, 6H), 1.91 – 1.84 (m, 4H).

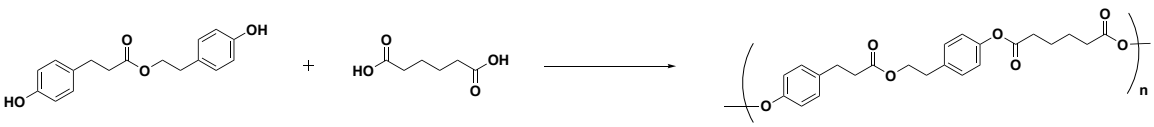

Scheme 3.13. Reaction schematic for the synthesis of poly(DTy adipate).

3.3.5.12 Synthesis of poly(DTy pimelate) (pDTy5).

GPC (Chloroform + 0.1% TFA): M_n = 103.1 kDa, M_w = 189.3 kDa, PDI = 1.84. ^{1}H NMR (500 MHz, Chloroform-*d*) δ 7.18 (t, *J* = 8.5 Hz, 4H), 7.01 (d, *J* = 8.6 Hz, 2H), 6.97 (d, *J* = 8.6 Hz, 2H), 4.27 (t, *J* = 7.1 Hz, 2H), 2.91 (q, *J* = 7.0 Hz, 4H), 2.66 – 2.54 (m, 6H), 1.81 (p, *J* = 7.5 Hz, 4H), 1.54 (p, *J* = 7.9 Hz, 2H).

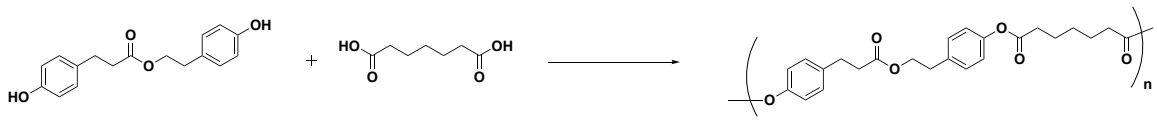

Scheme 3.14. Reaction schematic for the synthesis of poly(DTy pimelate).

3.3.5.13 Synthesis of poly(DTy suberate) (pDTy6).

GPC (Chloroform + 0.1% TFA): M_n = 77.5 kDa, M_w = 138.4 kDa, PDI = 1.79. ^{1}H NMR (500 MHz, Chloroform-*d*) δ 7.19 (t, *J* = 8.4 Hz, 4H), 7.01 (d, *J* = 8.5 Hz, 2H), 6.97 (d, *J* = 8.5 Hz, 2H), 4.27 (t, *J* = 7.1 Hz, 2H), 2.91 (q, *J* = 7.1 Hz, 4H), 2.60 (t, *J* = 7.8 Hz, 2H), 2.56 (td, *J* = 7.5, 2.5 Hz, 4H), 1.77 (tt, *J* = 7.5, 3.3 Hz, 4H), 1.48 (dt, *J* = 7.2, 3.8 Hz, 4H).

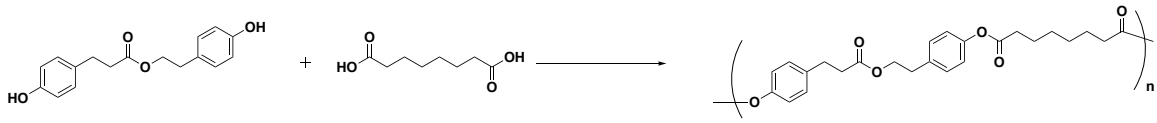

Scheme 3.15. Reaction schematic for the synthesis of poly(DTy suberate).

3.3.5.14 Synthesis of poly(DTy azelate) (pDTy7).

GPC (Chloroform + 0.1% TFA): M_n = 73.8 kDa, M_w = 150.3 kDa, PDI = 2.04. ^{1}H NMR (500 MHz, Chloroform-*d*) δ 7.18 (t, *J* = 8.4 Hz, 4H), 7.01 (d, *J* = 8.5 Hz, 2H), 6.97 (d, *J* = 8.5 Hz, 2H), 4.26 (t, *J* = 7.1 Hz, 2H), 2.90 (q, *J* = 7.1 Hz, 4H), 2.60 (t, *J* = 7.8 Hz, 2H), 2.54 (td, *J* = 7.5, 2.6 Hz, 4H), 1.76 (p, *J* = 7.2, 6.8 Hz, 4H), 1.44 (d, *J* = 15.3 Hz, 6H).

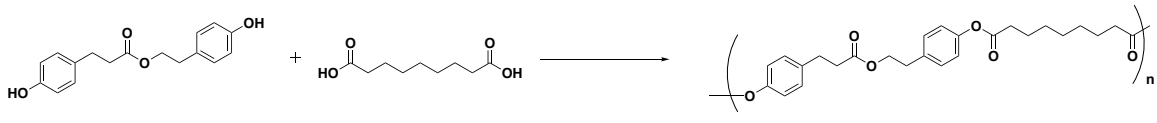

Scheme 3.16. Reaction schematic for the synthesis of poly(DTy azelate).

3.3.5.15 Synthesis of poly(DTy sebacate) (pDTy8).

GPC (Chloroform + 0.1% TFA): M_n = 80.7 kDa, M_w = 154.4 kDa, PDI = 1.91. ^{1}H NMR (500 MHz, Chloroform-*d*) δ 7.18 (t, *J* = 8.3 Hz, 4H), 7.01 (d, *J* = 8.5 Hz, 2H), 6.97 (d, *J* = 8.5 Hz, 2H), 4.27 (t, *J* = 7.1 Hz, 2H), 2.91 (q, *J* = 7.1 Hz, 4H), 2.60 (t, *J* = 7.8 Hz, 2H), 2.54 (td, *J* = 7.5, 2.6 Hz, 4H), 1.75 (p, *J* = 7.2 Hz, 4H), 1.41 (dd, *J* = 15.0, 7.7 Hz, 8H).

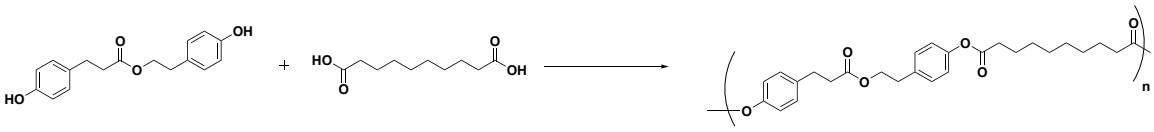

Scheme 3.17. Reaction schematic for the synthesis of poly(DTy sebacate).

3.3.5.16 Synthesis of poly(DTy dodecanedioate) (pDTy10).

GPC (Chloroform + 0.1% TFA): M_n = 89.7 kDa, M_w = 184.5 kDa, PDI = 2.06. ^{1}H NMR (500 MHz, Chloroform-*d*) δ 7.18 (t, *J* = 8.3 Hz, 4H), 7.01 (d, *J* = 8.5 Hz, 2H), 6.97 (d, *J* = 8.5 Hz, 2H), 4.27 (t, *J* = 7.1 Hz, 2H), 2.91 (q, *J* = 7.1 Hz, 4H), 2.60 (t, *J* = 7.8 Hz, 2H), 2.54 (td, *J* = 7.5, 2.6 Hz, 4H), 1.74 (p, *J* = 8.3, 7.8 Hz, 4H), 1.45 – 1.28 (m, 12H).

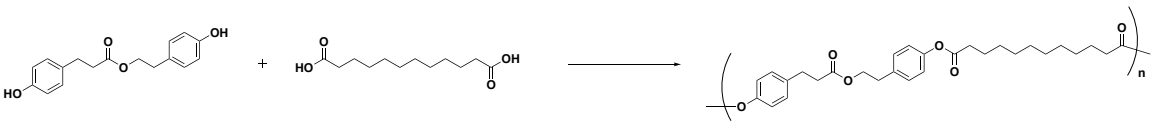

Scheme 3.18. Reaction schematic for the synthesis of poly(DTy dodecandioate).

3.3.5.17 Synthesis of poly(HTy diglycolate) (pHTyDG).

GPC (Chloroform + 0.1% TFA): M_n = 9.5 kDa, M_w = 23.5 kDa, PDI = 2.4. ^{1}H NMR (500 MHz, Chloroform-*d*) δ 7.24 (d, *J* = 8.1 Hz, 2H), 7.14 (d, *J* = 8.1 Hz, 2H), 7.07 (d, *J* = 8.1 Hz, 2H), 7.03 (d, *J* = 8.1 Hz, 2H), 4.56 (s, 4H), 4.30 (t, *J* = 6.7 Hz, 2H), 3.58 (s, 2H), 2.90 (t, *J* = 6.6 Hz, 2H).

Scheme 3.19. Reaction schematic for the synthesis of poly(HTy diglycolate).

3.3.5.18 Synthesis of poly(DTy diglycolate) (pDTyDG).

GPC (Chloroform + 0.1% TFA): M_n = 55.0 kDa, M_w = 89.4 kDa, PDI = 1.6. ^{1}H NMR (500 MHz, Chloroform-*d*) δ 7.20 (m, *J* = 8.3, 2.9 Hz, 4H), 7.10 – 7.01 (m, 4H), 4.56 (s, 4H), 4.27 (s, 2H), 2.91 (d, *J* = 6.3 Hz, 4H), 2.61 (t, *J* = 7.6 Hz, 2H).

Scheme 3.20. Reaction schematic for the synthesis of poly(DTy diglycolate).

3.3.5.19 Synthesis of poly(HTy transhexenedioate) (pHTytHex).

GPC (Chloroform + 0.1% TFA): M_n = 80.1 kDa, M_w = 153.6 kDa, PDI = 1.92. ^{1}H NMR (500 MHz, Chloroform-*d*) δ 7.24 (d, *J* = 8.4 Hz, 2H), 7.15 (d, *J* = 8.4 Hz, 2H), 7.05 (d, *J* = 8.5 Hz, 2H), 7.01 (d, *J* = 8.5 Hz, 2H), 5.91 (d, *J* = 3.7 Hz, 2H), 4.29 (t, *J* = 6.9 Hz, 2H), 3.58 (s, 2H), 3.38 (s, 4H), 2.90 (t, *J* = 6.8 Hz, 2H).

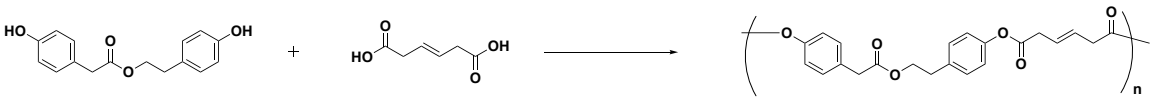

Scheme 3.21. Reaction schematic for the synthesis of poly(HTy transhexenedioate).

3.3.5.20 Synthesis of poly(DTy transhexenedioate) (pDTytHex).

GPC (Chloroform + 0.1% TFA): M_n = 74.2 kDa, M_w = 156.8 kDa, PDI = 2.11. ^{1}H NMR (500 MHz, Chloroform-*d*) δ 7.18 (t, *J* = 8.5 Hz, 4H), 7.03 (d, *J* = 8.5 Hz, 2H), 6.99 (d, *J* = 8.5 Hz, 2H), 5.89 (tt, *J* = 3.8, 1.4 Hz, 2H), 4.27 (t, *J* = 7.0 Hz, 2H), 3.37 (dq, *J* = 3.6, 1.7 Hz, 4H), 2.90 (s, 4H), 2.63 – 2.58 (m, 2H).

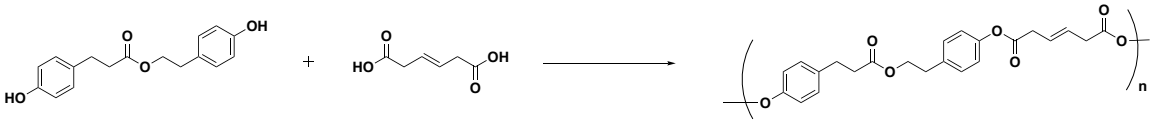

Scheme 3.22. Reaction schematic for the synthesis of poly(DTy transhexenedioate).

3.3.5.21 Synthesis of poly(HTy phenylenediacetate) (pHTyPDA).

GPC (Chloroform + 0.1% TFA): M_n = 82.4 kDa, M_w = 156.0 kDa, PDI = 1.89. ^{1}H NMR (500 MHz, Chloroform-*d*) δ 7.38 (s, 4H), 7.22 (d, *J* = 8.6 Hz, 2H), 7.12 (d, *J* = 8.5 Hz, 2H), 7.02 (d, *J* = 8.5 Hz, 2H), 6.98 (d, *J* = 8.5 Hz, 2H), 4.27 (t, *J* = 6.9 Hz, 2H), 3.84 (s, 4H), 3.56 (s, 2H), 2.88 (t, *J* = 6.9 Hz, 2H).

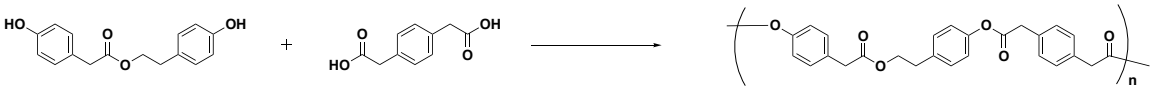

Scheme 3.23. Reaction schematic for the synthesis of poly(HTy phenylenediacetate).

3.3.5.22 Synthesis of poly(DTy phenylenediacetate) (pDTyPDA).

GPC (Chloroform + 0.1% TFA): M_n = 83.0 kDa, M_w = 192.3 kDa, PDI = 2.32. ^{1}H NMR (500 MHz, Chloroform-*d*) δ 7.37 (s, 4H), 7.16 (t, *J* = 8.2 Hz, 4H), 7.01 – 6.95 (m, 4H), 4.25 (t, *J* = 7.0 Hz, 2H), 3.84 (s, 4H), 2.89 (q, *J* = 7.0, 6.6 Hz, 4H), 2.58 (t, *J* = 7.8 Hz, 2H).

Scheme 3.24. Reaction schematic for the synthesis of poly(DTy phenylenediacetate).

3.3.5.23 Synthesis of poly(HTy cyclohexanedioate) (pHTyCHD).

GPC (Chloroform + 0.1% TFA): M_n = 100.9 kDa, M_w = 226.0 kDa, PDI = 2.24.

Scheme 3.25. Reaction schematic for the synthesis of poly(HTy cyclohexandioate).

3.3.5.24 Synthesis of poly(DTy cyclohexanedioate) (pDTyCHD).

GPC (Chloroform + 0.1% TFA): M_n = 119.7 kDa, M_w = 220.8 kDa, PDI = 1.85.

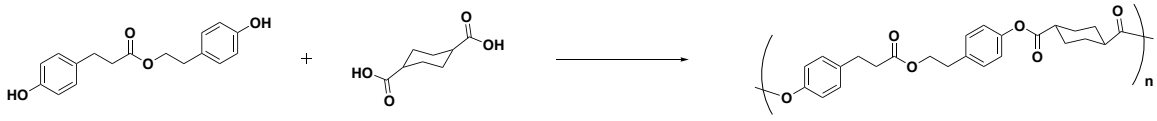

Scheme 3.26. Reaction schematic for the synthesis of poly(DTy cyclohexandioate).

3.4 Results and Discussion

3.4.1 Monomer Library Design

The main goal of this work is to design polymers that are both degradable and resorbable. In order to do so, the degradation components must be soluble in aqueous environments. Previously designed tyrosine derived polymers contained an amide linkage, which hydrolyze at much slower rates compared to the esters or carbonates bonds in the polymers. This meant that resorption relied on solubilization of the diphenol component. Given the bulky aromatic structure with pendant side chains, solubility was minimal. One example, DTE, which contained an ethyl ester pendant chain, has a reported solubility of 0.03 mg/mL in PBS. This was extremely low compared to lactic acid and glycolic acid which have solubilities of 1000 mg/mL and 608 mg/mL, respectively. In an effort to improve solubility of the degradation products while maintaining the biocompatibility and structural rigidity observed in tyrosine polymers, replacing the amide with an ester was investigated (Figure 3.27A). It is also hypothesized that removing the pendant group from the diphenol will result in tighter packing of the polymer chains. As such, molecular geometries of the diphenol can play a role. To better understand the structural implications, both HPAA and DAT were used in the monomer synthesis. When compared to tyrosol which contains two methylene groups, HPAA provides asymmetry around the ester with one methylene group while DAT provides symmetry with two (Figure 3.27B-C). This can play a significant role in solubilities of the monomers and a wide range of polymer properties.

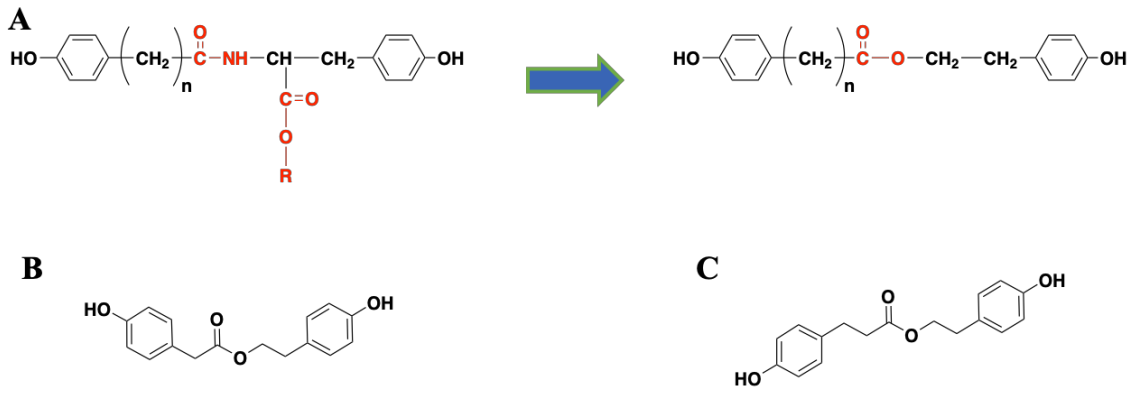

Figure 3.27. Change in chemistry structure from a backbone amide to a backbone ester (A) and the resulting monomers HTy (B) and DTy (C).

3.4.2 Synthesis of Monomers

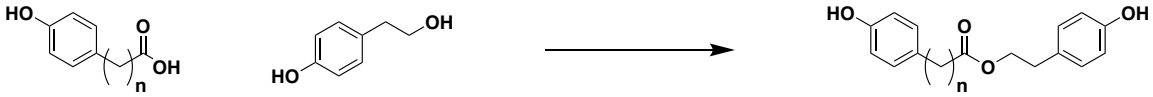

Scheme 3.28. Synthesis of tyrosol-derived diphenol compounds.

Monomers were obtained through Fischer esterification between an aliphatic acid and aliphatic alcohol. Tyrosol was reacted under reflux with either HPAA or DAT (Scheme 3.28). While phenolic alcohols were present in the reaction, they were less reactive than the aliphatic alcohol due to resonance stability. It was found that increasing the amount of excess tyrosol in the reaction mixture led to additional formation of the undesired phenolic ester. Synthesis optimization investigated the effect of excess tyrosol, acid types, and solvents (Table 3.1). All three play a role in the kinetics of the reaction and minimization of unwanted side products.

Excess tyrosol played a role in the presence of phenolic esters and free tyrosol. While neither act as chain terminators in the subsequent polymerization, they can produce

unwanted bonds, affecting both polymer properties and expected degradation products. Tyrosol's aromatic and aliphatic alcohol inhibit the efficacy of common extraction techniques to purify the monomer. As a result, minimizing the excess tyrosol added to the reaction is essential to final product purity. In order to ensure complete reaction, an excess of tyrosol was required to prevent free acid present in the monomer and as such, it was found that an excess of 0.01 molar equivalent was sufficient enough.

Acid choice played a primary role in the workup procedure of the monomer. p-toluenesulfonic acid (PTSA), which was traditionally used for tyrosine ester synthesis, required complex salting out procedures due to the hydrophobicity of the acid itself. These salting out procedures are difficult and require large excesses of solvent. PTSA also has a pKa of -2.8, making it a strong acid which could facilitate more phenolic ester formation. Switching to phosphoric acid, with a pKa of 2.16, and excellent water solubility, allowed for simpler workup procedures involving water washes

The last reaction condition that played a large role in monomer purity was the solvent type. Given the hydrophobic nature of these materials, they tend to be most soluble in chlorinated solvents. 1,2-dichloroethane, a higher boiling point and less volatile chlorinated solvent, led to a larger degree of phenolic esters present and also resulted in more discoloration of the final product. This is most likely due to thermal decomposition of the solvent during the reaction. Heptane was tried as a lower boiling point solvent but still resulted in impure product. Switching to toluene kept the reflux temperature low enough to prevent phenolic ester formation and was also easier to remove in DTy, which simply precipitated out, and HTy, which precipitated with a hexanes wash. Minimizing

phenolic ester formation, aromatic oxidation, and complex workup with chain terminators such as alcohols is essential to the ease of subsequent polymerizations.

Table 3.1. Synthetic conditions and implications in monomer purity.

Reaction No.	Tyrosol Excess	Acid	Solvent	Phenolic Ester	Yield
i	1:1	pTSA (0.05 equiv)	DCE	NC	75.5
ii	1.01:1	pTSA (0.05 equiv)	Heptane	6.5 %	NC
iii	1.1:1	pTSA (0.05 equiv)	Heptane	14.9 %	NC
iv	1.1:1	H_3PO_4 (0.05 equiv)	Toluene	38.0 %	NC
v	1:1	H_3PO_4 (0.05 equiv)	Toluene	1.7 %	79
vi	1.05:1	H_3PO_4 (0.05 equiv)	Toluene	3.8 %	NC
vii	1.01:1	H_3PO_4 (0.1 equiv)	Toluene	2.9 %	84.6

^{1}H NMR and FTIR were used to confirm monomer synthesis and any structural features. When comparing the phenolic protons in NMR, the HTy phenolic peaks around 9.25 ppm were broader compared to phenolic peaks in DTy. This is most likely due to slight differences in the phenols resulting from symmetry or lack thereof around the ester bond. In the FTIR spectrum, the differences in phenol were more evident with two distinct peaks around 3500 cm^{-1} with different intensities and broadness, whereas the DTy phenols were very similar in both wavenumber and intensity. The aromatic region from 700 – 900 cm^{-1} also show the presence of two sharp peaks in the HTy spectrum that are distinct

compared to in DTy spectrum, which has two peaks very close to each other. This data indicates that DTy exhibits pseudo 2,2 symmetry around the ester linkage while HTy has 1,2 asymmetry (Figure 3.29A). When observing the aromatic region of polymers in NMR, the coupling patterns are very similar weight two sets of doublets visible in each monomer. The chemical shifts for DTy are slightly upfield compared to HTy (Figure 3.29B-C) . This is most likely a result of the proximity of the aromatic hydrogens to the carbonyl oxygen.

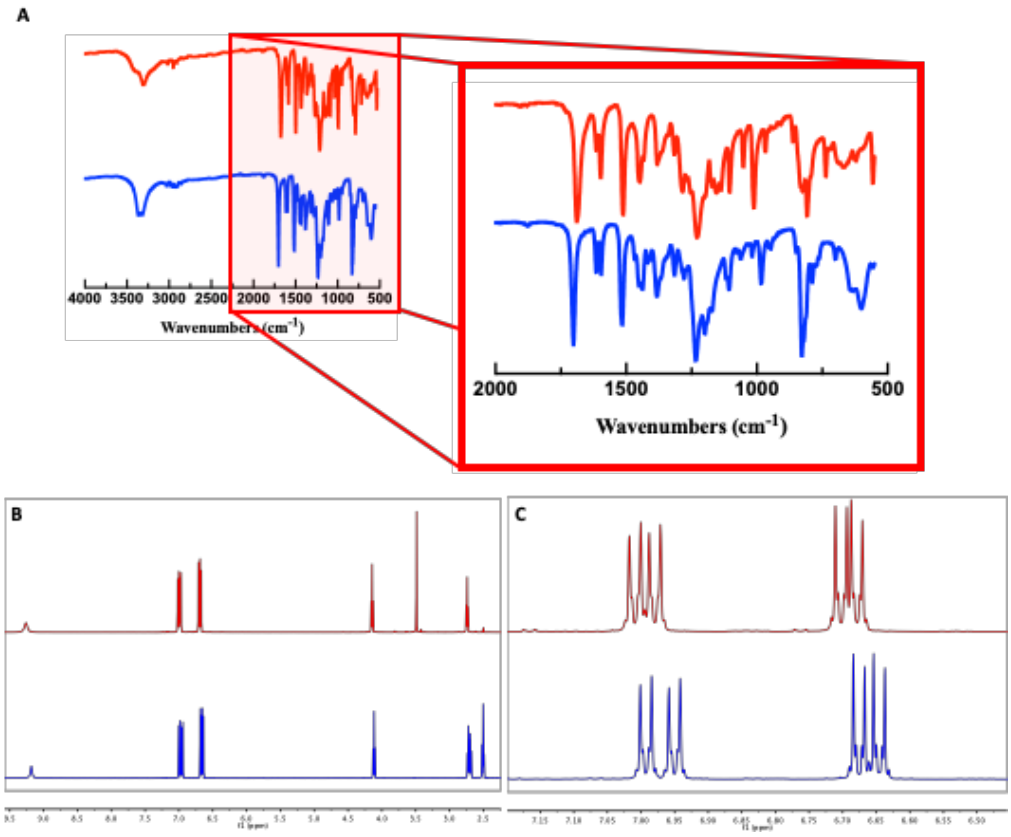

Figure 3.29. (A) FTIR and ^{1}H NMR of HTy (red) and DTy (blue) (B-C).

Symmetry is hypothesized to have an impact on the monomer and resulting polymer properties. One example of this was observed in the workup of the monomers. DTy precipitated upon cooling in toluene, allowing for faster removal of excess solvent

and more efficient purification measures while HTy preferred to stay as an oil. Additionally, the thermal properties of the diphenol themselves were characterized. HTy, had a lower melting temperature, 94.5 °C, compared to the "pseudo-symmetric" DTy, 124.8 °C (Figure 3.30). Likewise, upon cooling and then reheating, HTy did not recrystallize and showed a glass transition temperature while DTy crystallized and subsequently melted.

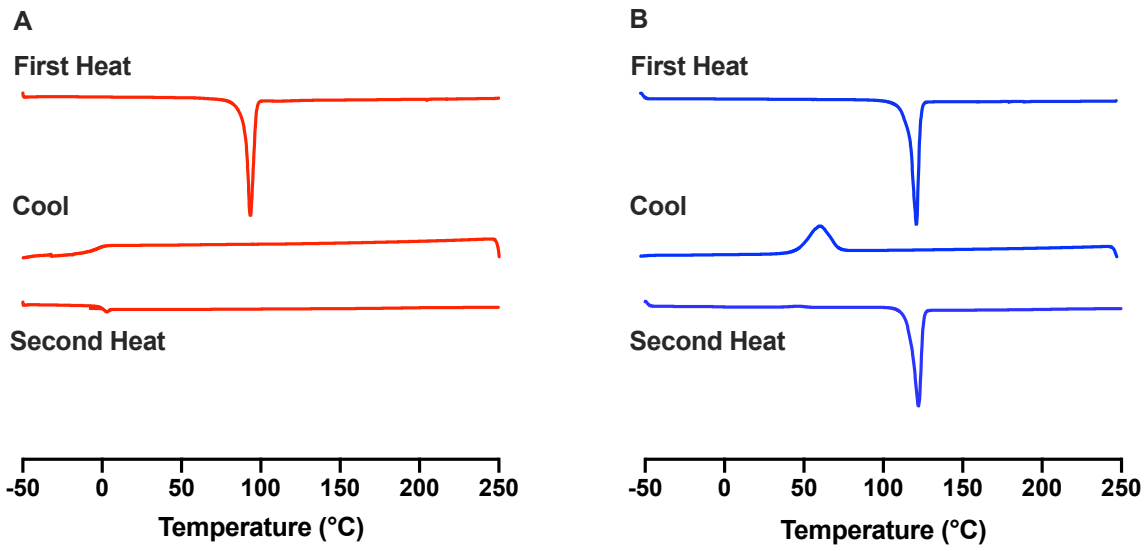

Figure 3.30. DSC Thermograms of diphenols HTy (red, A) and DTy (blue, B) including both heating and cooling patterns.

3.4.3 Solubility of Diphenol Monomer Units and Diacids

Once monomers were synthesized, an initial solubility study was performed to test whether or not the resulting polymers will be faster resorbing compared to those designed with tyrosine. The hypothesized degradation pathway for these polymers starts with hydrolysis of the arylate bond, which is an activated ester due to the electron donating of

the aromatic ring. Cleavage of that bond leads to the formation of the diphenol (DTy or HTy) and the diacid. The diphenol can then further degrade into the acid-phenol (HPAA or DAT) and tyrosol (Scheme 3.31). Alternatively, albeit less expected, the aliphatic ester can degrade first followed by the arylate bond, resulting in the same byproducts. For the purposes of these studies, we will evaluate solubilities of the degradation products from the former pathway. A benefit of tyrosol-derived polymers is their ability to degrade into their starting materials compared to PLA, PGA, and PCL, which degrade into lactic acid, glycolic acid and caprolactic acid, respectively.

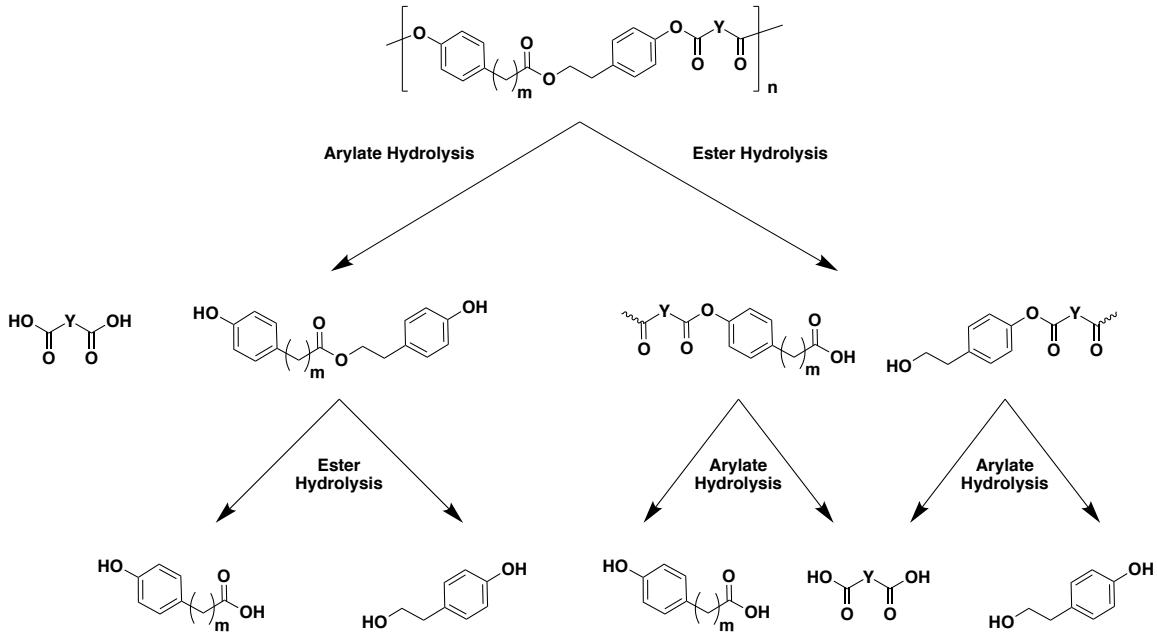

Scheme 3.31. Hypothesized schematic of degradation pathways.

In order to measure solubility, standard calibration curves were made for all the hypothesized degradation products using known concentrations. An HPLC method was then developed and used to plot area under the curve (AUC) against concentration.

Saturated solutions of each compound were prepared of each compound and incubated at 37 °C with shaking for 24 hours. Supernatant was analyzed by HPLC to determine a solubility limit. These values were compared to controls reported in the literature including tyrosine-derived DTE, as well as commercially relevant lactic acid and glycolic acid.

Overall it was found that the novel diphenol monomers have higher solubility than tyrosine diphenols, suggesting faster resorption that was independent of further hydrolysis of the aliphatic ester. Once the aliphatic ester was cleaved, solubility was increased even more and faster resorption would be expected. Though lactic acid and glycolic acid have significantly higher solubility in water at 100 mg/mL and 600 mg/mL, respectively, they can cause high concentrations of local acidity. It was found that DTy was the most hydrophobic compound with a solubility of 0.36 mg/mL compared to HTy with a solubility of 1.89 mg/mL (Table 3.2). This is comparatively better than tyrosine derived DTE compound which has a solubility of 0.03 mg/mL.

Table 3.2. Solubility studies and calculations for monomers and expected degradation products from the diphenol.

Compound	Calibration Curve	AUC	Dilution Factor	Solubility at 37 °C in PBS (mg/mL)
DTy	18.65x + 3.18	681	1:10	0.36
HTy	23.15x + 40.39	2776.1	1:16	1.89
DAT	23.64x + 8.10	839.6	1:1000	35.2
HPAA	22.94x + 6.75	1232.5	1:1000	53.4
Tyrosol	27.61x + 13.40	1284.6	1:1000	46.0

Additionally, the solubility of diacids used must be considered to ensure that the polymer remains resorbable. There is an odd-even effect with the diacid and its solubility.[99] Shorter chains and diacids with an odd number of carbons are much more soluble than the those with even numbers and long chains. Rigidity also led to increased hydrophobicity and limited solubility (Table 3.3). Another key point to note is the acidity of the degradation components. Comparatively, degradation components in tyrosol polyesters have higher pKa, and are therefore less acidic then the products of commercially available materials like PLA and PGA. Non-acidic degradation avoids a drop in local pH to the device implant site during later stages of degradation.

Table 3.3. pKa and Solubility data for predicted degradation products.

Compound	pKa[a]	Solubility (mg/mL)
Lactic acid	3.86[100]	1000[c]
Glycolic acid	3.53[c]	608[c]
Succinic acid	4.21[c]	88[101]
Glutaric acid	4.34[c]	1160[101]
Suberic acid	4.15[c]	2.46[102]
Dodecanedioic acid	4.65[c]	0.04[c]
4-Hydroxyphenylacetic acid	4.8[103]	60.7[d]
Desaminotyrosine	6.5[103]	2.7[d]
Tyrosol	10.0[104]	25.3[d]
HTy	9.81[b]	1.76[d]
DTy	9.91[b]	0.6[d]

[a]Based on the strongest acid, [b]Based on predictive values, [c]Based on values found on Human Metabolome Database or Drug Bank Database [d]Based on experimental data in PBS at 37 °C.

3.4.6 Biocompatibility of Polymer Byproducts

Another key component to the design of new polymers is assuring that when degraded, the products will be non-cytotoxic. A specific guideline, denoted as ISO 10995:3 focuses on *in vitro* biocompatibility studies. First, all monomeric components including HTy, DTy, tyrosol, HPAA, DAT were evaluated to determine if there was toxicity at any concentration. Per the ISO guidelines, predicted degradation byproducts were dissolved in culture media at a concentration close to the solubility limit. Serial dilutions were completed to identify concentrations in which a toxic response, or loss of at least 50% cell viability was observed. In all, it was determined that DTy was non-cytotoxic above 0.25 mg/mL which was the tested limit for this study. HTy had a lower value at 0.11 mg/mL but some of which is most likely a result of residual solvents present. As expected all other reagents were deemed suitable at concentrations over 1 mg/mL (Figure 3.32). Based on these results, it is expected that these polymers will not cause a toxic response during the degradation process.

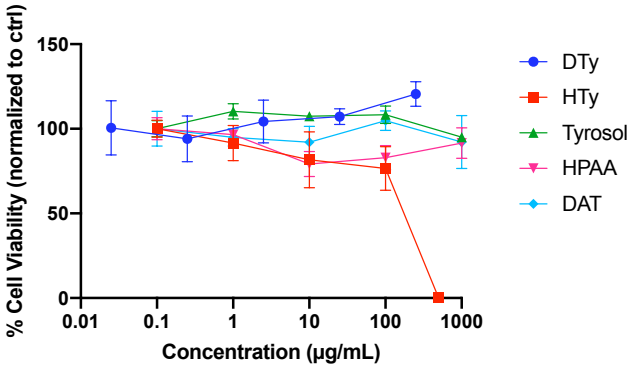

Figure 3.32. Cytotoxicity of degradation components for tyrosol-derived polymers.

3.4.2 Synthesis of Polymers and Reaction Kinetics

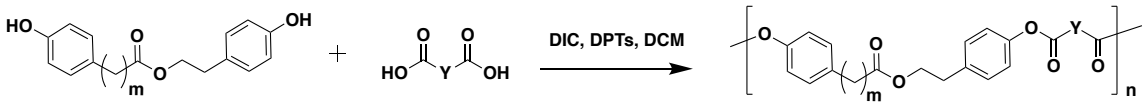

Scheme 3.33. Reaction schematic for tyrosol-derived poly(ester-arylate)s.

Table 3.4. Nomenclature reference for tyrosol-derived polymers based on Scheme 3.33.

Polymer	Index	m	Y
poly(HTy succinate)	pHTy2	1	$-(CH_2)_2-$
poly(HTy glutarate)	pHTy3	1	$-(CH_2)_3-$
poly(HTy suberate)	pHTy6	1	$-(CH_2)_6-$
poly(HTy dodecanedioate)	pHTy10	1	$-(CH_2)_{10}-$
poly(HTy diglycolate)	pHTyDG	1	$-CH_2-O-CH_2-$
poly(HTy transhexendioate)	pHTytHex	1	$-CH_2-CH=CH-CH_2-$
poly(HTy phenylenediacetate)	pHTyPDA	1	$-CH_2-Ar-CH_2-$
poly(DTy succinate)	pDTy2	2	$-(CH_2)_2-$
poly(DTy glutarate)	pDTy3	2	$-(CH_2)_3-$
poly(DTy suberate)	pDTy6	2	$-(CH_2)_6-$
poly(DTy dodecanedioate)	pDTy10	2	$-(CH_2)_{10}-$
poly(DTy diglycolate)	pDTyDG	2	$-CH_2-O-CH_2-$
poly(DTy transhexendioate)	pDTytHex	2	$-CH_2-CH=CH-CH_2-$
poly(DTy phenylenediacetate)	pDTyPDA	2	$-CH_2-Ar-CH_2-$

Subsequent polymerization of the diphenol with varying diacid structures was completed using carbodiimide chemistry (Scheme 3.30). All polymerizations used DIC as a catalyst due to its ability to work in chlorinated solvents required for polymer solubility and easier removal compared to DCC. Diacids including aliphatic carbon chains, alkenes, heteroatoms, aromatic rings, and saturated rings were investigated (Table 3.4). One of the main drawbacks to this method of synthesis is the formation of water in the reaction vessel. While this can lead to molecular weight inhibition and ultimately, degradation of the polymer through hydrolysis, the trace water did not hinder molecular weight growth.

Kinetically, molecular weight growth over time was largely dependent on the type of diacid in the polymer (Figure 3.31). Shorter chain diacids like glutarate-containing copolymers took several days to reach higher molecular weights compared to the longer chain diacids like suberate and dodecanedioate-containing copolymers which took hours. Additionally, succinate copolymers exhibited lower obtainable molecular weights with the DTy copolymer only reaching a DP of ~80 after one week. It is hypothesized that this is due to symmetry within the polymer chains, increasing intermolecular interactions and resulting in precipitation out of solution.

Bond rigidity has minimal effect on the rate of polymer molecular weight growth, with alkene-containing copolymers having comparable rates to aromatic bond-containing ones. Diglycolate copolymers were also limited in molecular weight growth, most likely due to poor solubility of diacid in the reaction solvent, methylene chloride. Polydispersities of the resulting polymers were slightly lower than 2.3, which is the theoretical polycondensation PDI, most likely a result of fractionation during precipitation.

When comparing bond rigidity's impact on molecular weight growth rates, early time points were largely unaffected. Heteroatom containing diglycolic acid, double bond containing transhexenedioic acid, saturated ring containing cyclohexanedicarboxylic acid, and aromatic containing phenylenediacetic acid, were all compared. Polymers containing both double bond and aromatic diacids exhibited molecular weight growth comparable to those with long chain diacids. Conversely, polymers with cyclohexane- or oxygen-containing diacids were considerably slower, only reaching a DP of about 75 after one week. This is most likely a result of steric hindrance and solubility, respectively.

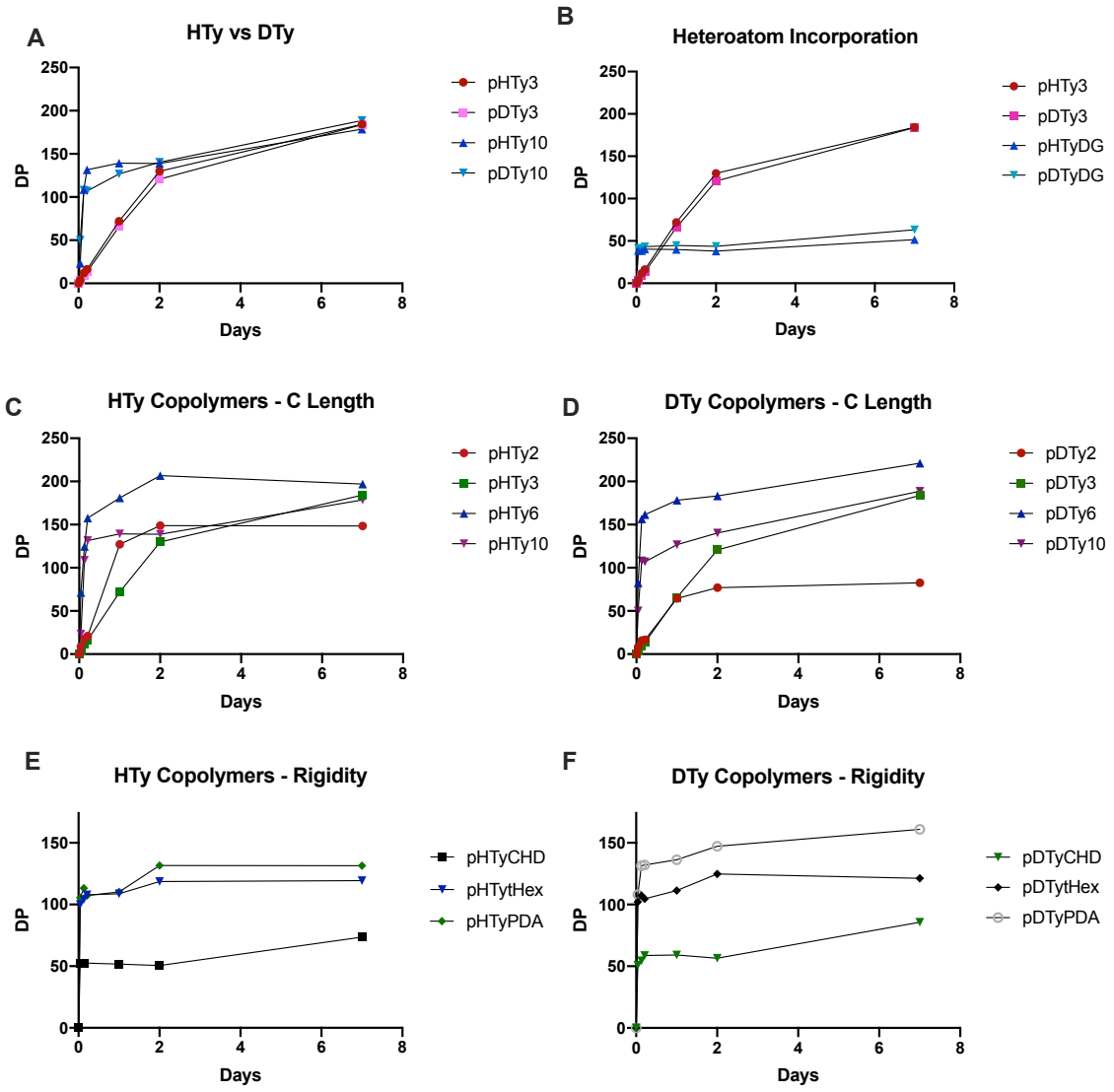

Figure 3.31. Kinetic studies comparing (A) diphenols, (B-C) diacid chain length, (D-E) bond rigidity, and (F) heteroatom incorporation. All reactions used a molar ratio of 0.98:1 diacid:diphenol.

Table 3.5. Molecular weights obtained of polymer compositions.

Index	Mn[a] (kDa)	Mw[a] (kDa)	PDI	Index	Mn[a] (kDa)	Mw[a] (kDa)	PDI
pHTy2	95.0	175.4	1.8	pDTy2	25.2	37.6	1.5
pHTy3	90.9	157.6	1.7	pDTy3	83.6	177.8	2.1
pHTy6	95.5	184.8	1.9	pDTy6	77.5	138.4	1.8
pHTy10	104.9	191.0	1.8	pDTy10	89.7	184.5	2.1
pHTytHex	80.1	153.6	1.9	pDTytHex	74.2	156.8	2.1
pHTyDG[b]	9.5	23.5	2.4	pDTyDG	55.0	89.4	1.6
pHTyPDA	82.3	156.0	1.9	pDTyPDA	83.0	192.3	2.3

[a] All values were measured relative to polystyrene standards in chloroform with 0.1% trifluoroacetic acid, [b] GPC values are prior to precipitation due to low molecular weights achieved.

By varying the ratio of diacid to diphenol between 0.97 and 0.99, molecular weights of 150 kDa were obtained for most polymers *via* GPC using polystyrene standards (Table 3.5). One important note is that GPC measures hydrodynamic volume, which is solvent dependent and can cause values to change slightly. As previously detailed, pDTy2, pHTyDG, and pDTyDG were the exception to this. GPC curve shape can help identify the distribution of molecular weights in the polymers. Molecular weights were normalized to polystyrene calibration standards due to similarities from the aromatic rings. All curves looked relatively similar with representative ones presented in Figure 3.32. Slight shouldering was observed but all PDI's stayed at or below 2.3 which is the expected polydispersity for a polycondensation reaction. The exception to this was pHTyDG which was due to lack of polymerization, only forming oligomers.

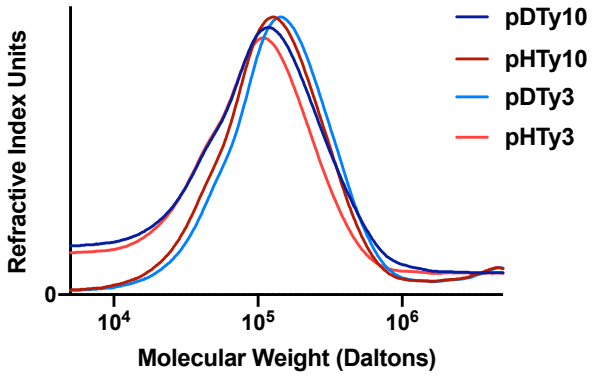

Figure 3.32. Representative GPC curves of tyrosol-derived poly(ester-arylate)s.

Chemical composition was confirmed *via* ^{1}H NMR and FTIR. Characteristic NMR peaks indicating reactivity were from 2.5 – 2.75 ppm corresponding to the methylene protons next to the arylate bond. Methylene peaks at 1.25 ppm, corresponding to aliphatic diacids (Figure 3.33A-B), alkene methines around 5.9 ppm for tHex polymers, and an aromatic peak around 7.4 ppm for PDA polymers were used to confirm incorporation of the diacid (Figure 3.33C). "pseudo-symmetry" in DTy was confirmed by apparent triplets in the aromatic region indicating chemical similarity, while HTy containing polymers maintained distinct sets of doublets (Figure 3.33D).

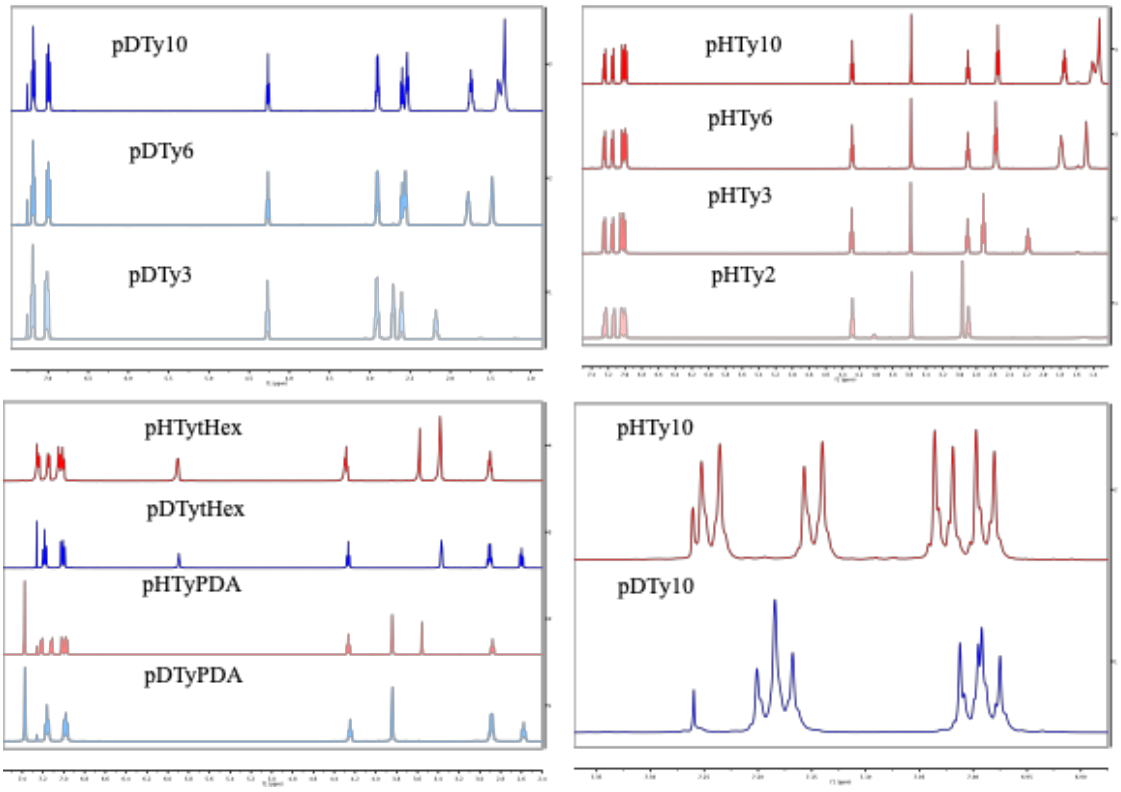

Figure 3.33. NMR spectrum of polymers with varying diacid chain length for HTy (A) and DTy (B) copolymers. Spectra with varying diacid ridgidity for HTy (C) and DTy (D) copolymers are presented.

FTIR was used to confirm structural features of the polymers (Figure 3.34). As expected, long aliphatic diacid containing polymers had the sharpest CH stretching peaks. All of the polymers contained carbonyl C=O stretch peaks around 1700 cm^{-1} indicative of the esters present in the polymers. The one major difference was the aromatic containing polymers contained two distinct carbonyl C=O stretches while all other polymers had C=O stretches that significantly overlapped with one another.

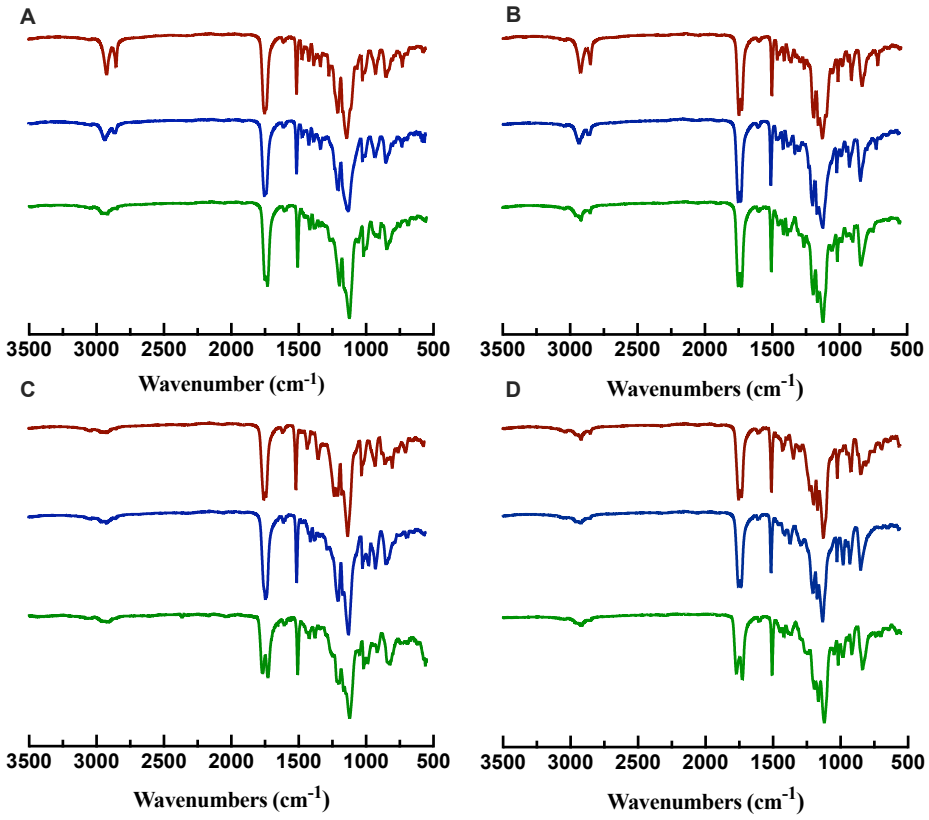

Figure 3.34. FTIR spectra of polymers with varying diacid chain length for HTy (A) and DTy (B) copolymers. Representative spectra of 10 carbons (top), 6 carbons (middle), and 3 carbons (bottom) are presented. Additional spectra with varying diacid ridgidity for HTy (C) and DTy (D) copolymers for oxygen (top), alkene (middle), and aromatic (bottom) containing groups are presented.

3.5 Conclusion

A new library of tyrosol-derived polymers was designed with improved solubility over tyrosine-derived polymers, less acidic degradation byproducts compared to PLA, PGA, and PLGA, and increased expected degradation compared to PCL. Synthetic methods for two tyrosol-derived diphenols, HTy and DTy synthesis were optimized by exploring stoichiometry, acid catalysts, and solvents in the reaction. Solubilities were characterized and confirmed to be over 10 times higher than the tyrosine diphenols previously reported in the literature. Monomers and their expected degradation byproducts were analyzed for cytotoxicity. None of the compounds elicited a severe toxic response confirming their validity as biomaterials. Subsequent polymerizations with the tyrosol diphenols and diacids with varying chemical structures were carried out successfully. Most polymers were easily obtained at molecular weights around 150 kDa by GPC. Three trends were explored in the design of the polymer library: (i) symmetry in the diphenol, (ii) diacid carbon chain length and (iii) diacid bond rigidity. Structure-property relationships were evaluated for chemical and degradative properties.

CHAPTER 4: EVALUATION OF STRUCTURE-PROPERTY-PROCESSING RELATIONSHIPS IN TYROSOL-DERIVED POLYARYLATES

4.1 Abstract

Tyrosol-derived poly(ester-arylate)s with tunable properties were explored and structure-property relationships established using both experimental and theoretical approaches. This data illustrates the wide range of properties attainable for these polymers through small compositional changes. Chemical properties including hydrophobicity, biocompatibility, and degradation were evaluated. Increasing the diacid chain length increased the polymer hydrophobicity, resulting in slower degradation rates. Polymers containing alkenes or aromatic rings degraded the fastest of any polymers. Diacids played a significant role in thermal properties, with glass transition temperatures and melting temperatures ranging from 4 °C to 45 °C and 80 °C to 200 °C, respectively. This was confirmed with modeling approaches to the thermal properties, specifically using mass-per-flexible bond approach and group contribution theory. Mechanical properties were tunable based primarily on diacids. Defined structure-property relationships were used in a case study to identify lead polymers for use as nerve guidance conduits. Braiding for the conduits required polymers with increased mechanical toughness. Processing of polymer films to orient polymer chains increased moduli as much as 3.5-fold. Polymer crystallinity was also characterized for several polymers and increasing chin-axis repeat units were largely dependent on diacid chain length. The properties identified establish a basis for a wide range of biomaterial applications that can utilize these resorbable polymers.

4.2 Introduction

Biomaterial applications range from tissue regeneration to sustained drug delivery, requiring a wide array of material properties. Specifically, biodegradable polymers require a balance between base properties, processing and device design, all of which contribute to the final device's behavior. Base properties are largely dependent on the chemical makeup of the material. Thermal and mechanical properties are impacted by intermolecular and intramolecular chain interactions, while chemical and biological responses are a result of the atomic composition. The balance between a multitude of parameters leads to large sets of data which are often not easily understood and complex to plot. As a result of the ongoing desire to understand large sets of data, the introduction of the omics era into biomaterials has taken place. Omics is the use of computational modeling and data arrays to understand a system in a fast and efficient manner. While this approach has been largely integrated into biological sciences including proteomics and genomics, it has been slower to implement in material design. The efficiency of data-driven models and predictive methods requires large amounts of experimental design with high precision and control of chemical or biological composition. While the omics approach will not be presented in this thesis, a simpler method using structure-property-relationships (SPR) will be assessed. This requires smaller experimental data sets and uses correlations to efficiently determine chemical implications in material properties.

Ideally, monomers and/or oligomers in a polymer can be incorporated to address specific properties including degradation, mechanical stiffness, and processability separately, to make a terpolymer (Figure 4.1). Each component would contribute as an independent additive characteristic. Unfortunately, many polymer properties are

intertwined and therefore can be challenging to decouple. For example, monomers that promote degradation will often limit thermal processability and the incorporation of bioactive molecules will limit solubility and maximum temperatures the material can be exposed to.

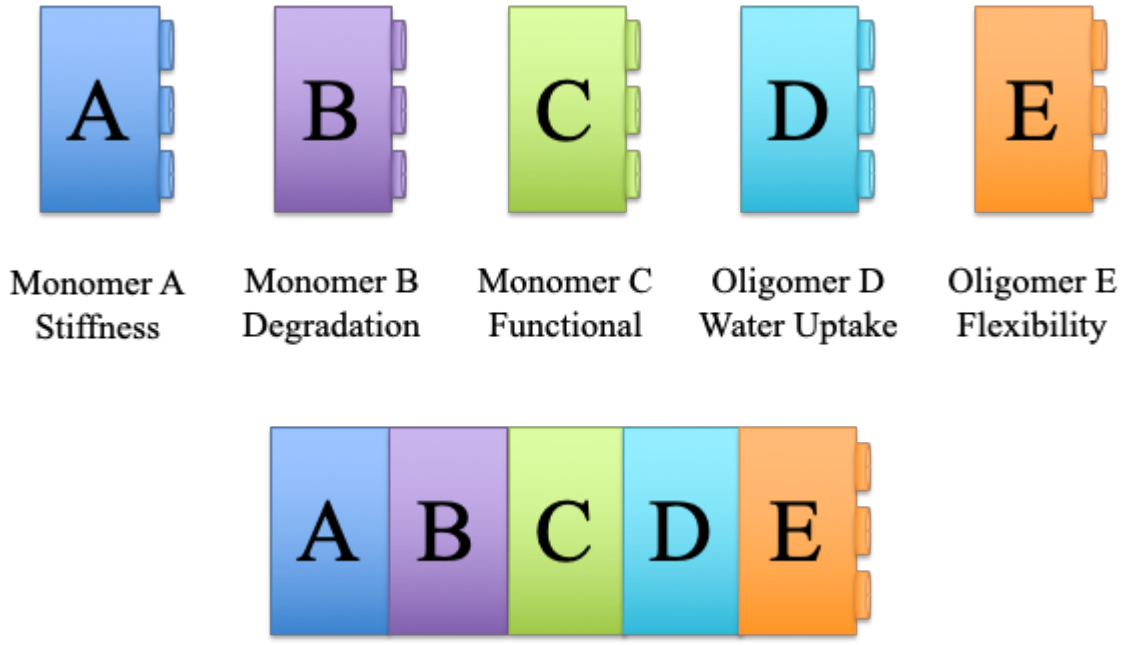

Figure 4.1. Idealistic interpretation of material design through combining different monomers and oligomers to match an application's required property profile.

Material properties are all interrelated and play a crucial role in the development of a new material (Figure 4.2). Hydrophobicity will dictate protein adhesion and diffusion of water into the polymer matrix while degradation and resorption rates will determine a material's application potential. Thermal properties help determine what processing techniques can be used. Many devices use thermal processes such as injection molding,

additive manufacturing, and extrusion, ideally performed just above the melting point of a material if present. Thermal processing allows for manipulation of the chain orientation of a polymer to increase the limits of a polymer's mechanical strength and crystallinity. Similarly, the mechanical properties of a material are largely dependent on the scaffold architecture, infill, and material's crystallinity. Mechanical properties need to match the desired application. Tensile and compressive properties are required for different applications depending if the injury site is load bearing or not.

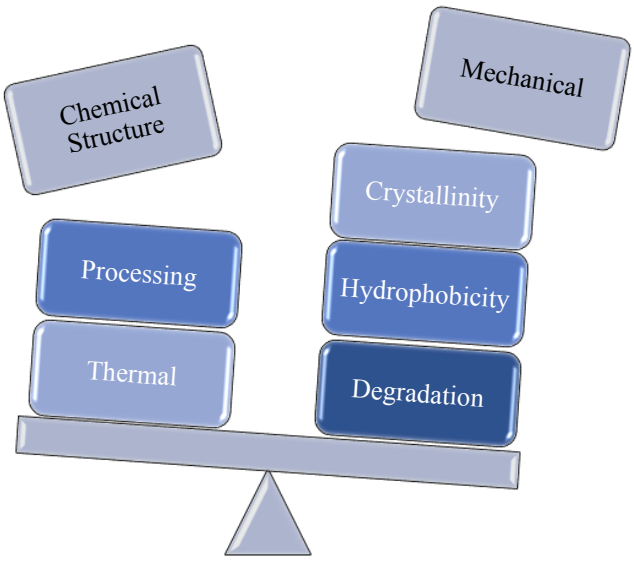

Figure 4.2 Balance of material properties.

One comparable material library that has been investigated using structure property relationships is copolymers of lactide and glycolide. Poly(lactic acid) (PLA) has been extensively used in biomaterial applications and is a man component in several FDA-approved devices including sutures, ligatures, and meshes.[105, 106] These can be used in surgical procedures and can often incorporate active pharmaceutical ingredients (APIs) to further aid the healing process. Poly(lactide-co-glycolide) (PLGA) copolymers are a

combination of lactic acid and glycolic acid, which are both naturally derived, on the FDA generally regarded as safe (GRAS) list, and found in the body. They are synthesized using ring opening polymerization and scalable. SPR of the copolymers has found that these polymers are semicrystalline and can range between 0 % (amorphous) to 50 % crystallinity. This has a further impact on the mechanical properties and biodegradation time (Table 4.1).

Table 4.1. Polymer properties for copolymers of lactic acid and glycolic acid.

Polymer	Tg (°C)	Tm (°C)	% Crystallinity	E (GPa)	Biodegradation Time (months)	Reference
PLLA	64	173	37	2.7	12-18	46, 107
PLGA (85:15)	57	140	Amorphous	2.0	5-6	46, 108
PLGA (72:25)	50	N/A	Amorphous	2.0	4-5	46, 109
PLGA (50:50)	31	N/A	Amorphous	2.0	1-2	46, 107
PGA	42	224	45-55	7.0	6-12	46, 107, 110

Libraries that can drastically change material properties with minimal change in chemical composition are ideal within medical device development due to ease in FDA approval pathways. Alternatively, in polyesters, the dialcohol or diacid can be exchanged or slightly modified to dictate polymer properties. Herein, we investigate the compositional components of tyrosol-derived polyarylates for their effect on degradative, thermal and

mechanical properties. The relationships established are then used to identify lead polymer candidates for making nerve guidance braided conduits. Annealing and drawing of polymer films, impacting polymer crystallinity, was used to improve the mechanical toughness of the polymers. Preliminary *in vitro* cell studies using human Schwann cells (HSCs) specific to neural regeneration were performed.

4.3 Materials and Methods

4.3.1 Materials

All chemicals and reagents, previously defined, were purchased from TCI America (Portland, OH), Sigma Aldrich (St. Louis, MO), VWR (Radnor, PA) or Fisher Scientific (Waltham, MA). Human Schwann cells (HSC #1700) and culture medium were purchased from ScienCell Research Laboratory. Tissue culture treated polystyrene (TCP) flask, multi-well plates were purchased from VWR.

4.3.2 Computational Calculations of logP

LogP calculations were completed using MarvinView programming. Calculations were based on monomer repeat units without consideration for the end group functionality. Using the logP predictor plugin, logP for each polymer was reported.

4.3.3 Determination of Air-Water Contact Angle

Polymer coated coverslips were prepared by spin coating a 2 wt.% solution of polymer in dichloromethane. To a 12 mm diameter glass cover slip, 100 μL polymer solution was added and spun at 3000 rpm for 30 s. The samples were then dried for 48 hours under vacuum at 40 °C to remove solvent and prevent particulate build up. Air-water contact angles were measured using a goniometer (RameHart Model 100-00) following ASTM C813. In short, 40 μL reagent grade water was placed on the polymer surface. The angle of the droplet was measured in 3 drops per film and in 3 separate spin-coated films.

4.3.4 *In Vitro* Degradation of Polymers

Polymers were compression molded into films and 8 mm diameter discs were punched using 8 mm diameter biopsy punches. Samples were place in a 1.5 mL polypropylene tube with a cap and o-ring to prevent loss of moisture. Mass was collected prior to incubation and at predesignated time points. Samples were incubated in 1.5 mL PBS (pH 7.4) solution with 0.02 % sodium azide to prevent bacteria growth. At each time point, samples were removed in triplicate, washed 3 times with DI water to remove salts and then frozen and lyophilized. Samples were weighed post degradation to calculate mass retention and then analyzed by GPC to determine molecular weight retention. At designated time points, media of the samples was exchanged to ensure sink conditions throughout the study.

4.3.5 Thermal Properties of Polymers.

Differential scanning calorimetry (DSC, Mettler Toledo) was used to evaluate melting temperatures (T_m), glass transition temperatures (T_g), and crystallization temperatures (T_c) for monomers and/or polymers. Briefly, samples were run in a 5-step program that included heating from 25 °C to 250 °C at a rate of 10 °C/min, followed by a hold at 250 °C for 2 min, cooling to -50 °C at 10°C/min, a hold a -50 °C for 2 min, and then heating to 250 °C at 10 °C/min. T_g and T_m are reported on the second heat unless otherwise noted. Thermogravimetric analysis (TGA, TA Instruments) was used to measure volatiles and decomposition temperature (T_d). Volatiles were calculated by the step transition between 50 °C and 150 °C, while T_d was calculated by the step transition from the plateau regions prior to and after mass loss.

4.3.6 Mechanical testing of polymer samples.

Polymer films were made by compression molding polymer solids with 100 μm shims at 30 °C above their T_m or 50 °C above their T_g if no melt was observed. Samples were heated for 3 min with no pressure followed by 3 min with 3000 lbs force producing films with a thickness between 150 – 300 μm. Specimens were cut into 3 mm x 40 mm strips. Mechanical properties of polymers were collected on an MTS Systems Tester with a 100 N load cell and a 10 mm/min displacement rate. The elastic modulus was calculated from the slope of the tangent drawn at the linear portion of the stress-strain curve (between 0 % and 2 %). Strain was calculated based on the displacement between the grips from the initial position. All measurements were collected on a minimum of 3 specimens per sample.

4.3.7 Orientation and/or Crystallization of Polymer Films.

To induce crystallization, annealed (an) samples were placed in an oven at approximately 50 % between T_g and T_c for 2 hours. To orient polymer chains, drawn (dr) samples were prepared by straining polymers above their T_g to ~50 % prior to break. Samples that were annealed post drawing (dr, an) were placed in an oven at 50 % between T_g and T_c in a constrained device to prevent shrinkage.

4.3.8 X-Ray Diffraction

1D wide-angle X-ray diffraction (WAXD) patterns from unoriented films were obtained in parafocus mode on a Xpert diffractometer (Malvern Panalytical, United Kingdom). 2D WAXD patterns from oriented films were collected in transmission geometry using an AXSs Hi-Star multiwire area detector Bruker (Billerica, MA). Nickel filtered copper radiation (Cu Kα, λ = 1.542 Å) was used in both instances. The 2D patterns were processed using the manufacturer's GADDS software to obtain 1D radially averaged scans, as well as equatorial, meridional and azimuthal scans. The radially averaged scans were profile fitted using MDI software to obtain the crystallinity and crystallite size using published methods. Azimuthal scans were used to determine the degree of orientation.64 Position of the peaks in the meridional scans were used to calculate the repeat distance along the stretch direction, which based on the equatorial scans and the total 2D pattern corresponds to chain-axis repeat.

4.3.9 Cell Adhesion and Proliferation Assays

HSC were cultured and maintained following the manufacturer's instructions. 10 mm/disc of polymer films were sterilized under UV for 1 h. Polymer films were placed in the wells of non-tissue culture treated 48-well plate and held in place by O-rings. Cells were trypsinized from an 80% confluent culture and counted. $2x10^4$ cells were added to each well containing polymer film and incubated at 37°C with 5% CO_2 and 95% humidity. After 24 h, medium was removed from each well and cells were washed once with PBS. 0.2 mL of medium containing 10% alamarBlue was added to each well. After incubated at 37°C for 45 min, the fluorescent intensity was read using TECAN Spark plate reader with Ex/Em=540nm/590nm. After the assay, cells were washed with PBS twice and continued to culture for 3 days. On Day 4, the viability of cells in each well was measured using alamarBlue assay. Repeat the viability measurement on Day 7. The proliferation of cells on Day 4 or Day 7 on each polymer surface was normalized to that of Day 1.

4.4 Results and Discussions

4.4.1 Degradation and Resorption

4.4.1.1 Hydrophobicity of Polymers

The hydrophobicity of a polymer acts as a predictor of polymer degradation rates, controlling diffusion of water into the polymer matrix. Two ways to measure this include computational modeling of monomer units to calculate the logP or experimentally measured air-water contact angles which look at the surface properties of polymers. LogP of the repeat unit increases with increasing chain length. This indicates the hydrophobic nature of long chain diacids versus the shorter chains. Oxygen-containing diglycolate

copolymers had the lowest logP which matched expectations due its polar ether group, and increasing rigidity resulted in increasing hydrophobicity, most likely due to steric effects (Figure 4.3).

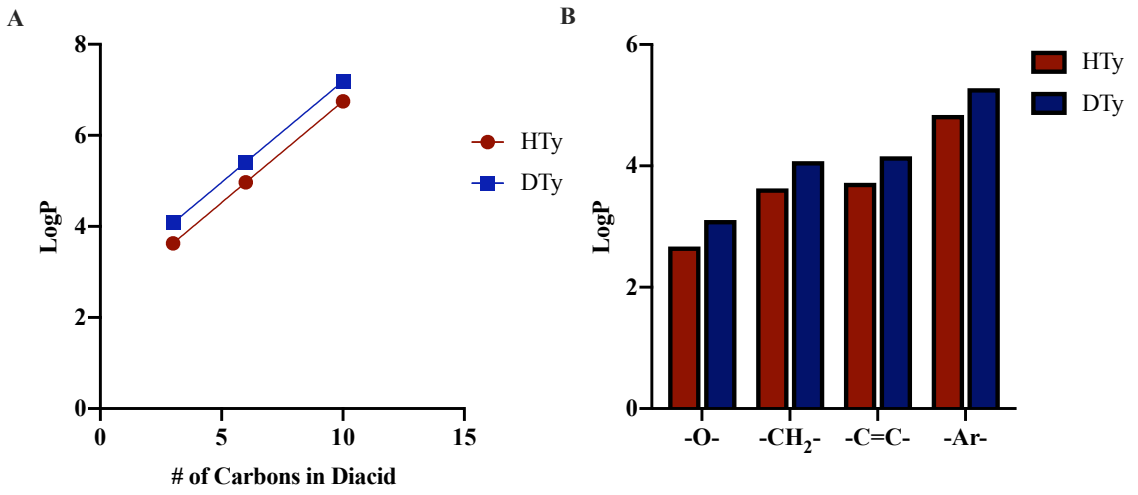

Figure 4.3. Calculated LogP of polymer repeat unit.

An experimental method for measuring polymer hydrophobicity is the use of air-water contact angle. By looking at a drop of water on the polymer surface, hydrophobicity can be evaluated. For hydrophobic materials, the drop of water will ball up and the angle will be greater than 90°. On the contrary, hydrophilic materials have lower angles, typically below 45° (Figure 4.4).

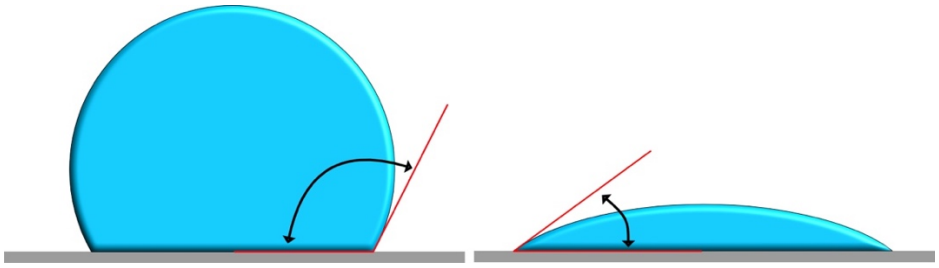

Figure 4.4. Schematic of air-water contact angle measurements with illustrated droplets on hydrophobic (left) and hydrophilic (right) surfaces. Angles are represented by arrows and show that those greater than 90° are hydrophobic whereas less than 90° are hydrophilic.

All polymers were moderately hydrophobic due to the presence of aromatic ring in the diphenol. Diacid chain length had the largest impact on changes in polymer hydrophobicity. As expected, increasing chain length resulted in more hydrophobicity, albeit only over a 15 ° range. Interestingly, bond rigidity had minimal impact on the hydrophobicity of the polymer (Figure 3.36B). When comparing the slopes of DTy and HTy copolymers with linear chain diacids, 1.086 and 0.539 respectively, DTy copolymers were more sensitive to changes in the diacid chain length (Figure 3.36A). Another expected trend in hydrophobicity is the incorporation of an ether bond in the diacid (glutarate vs. diglycolate). The oxygen promotes hydrogen bonding and helps bring water into the polymer matrix. This results in a drop in contact angle from 75 ° to 70 °. When comparing the LogP and AWCA there was a weak correlation between the two with better fit for more hydrophilic polymers (Figure 4.6).

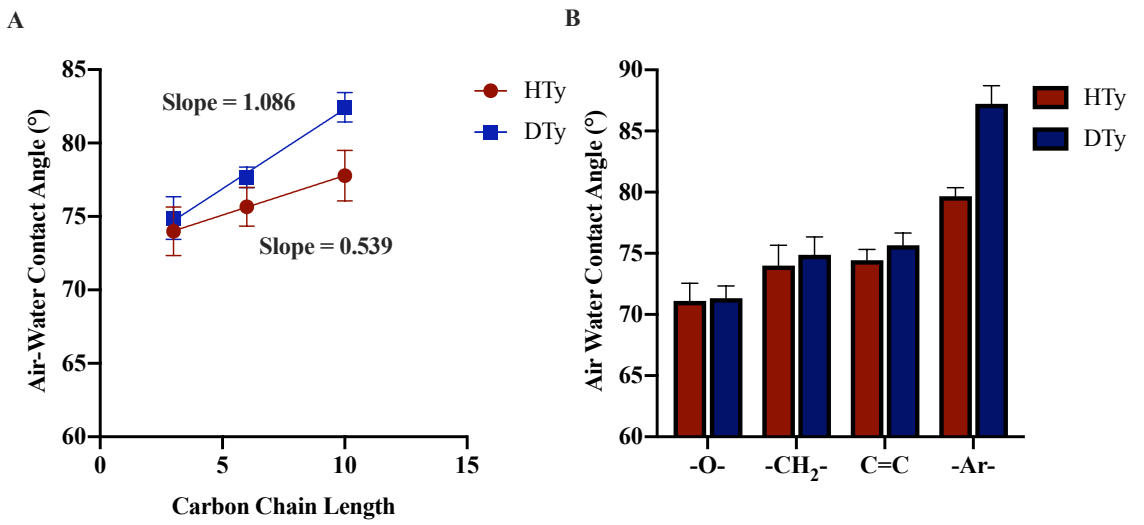

Figure 4.5. Polymer hydrophobicity using air-water contact angle measurements investigating (A) carbon chain length and (B) bond rigidity.

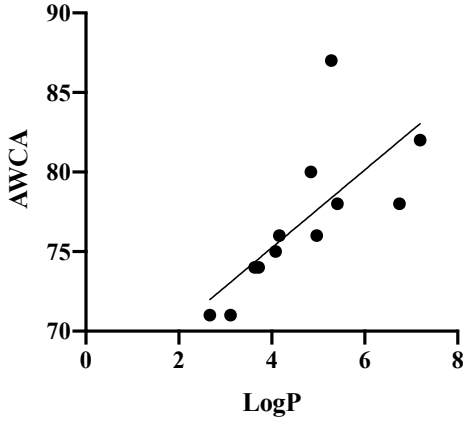

Figure 4.6. Correlation between experimental and theoretical hydrophobicity data.

4.4.1.2 *In Vitro* Degradation Under Physiological Conditions

In vitro degradation studies were carried out under physiological conditions and number average and weight average molecular weight retention were calculated. Additionally, mass retention was measured over time to understand the resorption profile of the polymers. Compared to commonly used PLA and tyrosine-derived poly(DTE-co-10%DT-co-1%PEG_{1K} carbonate) (E1001(1k)), these tyrosol polyarylates resorb at a faster rate. When comparing earlier time points, E1001 (1k) degraded at a slightly faster rate compared to pHTy3, most likely due to the presence of PEG. After 200 days, pHTy3 exhibited higher mass loss compared to E1001(1k) signaling faster resorption *in vitro* (Figure 4.7).

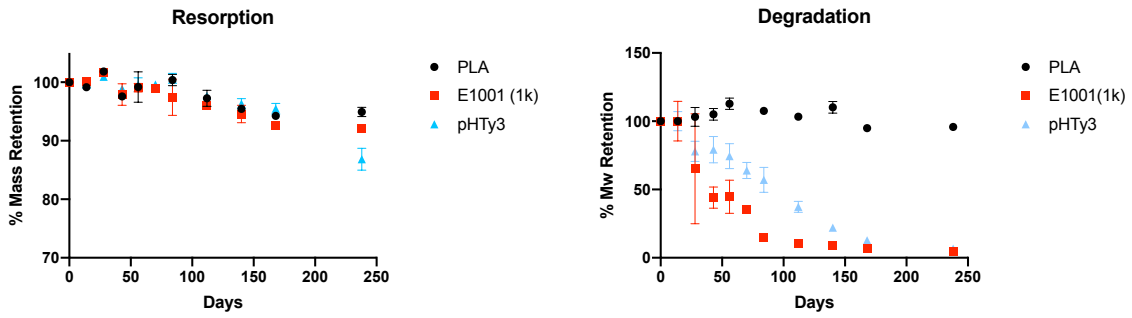

Figure 4.7. Degradation and resorption profiles of tyrosol polymer pHTy3 compared to commercial standard PLA and internal standard E1001(1k).

When comparing polymers within the tyrosol polyarylate library, all three trends investigated above played a role in the degradation and resorption. Increases in diacid chain length resulted in increased polymer hydrophobicity and slower degradation and resorption times. Inversely, shorter chain diacids were faster to degrade and resorb. One polymer,

poly(HTy succinate), did not follow this trend and was slower degrading, comparable to the longer chain diacids. This may be due to spatial distance between the bulky hydrophobic aromatic rings. Additionally, the copolymers with diacids containing double bonds or aromatic rings observed accelerated degradation and resorption. It is hypothesized that this is a result of the higher processing temperatures required to form compression molded films from these polymers, leading to degradation prior to incubation due to the presence of free acid end groups which could catalyze hydrolysis. Another important observation during this study was the appearance of the polymer discs. First, many of the HTy based polymers were clear to slightly cloudy upon starting the experiment. After 14 days almost, all polymers with the exception of pHTy2 had turned completely opaque and white. Some of the double bond containing polymers had a yellowish-brown tinge to them. The transhexenedioate containing polymers became extremely brittle after 2 months of incubation. This is most likely a result of the formation of low molecular weight oligomers. Comparatively, pHTy10 and pDTy10 maintained their form throughout the year duration of the study. All polymers towards the end of the study were opaque and held shape as a result of water-induced crystallization of the polymers.

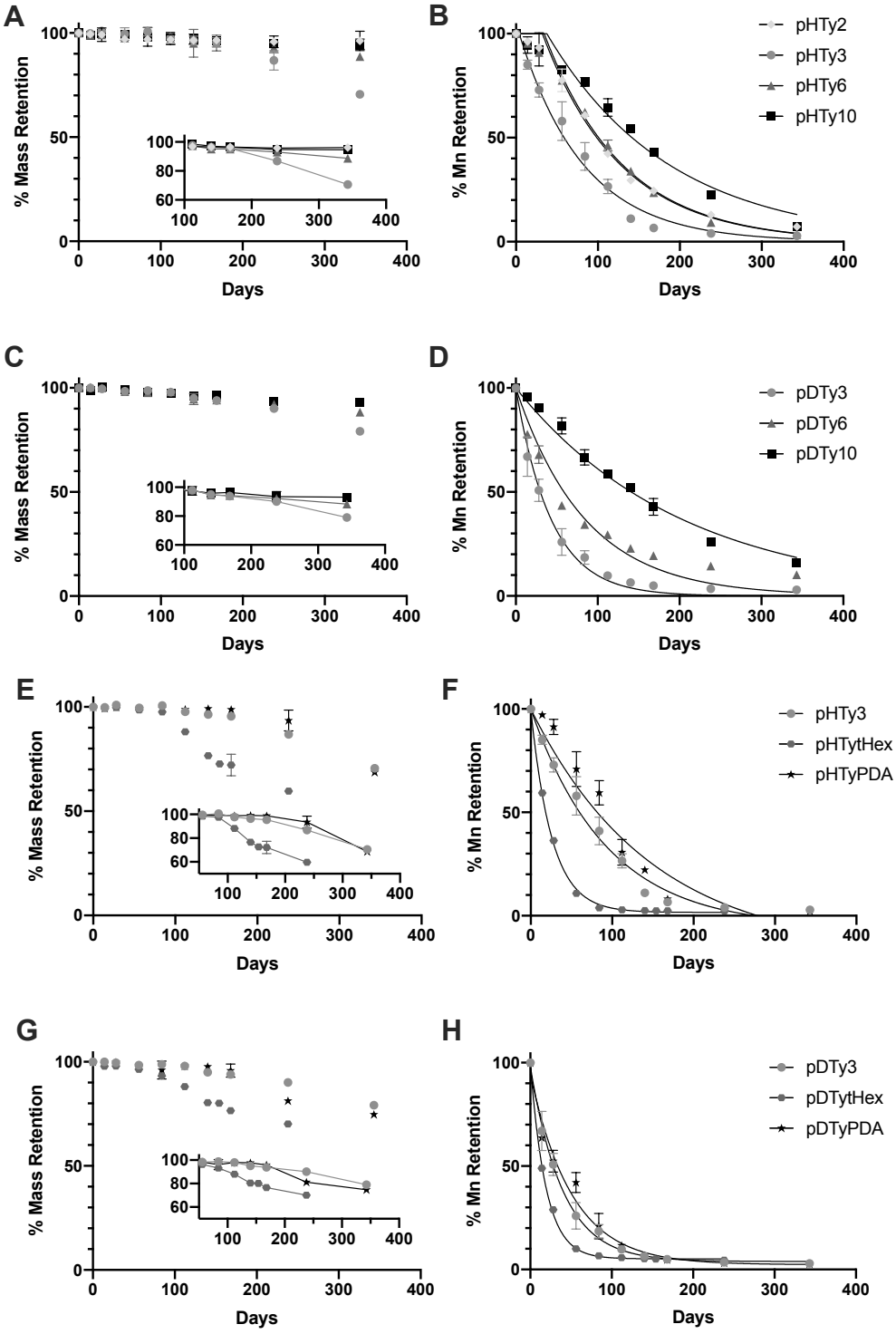

Figure 4.8. Degradation of polymers with varying (A-D) chain length and (E-H) bond rigidity. Degradation was determined by M_n retention and resorption by mass retention. All Studies Were Carried Out at 37 °C in PBS pH 7.4.

4.4.2 Thermal Properties

Tyrosol-derived polyarylates are classified as semi-crystalline polymers containing both amorphous and crystalline domains. Glass transition temperature measures amorphous region properties and is important to understand how the polymer will behave in a physiological environment or during processing. Melt temperatures will dictate under what conditions a polymer can be thermally processed. Having control over these parameters can aid in identifying polymers with unique properties, such as the ability to mold a material when handling due to increased temperature.

4.4.2.1 Experimental Thermal Properties

The glass transition temperature was found to be primarily dependent on the diacid in the backbone and less so dependent on the change from HTy to DTy. As expected, increasing the diacid chain length from 2 carbons to 10 carbons drastically reduced the T_g from 44 °C to 4 °C, respectively, due to increased chain flexibility (Figure 4.9A). Incorporating various chemical structures such as double bonds, ring structures, and aromatic groups leads to differing glass transitions (Figure 4.9B). Interestingly, slight modifications from a carbon to an oxygen led to an increase of 10 °C in glass transition temperature most likely as a result of electron density and electronegativity (Figure 4.9C). This phenomenon has been previously presented in copolymers of glutaric acid, diglycolic acid, and thiodiglycolic acid with aliphatic diols.[111]

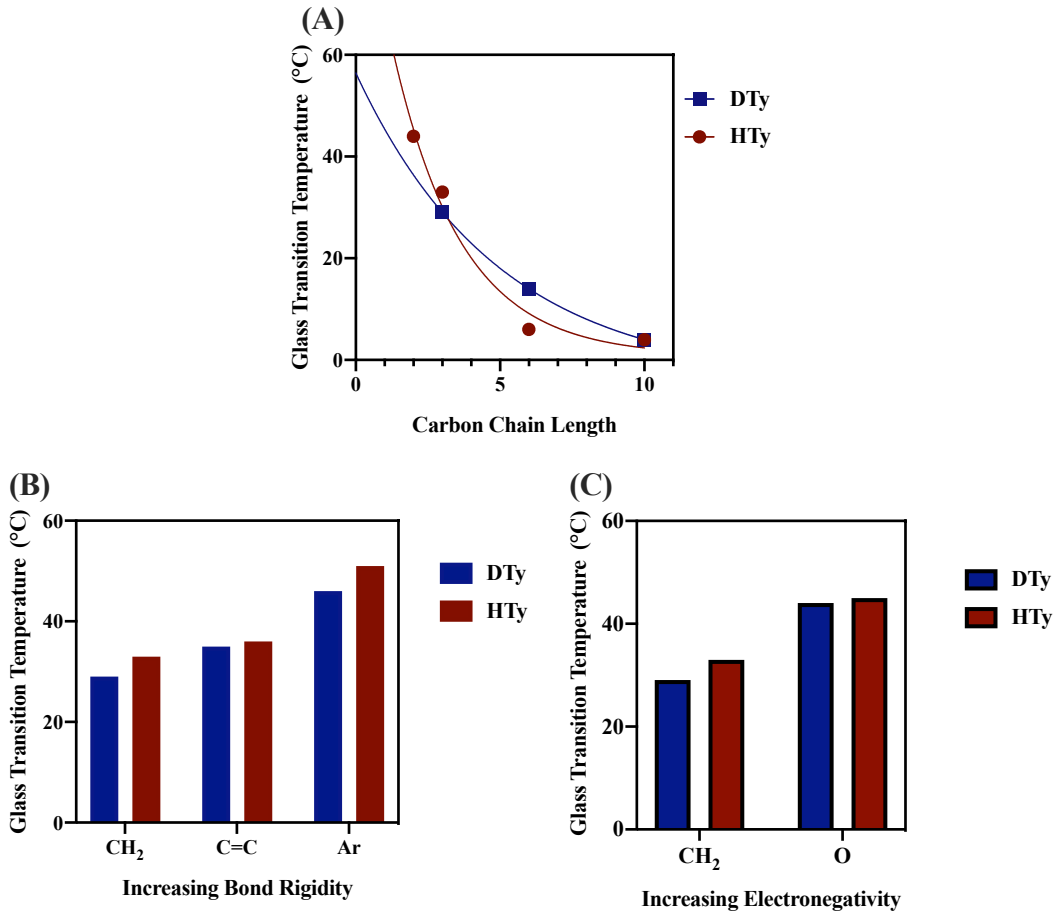

Figure 4.9. Glass transition temperature trends with changing (A) diacid chain length, (B) bond rigidity, and (C) electronegativity.

Along with glass transition temperatures, melting temperatures play a crucial role in biomaterial design. Many applications require thermally processed devices, including braided conduits, extruded rods, injection molded pins or screws, and 3D printed complex architectures. The difficulty with these processing methods is resulting thermal degradation that can occur. Ensuring the gap between melting temperature and decomposition temperature is large enough will help prevent changes in chemical structure as well as molecular weight loss. When comparing DTy and HTy copolymers, one noticeable trend

was that all of the DTy copolymers had higher melting temperatures than their HTy counterparts. This is hypothesized to be due to the "pseudosymmetry" in the molecular structure, resulting in tighter packing of the polymer chains and a more crystalline material. Another trend observed was a commonly reported odd-even effect (Figure 4.10A).[112] This indicates that polymers composed of diacids with an even number of carbons typically will have higher melting points and lower solubility due to packing. One deviation in this trend is pHTy3 which is higher than both pHTy2 and pHTy4. Some thermograms show a double melting peak. This is due to the presence of defects in crystal structure. Smaller crystals may form which lead to additional melting points. Bond rigidity did play a large role on the melting point of the polymers. Double bond containing polymers had lower melting temperatures than the carbon containing glutarates or aromatic containing phenylenediacetates (Figure 4.10B). All of these polymers have symmetry in the diacid which can help packing and lead to higher melting temperatures.

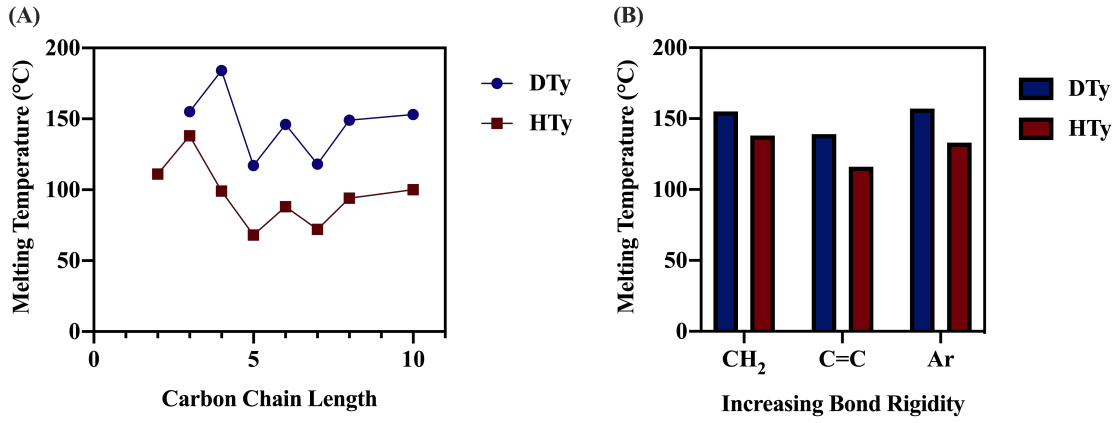

Figure 4.10. Melting temperatures of polymers with varying (A) carbon chain diacid length and (B) bond rigidity.

4.4.2.2 Modeling Thermal Properties

In addition to experimental data with drawn correlations, predictive models using approaches such as group contribution theory, molecular dynamics, and quantitative structure-property relationships (QSPR) can be employed. Thermal properties are the most common polymer property that can be predicted due to their large dependence on chemical structure. Previous work in the Kohn lab investigated the use of mass-per-flexible bond as a way to predict a polymer's glass transition temperature.[113] This semi-empirical approach compared the molecular weight of a repeat unit, the flexibility of bonds in a repeat unit, and measured T_g to find a correlation, obtaining linear fits with an R^2 greater than 0.900. Some of the key findings of this work were that: (i) aromatic rings have flexibility across the center of axis (ii) amides are not considered flexible due to resonance stability, and (iii) methyl groups and alcohols have no flexibility due to the small size of the hydrogen atoms.

Newly developed tyrosol-derived polyarylates were tested against this method. Upon evaluation, three categories were considered: flexibility of the diphenol, diacid chain length or rigidity, and intermolecular interactions. Figure 4.11A shows the assigned flexibility for tyrosol-derived diphenols and indicates small differences in mass-per-flexible bond value of 34.03 and 31.53 for HTy and DTy, respectively. For the poly(ester-arylate)s library, a small set of polymers were used with diacid extremes such as short, medium, or long aliphatic diacids, along with double bond and aromatic containing polymers for rigidity. Diglycolate polymers were not used as they have intermolecular interactions that interfere with the efficacy of the model. When plotting the M/f value against experimental glass transition temperatures in K, a correlation of 0.8864 was obtained (Figure 4.11). The one major deviation from the trendline was pHTy6.

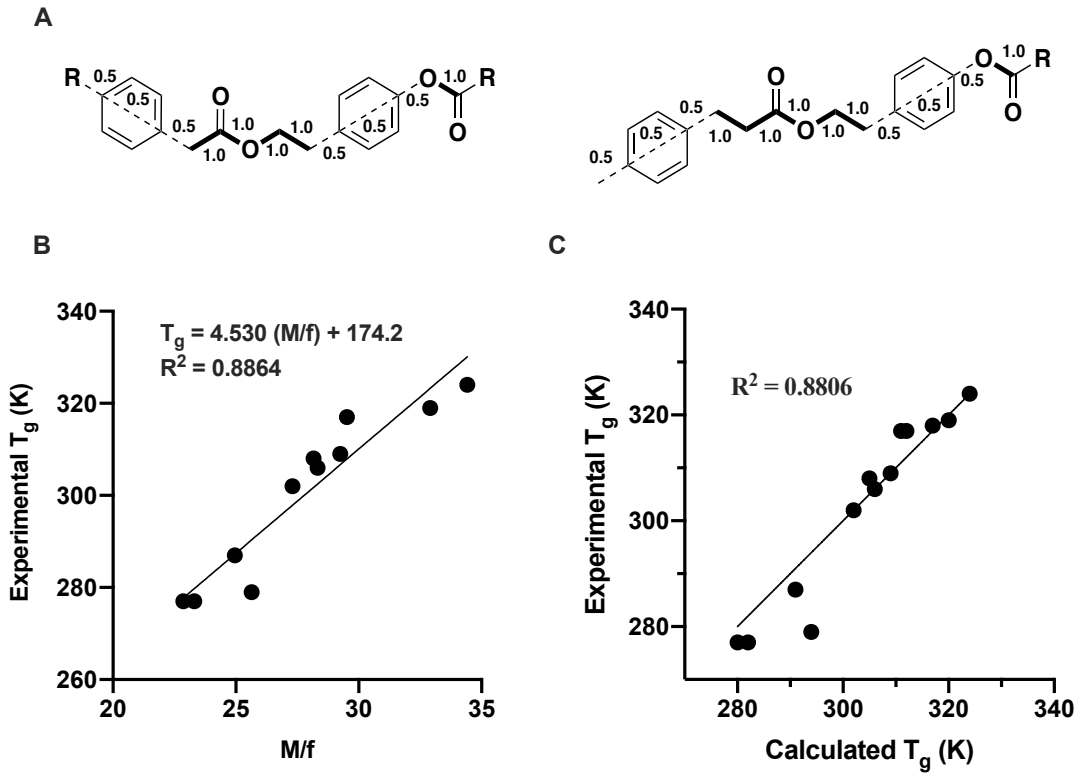

Figure 4.11. Mass-per-flexible bond calculations to predict glass tranisition temperature. (A) Flexibility indices for HTy (left) and DTy (right), (B) correlation between M/f and T_g, and (C) Correlation between predicted and experimental T_g.

Alternatively, group contribution theory can be used to predict polymer properties. This approach is more widely known and employs large experimental data sets for polymers and correlates their values to distinct chemical features. These features can then be correlated with mass of the repeat unit to calculate the T_g. Specifically, T_g (K) = 1000 * Yi / M where Yi is the sum of all group contribution factors in the repeat unit and M is the molar mass of the repeat unit. The benefit to this approach is the ability to predict properties without any experimental data. Goodness of fit can be performed by comparing experimental data to theoretical. This approach was used as a comparison to the previously

explained Mass-per-flexible bond theory. The small subset used in the previous approach was applied to GCT and theoretical values were compared (Table 4.2). Similarly, pHTy6 showed the highest error again. This potentially indicates a non-chemical interaction leading to the outliers.

Table 4.2. Group contribution theory additive data for determination of glass transition temperature.

Polymer	Diphenol		Diacid		Sum		Calc.	Exp.	%
	Yi	M	Yi	M	Yi	M	Tg (K)	Tg (K)	Error
pHTy2	79.6	238.2	30.4	116	110	354.2	311	317	2.03%
pHTy3	79.6	238.2	33.1	130	112.7	368.2	306	306	0.03%
pDTy3	82.3	252.2	33.1	130	115.4	382.2	302	302	0.02%
pHTy6	79.6	238.2	41.2	172	120.8	410.2	294	279	5.55%
pDTy6	82.3	252.2	41.2	172	123.5	424.2	291	287	1.44%
pHTy10	79.6	238.2	52	228	131.6	466.2	282	277	1.91%
pDTy10	82.3	252.2	52	228	134.3	480.2	280	277	0.97%
pHTyDG	79.6	238.2	37.6	132	117.2	370.2	317	318	0.44%
pDTyDG	82.3	252.2	37.6	132	119.9	384.2	312	317	1.55%
pHTytHex	79.6	238.2	37.8	142	117.4	380.2	309	309	0.07%
pDTytHex	82.3	252.2	37.8	142	120.1	394.2	305	308	1.08%
pHTyPDA	79.6	238.2	59.9	192.1	139.5	430.3	324	324	0.06%
pDTyPDA	82.3	252.2	59.9	192.1	142.2	444.3	320	319	0.33%

When comparing the two theories for calculating the glass transition temperature, they both are fairly successful with deviations coming from similar polymers. A plot of theoretical polymer glass transition temperatures to those that were experimentally found

indicated that the GCT theory was slightly better at predicting T_g than the MPF approach. This was determined by calculating the goodness of fit to the data assuming a correlation of Experimental T_g = Theoretical T_g (Figure 4.12).

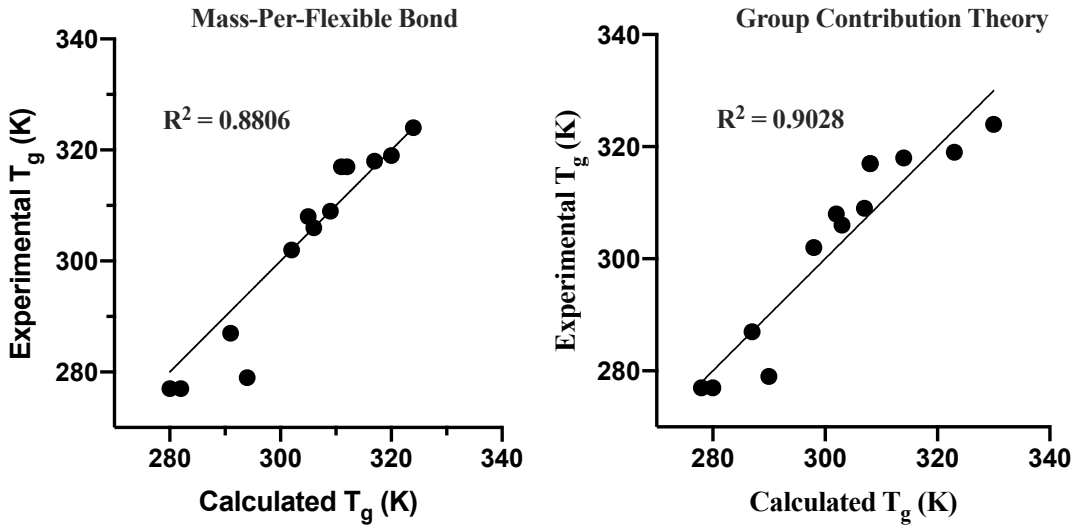

Figure 4.12. Comparison of calculated T_g versus experimental T_g for (left) mass-per-flexible bond and (right) group contribution theory approaches.

Additional properties can be modeled with GCT including melting temperature, tensile modulus, and density. The more a property is impacted by additional factors such as crystallinity and processing, the less efficient the model is. Modulus, for example was not appropriately predicted due to the ability of the polymer to reside in different phases. Semicrystalline polymers can be amorphous or crystalline, oriented or unoriented, all resulting in different properties as explained below. Melting temperature is another property that can be difficult to predict due to the impact of intermolecular chain interactions. When plotting the calculated values (Table 4.3) to the experimental values

(Figure 4.13), it was evident that the diglycolate polymers did not fit the model well. When removing that value, the goodness of fit goes from an $R^2 = 0.3011$ to 0.6211 (Figure 4.13). Additionally, pHTy3 is the next largest error which is expected due to deviation in the odd-even trend observed experimentally.

Table 4.3. Group contribution theory approach to predicting melting temperature.

Polymer	Diphenol		Diacid		Sum		Calc. Tm (K)	Exp. Tm (K)	% Error
	Yi	M	Yi	M	Yi	M			
pHTy2	84	238.2	52	116	136	354.2	384	384	0.01%
pHTy3	84	238.2	55	130	139	368.2	378	411	8.15%
pDTy3	105	252.2	55	130	160	382.2	419	428	2.19%
pHTy6	84	238.2	67.2	172	151.2	410.2	369	361	2.11%
pDTy6	105	252.2	67.2	172	172.2	424.2	406	419	3.12%
pHTy10	84	238.2	90	228	174	466.2	373	373	0.06%
pDTy10	105	252.2	90	228	195	480.2	406	426	4.68%
pHTyDG	84	238.2	72.4	132	156.4	370.2	422	359	17.68%
pDTyDG	105	252.2	72.4	132	177.4	384.2	462	444	4.00%
pHTytHex	84	238.2	63	142	147	380.2	387	389	0.61%
pDTytHex	105	252.2	63	142	168	394.2	426	412	3.44%
pHTyPDA	84	238.2	90	192.1	174	430.3	404	406	0.40%
pDTyPDA	105	252.2	90	192.1	195	444.3	439	430	2.07%

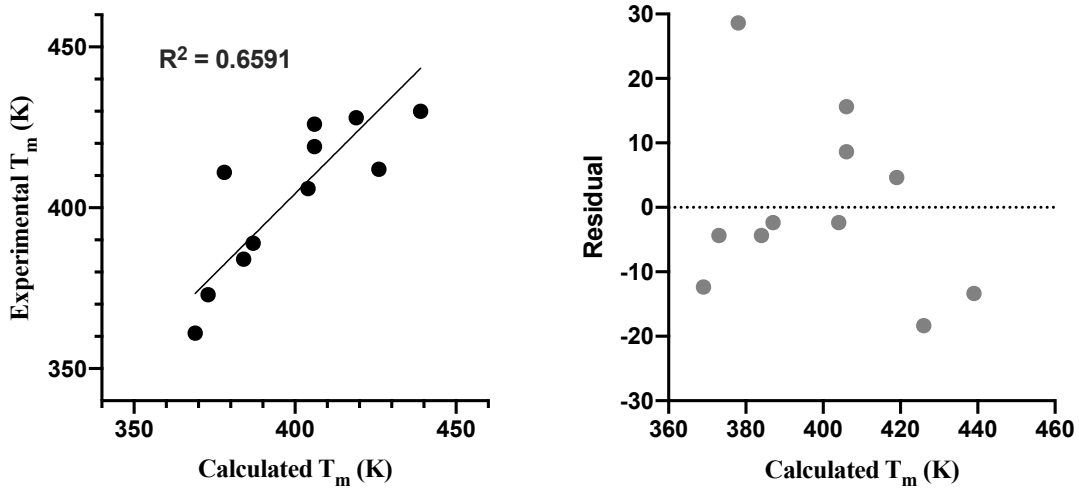

Figure 4.13. Melting temperature predictions based on GCT and the respective residual plot.

4.4.3 Mechanical Properties of Polymers

Tyrosol polyarylates as processed exhibit a wide range of properties with tensile moduli (E) ranging from 1100 MPa for short chain diacids down to 300 MPa for longer chains due to polymer flexibility. Likewise, their yield stress (σ_y) and strain (ε_y) can range from 1 to 22 MPa and 2 to 24 %, respectively (Table 4.4). One important note is that these polymers, being semicrystalline, can exhibit different mechanical properties depending on the form they are in. Polymers that are more crystalline can have higher moduli compared to their amorphous form. All polymers reported in Table 4.4 are quenched to minimize crystallization. Unfortunately, polymers containing DTy or long chain aliphatic diacids tend to crystallize rapidly and are more difficult to quench.

Table 4.4. Tensile properties for polymers as processed, most in the amorphous phase, n = 4 specimen per sample.

Polymer	*E*, (MPa)	σ_y (MPa)	ε_y (%)
pHTy2	1100 ± 130	21.6 ± 2.6	2.5 ± 0.7
pHTy3	1120 ± 60	15.5 ± 1.2	1.8 ± 0.3
pDTy3	1010 ± 100	14.5 ± 2.2	2.1 ± 0.3
pHTy6	7.00 ± 4.00	0.7 ± 0.4	23.8 ± 12.5
pDTy6	510 ± 20	12.4 ± 1.5	10.5 ± 0.8
pHTy10	280 ± 20	5.8 ± 0.5	6.5 ± 0.6
pDTy10	250 ± 20	6.6 ± 1.3	12.8 ± 2.8
pHTytHex	1420 ± 200	20.0 ± 1.2	1.9 ± 0.4
pDTytHex	450 ± 420	2.1 ± 2.4	1.4 ± 0.02
pHTyPDA	1340 ± 260	17.5 ± 3.1	1.8 ± 0.3
pDTyPDA	1740 ± 230	21.0 ± 7.5	2.1 ± 0.7

4.4.4 Case Study: Polymer Selection for Nerve Guidance Conduits

Peripheral nerve injuries are one of the more difficult regenerative processes to treat. Trauma to the nerve results in loss of motor and sensory functions causing vast patient complications.[114, 115] Formation of scar tissue in the defect space prevents axon growth from the proximal to distal stump inhibiting reconnection. Nerve guidance conduits provide a barrier to external factors such as fibroblasts, while also guiding axon growth across the gap.[116] Conduits also help retain growth factors secreted by axons at the nerve stump, accelerating regeneration. New materials that are biocompatible, resorbable, and mechanical robust are of extreme value to the nerve regeneration field and as such, tyrosol-derived poly(ester-arylate)s have been preliminarily explored.

Commercially available competitors NeuraGen® Nerve Guide and Neurotube® Device are nerve guidance conduits made of collagen and PGA, respectively. Both of these have limitations including weak mechanical properties or acidic degradation byproducts, as previously discussed.[117] As a result, tyrosine-derived polycarbonates have been explored for use as nerve guidance conduits. E1001(1k) was chosen based on its degradability, thermal processability, mechanical robustness, and excellent biocompatibility. A promising result of the study was that tyrosine-based nerve conduits promoted deposition of a pro-regenerative extra cellular matrix.[118] Unfortunately, a mismatch in the degradation and resorption led to device failure.

4.4.4.1 Selection Criteria

Device criteria specific to nerve guidance conduits include physical fit, degradability, and biocompatibility.[119] The conduit should hold shape to avoid nerve compression, and ideally have a wall thickness less than 0.81 mm and pores ~ 10-40 μm in diameter. Degradation and resorption should match the regenerative process. For most critical size defects, greater than 3 cm, regeneration takes 6-12 weeks depending on the gap. Comparable polymers degrade and resorb around 6-8 months. Polymers that degrade within a month typically cause inflammation and swelling around the defect site resulting in lack of regeneration while those that don't resorb past one year can compress the newly regenerated nerve. When evaluating the biocompatibility, polymers must be non-cytotoxic and promote Schwann cell adhesion and proliferation.[120] This is followed by secretion of growth factors that help with axon growth. This study aims to explore these three areas as the key considerations to new polymer design.

4.4.4.2 Identification of Small Library Subset

Tyrosol-based poly(ester-arylate)s show clear advantages over E1001(1k), specifically in areas causing device failure. Primarily, improved mechanical toughness and bioresorption were identified as advantages. In an effort to minimize the size of an *in vivo* study, processability, mechanical strength, degradability, and biocompatibility were explored *in vitro*. When evaluating the existing set of data collected two important considerations were that HTy-containing polymers had lower melting temperatures and increased resorption compared to their DTy counterparts. Additionally, the non-acidic and non-cytotoxic degradation byproducts were already confirmed. Mechanical properties were minimally explored by processing implications to these properties still needed to be completed. As such processing impacts and biocompatibility were explored specifically to further decide lead polymer candidates.

4.4.4.3 Improved Polymer Properties Through Processing

E1001(1k) was formed into a kink-resistant conduit through a braiding process, resulting in excellent porosity. Due to lack of mechanical strength, three polymer fibers needed to be twisted into a yarn prior to braiding. In an effort to eliminate the fiber twisting process and further increase porosity in the conduit, processing the polymer fiber to induce crystallization and/or chain orientation was explored. For semicrystalline polymers, drawing and annealing can significantly improve the mechanical properties. Through processing manipulation, moduli and yield stress were capable of increasing 3 to 4-fold for most polymers within the tyrosol polyarylate library (Figure 4.14). In general, shorter chain diacids were the stiffest materials post drawing and annealing. Some of the highest reported

moduli in this data set reach 4 GPa post drawing and annealing, comparable to PLA's tensile modulus of 3.8-4.0 GPa when oriented.[121] Yield stress and strain of the polymer were also improved as a result of increased toughness of the material. One notable observation was the minimal difference between drawn films and those that were drawn and subsequently annealed. This is most likely a result of the drawing process inducing crystallization prior to annealing. All polymers showed improved properties post processing. Based on these results, only the dodecanedioate-containing polymers did not meet the required properties for braiding.

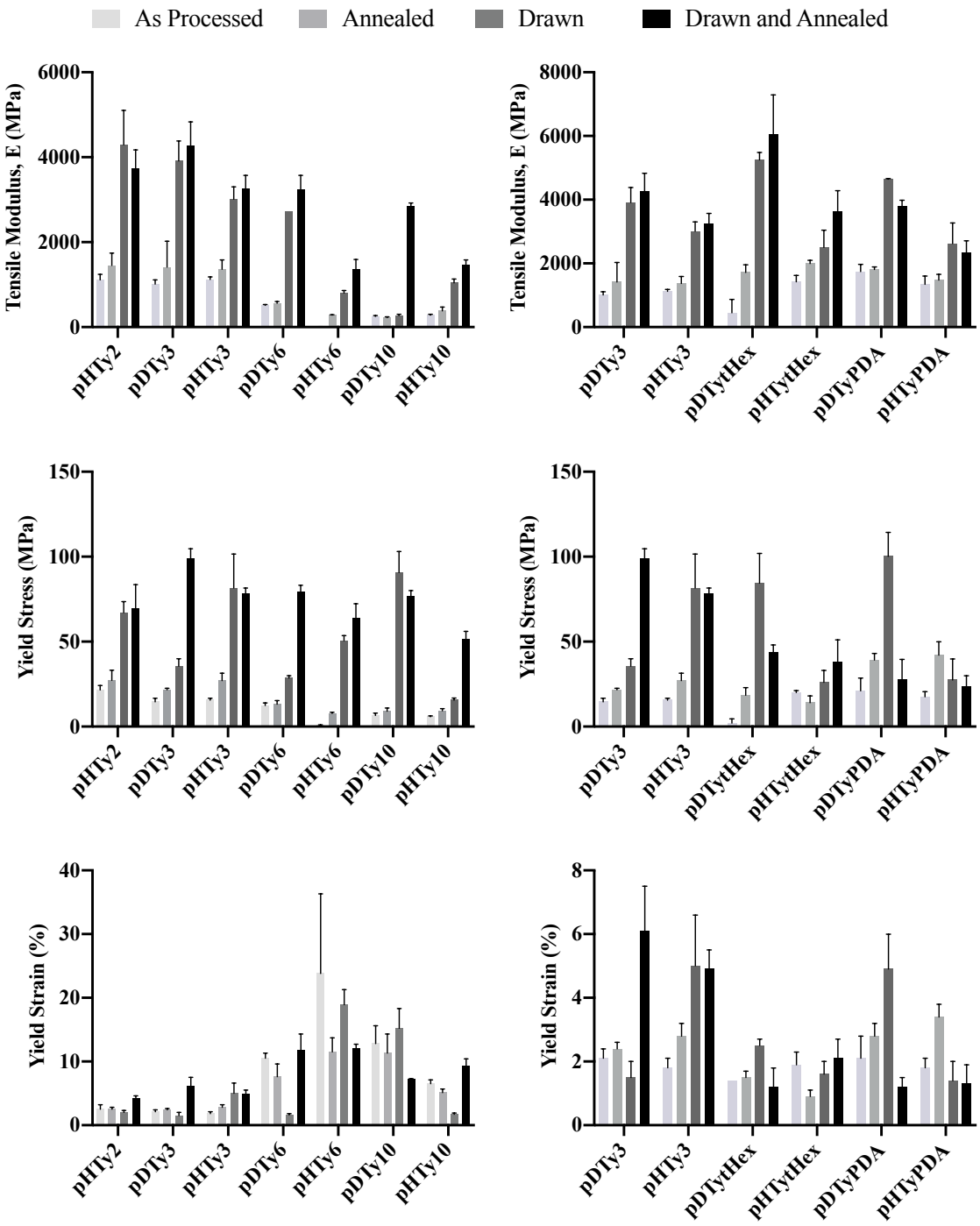

Figure 4.14. Polymer processing implications on (A,D) modulus, (B,E) yield stress, and (C,F) yield strain.

4.4.4.5 Processing Impacts on Crystallinity

Semicrystalline polymers contain both amorphous and crystalline regions. As such, they can change properties based on the fraction of each component. Polymers that are more amorphous typically have lower moduli but their strain to break are much higher compared to crystalline materials which are more brittle but often stronger; i.e., have higher modulus and strength. X-ray diffraction (XRD) is a method often used to analyze the structure and crystallinity of a material. Here, the influence of composition and processing on structure and properties is investigated using XRD. For instance, in pHTy3, the crystallinity of the polymer can be measured based on their processing parameters. Samples that underwent various processing manipulations were characterized using 2D XRD to evaluate their structure, orientation and crystallinity (Figure 4.15). In all polymers, there was an increase of crystallinity with drawing and/or annealing as a processing step as expected.

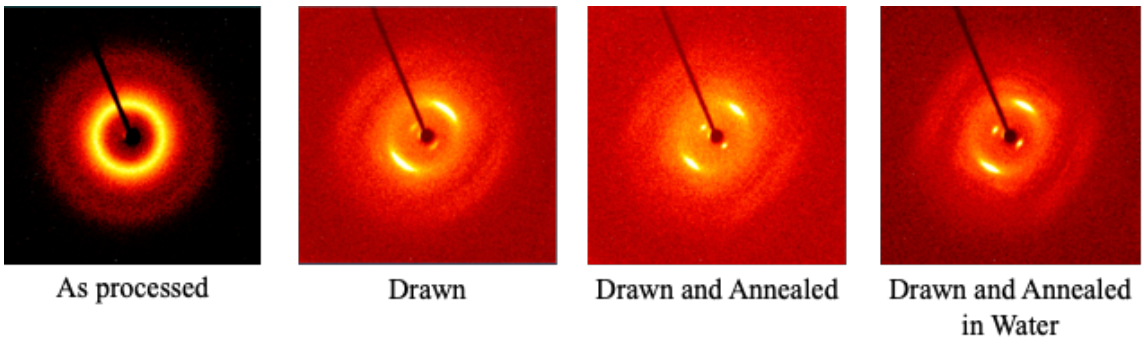

Figure 4.15. XRD patterns for pHTy3 after processing manipulations including drawn as well as drawn and annealed forms.

All polymers, were amorphous when quenched following compression molding and crystallized during drawing and annealing (Figure 4.16A). In an effort to understand the crystal packing, calculations were carried out to determine the unit cell parameters, most importantly the size along the chain-axis, the chain-axis repeat. A clear trend was evident between the length of the aliphatic diacid segment and the chain-axis repeat (Figure 4.16B). As expected, as the diacid chain length increased, so did the repeat length. This work is expected to be continued by others in lab investigating structural differences of these polymers and the implications they have on material properties.

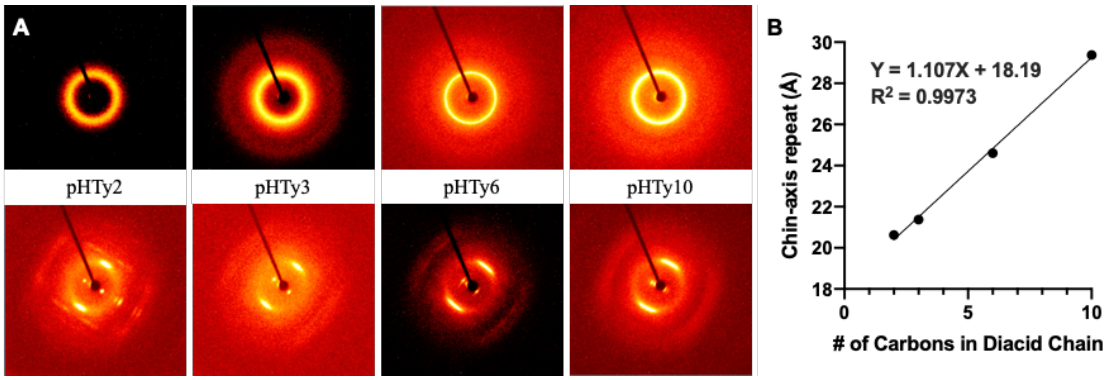

Figure 4.16. (A) Comparison of various diacid chain lengths for HTy copolymers quenched (top row) versus drawn and annealed (bottom row). (B) Chin-axis repeat dependence on diacid chain length.

4.4.4.7 Initial *In Vitro* Schwann Cell Studies

Recruitment of Schwann cells to the nerve gap site is crucial to the regenerative process.[122] When recruited, these cells express neurotrophic factors key to axon ingrowth and end-organ reinnervation. When comparing the adhesion of human Schwann cells (HSC) to tyrosol polymers versus TCPS, tyrosol polymers underperformed (Figure 4.17A).

While it is unclear as to why these polymers had significantly less cell adhesion compared to TCPS, they all promoted proliferation with the exception of pHTyPDA and pDTy6. Additionally, more hydrophobic materials and the best proliferation rates but at the price of degradation rates (Figure 4.17B-C).

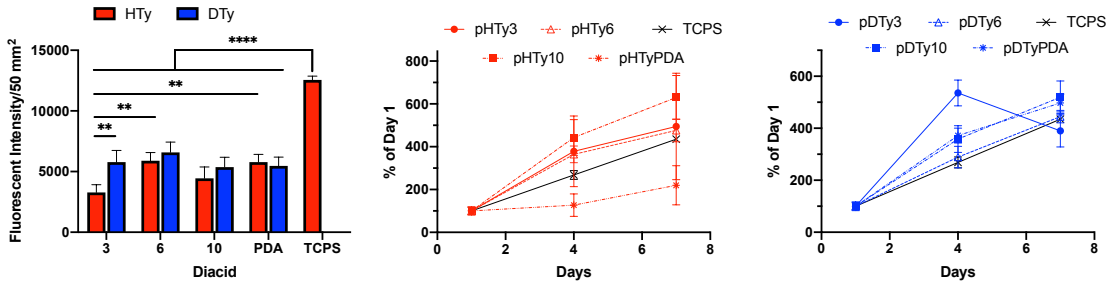

Figure 4.17. HSC adhesion (A) and proliferation (B-C) on tyrosol derived polymers. All samples had an n = 4, except TCPS which had an n = 2. Two-way ANOVA tests were run with post-hoc Tukey test where ** = $p< 0.01$ and **** = $p<0.0001$.

In all, nerve guidance conduits made from tyrosol-based polymers have potential for improved nerve growth following injury. In an effort to scale down the number of polymers to investigate *in vivo*, collected properties were evaluated. HTy-containing polymers were chosen over DTy-containing ones due to lower processing temperatures. Additionally, shorter chain diacids were favored since they had the highest mechanical properties of the aliphatic diacids. Double bond and aromatic polymers were excluded due to the cost of the raw materials. pHTy2 was also excluded because of its slow degradation, more comparable to pHTy10. As a result of this work, pHTy3 and pHTy6 were chosen to move forward with in animal studies. This work is ongoing and will be completed by others in the lab.

4.5 Conclusion

Structure-property-processing relationships were established for tyrosol-based poly(ester-arylate)s as a means to design biomedical devices more efficiently. Tunability in the polymer degradation and resorption, thermal properties, and mechanical properties increase the potential applications these polymers can be used for. Compared to PLA and E1001(1k) tyrosol polymers had increased resorption rates. Additionally, thermal properties were tunable over a range that spanned both above and below physiological and ambient temperatures. Modeled thermal properties were also used to expand on the experimental dataset explored in this thesis. Mechanical properties also were tunable primarily based on diacid and an even larger range of properties was attainable when the material underwent further processing. These relationships were used to identify lead polymer candidates for use in a nerve guidance conduit. Out of a library of over 30 experimentally tested polymers and many additional ones not explored in this work, 2 polymers, pHTy2 and pHTy3 were chosen for further *in vivo* work.

CHAPTER 5: BIODEGRADABLE POLYMERIC INKS WITH TUNABLE PROPERTIES FOR USE IN ADDITIVE MANUFACTURING

5.1 Abstract

3D printing has revolutionized the field of medicine over the past decade. Improvement's in instrumentation have led to the need for more materials. Herein, we investigate tyrosol-based poly(ester-arylate)s for their utility as biodegradable inks for use in direct ink writing. These semicrystalline polymers have been established with tunable properties, non-cytotoxic degradation components, and the ability to be functionalized. Evaluation of printing properties as they relate to chemical structure, molecular weight, and thermal properties was explored. Higher molecular weight polymers exhibit larger amounts of thermal degradation during printing and at some points, are even too viscous to print at all. It was determined that polymers with lower processing temperature and lower molecular weights were printable regardless of structure. pHTy6 is a low melting polymer that is processable up to 34 kDa with minimal degradation. Additionally, chemical improvements were made incorporate thiol-alkene click chemistry as a means for post-print curing. Low molecular weight pHTy6 was end capped with alkene functionality. This material was then formulated with either a dithiol for chain extension or tetrathiol for crosslinking. Scaffolds were cured post print for 5 to 60 min. Mechanical properties increased in all cases being much tougher than their base polymers. This design builds on the library of biocompatible polymers previously explored and aims to bring new biomaterials to the field of 3D printed personal medicine.

5.2 Introduction

3D printing is a tool gaining a lot of attention in biomaterials research due to its ability to transform medicine to be more patient specific. Specifically, tissue engineering,[123-125] dentistry,[126-129] and drug delivery[130-132] have benefited from the ability to design scaffolds and models with complex architectures. Comparatively, traditional methods for fabrication such as solvent casting, braiding, and compression molding often require additional surgical steps to allow an implant site to fit the device. The ability to use imaging such as computed tomography and magnetic resonance imaging which can be translated in computer assisted design software to a print specification. It can allow for fast turnaround during surgical procedures, using instrumentation already available in clinical facilities.[133, 134] One major hurdles that has been identified recently is the limited availability of biodegradable 3D printable ink libraries.[135] Biodegradable materials have been the focus of medical devices as they eliminate the need for future surgical procedures which carry the potential for infection and complications.[31] Current materials used in additive manufacturing include PLA and PCL.[136-138] Both polymers are available commercially in their filament form and have been used extensively in fused deposition modeling (FDM) printing. PLA and PCL are limited by their late stage degradation byproducts causing local tissue acidosis and poor degradability, respectively, leading to the need for new material libraries.

Kohn et al has focused their research on identifying new polymer libraries that can address these issues. Amino acid-based polymers have the benefit of increased inherent biocompatibility, chemical stability, and tunability. Specifically, tyrosine derived polymers have been successfully translated to the market, seeing use in drug eluting polymeric

coatings for hernia meshes and pacemaker pouches as well as cardiac stents.[84, 85] Unfortunately, the presence of amide functionality and pendant carbon chains results in amorphous materials with high processing temperatures. This limits their processability using methods such as direct ink writing (DIW). Semi-crystalline materials on the other hand exhibit melt properties favorable for printing. These materials often have the ability to flow in the melt form followed by rapid transition back to a solid after leaving the print head. Recently, the Kohn lab has identified tyrosol derived poly(ester-arylate)s as a new library of biocompatible, tunable polymers with semi-crystalline properties. These polymers have been further characterized and their structure property relationships identified with the ability to modulate thermal, mechanical, and degradative properties. Guvendiren and Kohn et al published the first article outlining the printability of one polymer within this library and indicated chemical and biological modifications to improve the bioactivity of the material.[139] Poly(HTy phenylenediacetate) was identified as a lead polymer candidate due to additional π-π stacking in the aromatic ring from the diacid. This was hypothesized to improve printability with limited thermal degradation due to its flow properties. Additionally, glutamate-derived functional monomers were incorporated into the polymer backbone to provide a pendant tethering site for bioactive molecules and other chemical structures. The focus of this was to improve on the bioactivity of the polymers as an improvement to traditional materials which are biologically inert.

Structure-property relationships have been a focus within polymer design and development for decades. Adding processing to the equation allows for an understanding of implications the material has on the processing technique and inversely, the fabrication's impact on material properties. It is hypothesized that by identifying the potential of tyrosol-

derived polymers in 3D printing, designing novel printed devices will be much faster and cost efficient. Chemical structure and molecular weight are expected to be main factors on the printability of these polymers. Low melting point polymers should print easier while high molecular weight polymers should be more difficult due to their melt viscosity. Thermal stability of degradable polymers is essential to ensuring retention of polymer properties and device reproducibility. Additionally, tunability in the thermal properties of the polymers provides unique phase changing capabilities following printing.

One of the main outcomes of this work is developing a new way to chemically modify a material to improve mechanical properties post printing using click chemistry. Low molecular weight polymers have weaker mechanical properties compared to the same polymer at higher molecular weights. It is hypothesized that through post printing modifications using thiol-ene click chemistry, chain extension or crosslinking can be achieved improving material properties. These changes combine the printability of low molecular weight polymers at lower temperatures, preventing degradation with the robust mechanical properties of a higher molecular weight polymers. Overall our results indicate the versatility of tyrosol-derived poly(ester-arylate)s in 3D printing and chemical modifications which allow for improved mechanical properties through crosslinking and/or chain extension and in the future, improved biofunctionality through tethering of bioactive molecules post printing.

5.3 Materials and Methods

5.3.1 Materials.

2-(4-hydroxyphenyl)ethanol, 2-(4-hydroxyphenyl)acetic acid, suberic acid, phenylenediacetic acid, dodecanedioic acid, and 4-butenoic were purchased from TCI America (Portland, OR). Glutaric acid, PETMP, and Irgacure 2959 were purchased from Sigma Aldrich (St. Louis, MO). Diisopropylcarbodiimide (DIC) was purchased from Oakwood Chemical (Estill, SC), catalysts including p-toluenesulfonic acid, dimethylaminopyridine, and phosphoric acid were purchased from Sigma Aldrich (St. Louis, MO), and solvents were purchased from Fisher Scientific (Houston, TX).

5.3.2 Polymer Synthesis and Selection.

Tyrosol-derived polymers were chosen as the base polymer library due to their tunable resorption rates and hydrophobicity. These polymers are semi-crystalline making them appropriate for 3D printing applications. Polymers are based on a specialized diphenol formed through the esterification of 2-(4-hydroxyphenyl)acetic acid with tyrosol, denoted as HTy. Subsequent polymerization with diacids using carbodiimide chemistry including DIC and DPTS was performed and molecular weights monitored by GPC. Polymers for this study looked at various molecular weights obtained through Carother's equation. This equation provided various ratios of diacid:diphenol to predict the molecular weight of the polymers. 4 different rations: 0.92, 0.95, 0.965, and 0.98 were compared. Polymers comprised of HTy were chosen due to favorable lower melting temperatures, preventing degradation of polymer during the print process. Specifically, copolymers with glutaric acid (pHTy3), suberic acid (pHTy6), dodecanedioic acid (pHTy10), and

phenylenediacetic acid (pHTyPDA) were used to compare slight variations in the hydrophobicity, thermal, and mechanical properties of the polymers.

5.3.2 Polymer Characterization

Polymers were characterized using NMR for chemical structure confirmation. Number average molecular weights (M_n), and weight average molecular weight (M_w) were determined using gel permeation chromatography (GPC, Waters 717) equipped with a differential refractometer (Waters 410). Agilent PLGel 5 μm columns (7.5 x 300 mm) with pore sizes of 10^5 and 10^3 Å in tandem were used in chloroform + 0.1% trifluoroacetic acid as a solvent. Results were relative to polystyrene standards in the range of 580 to 920,000 Daltons. Differential scanning calorimetry (DSC2520, Mettler Toledo) was used to evaluate melting temperatures (T_m), glass transition temperatures (T_g), and crystallization temperatures (T_c) for polymers. Briefly, samples were run in a 5-step program that including heating from 25 °C to 250 °C at a rate of 10 °C/min, followed by a hold at 250 °C for 2 min, cooling to -50 °C at 10°C/min, a hold a -50 °C for 2 min, and then heating to 250 °C at 10 °C/min. T_g and T_m are reported on the last heat unless otherwise noted.

5.3.3 Print Design and Methodology

Printability of the polymers was tested using an EnvisionTEC 3D Bioplotter Manufacturer Series printer (EnvisionTEC, Inc., Dearborn, MI). Models were designed in Sketchup (Google, Inc., Mountain View, CA) and exported as STL files to the Computer Aided Manufacturing (CAM) software, Perfactory Rapid Prototype (RP) (EnvisionTEC, Inc., Dearborn, MI) which translates the STL files into g-code files. The g-code was

exported to the 3D Bioplotter where it was assigned to the material file for a specific polymer. To show printability of the polymers, a 3D scaffold 10 cm W x 10 cm L x 2 cm H, was fabricated and assigned with 1 mm continuous strand distance with a z-offset of 0.32 mm and no contour. Polymers were loaded into a high temperature cartridge fitted with a stainless steel luer lock 22 G needle, 2 mm in length. The starting print temperature of the polymers was determined as 20 °C above their respective melting temperatures (T_m). At a pressure of 8 bar, the print temperature was increased at every 30 min by 5 °C until adequate extrusion was obtained. After determination of the optimum temperature for printing, a clean cartridge was used to load fresh polymer, eliminating any thermal degradation during method optimization. Printing pressure (bar) and speed (mm/s) were optimized using a built-in program on the EnvisionTec called `Manual Parameter Tuning`. Printability of the polymers was evaluated using the previously mentioned model.

5.3.4 Printhead Degradation Studies

Polymer degradation due to prolonged thermal exposure was characterized. Polymer was loaded in the printing cartridge and brought to the temperature defined by printability studies. Samples were then taken at 5 different time points: 0.5, 1, 2, 3, and 4 hours. This range was chosen to establish limitations to longer prints that may require several hours to complete. Samples were then prepared and run on GPC using the previously defined method. Results are reported based on molecular weight retention over time. Specifically, M_n was used to understand chemical degradation of the material while M_w was used to understand loss of material properties. Additionally, discoloration and physical changes to the polymers were noted.

5.3.5 Printed Strut Mechanical Properties

Polymer struts were printed at preestablished pressure, temperature, and speeds to form fiber-like architecture for mechanical testing. Three replicates were printed for each polymer and condition. Polymer fiber mechanical properties were characterized using a Mechanical Testing System (MTS). Tensile properties including Young's Modulus (E), yield stress (σ_y), and yield strain (ε_y) were reported. Samples were normalized to thickness, width, and length of the specimen. A 100 N load cell and a draw rate of 10 mm/min were used.

5.3.5 Polymer Modification and Characterization

One of the key contributions of this paper is the design of new materials with functionality to improve polymer properties post printing. Low molecular weight oligomers were synthesized with excess diphenol to have phenol groups on the ends of the polymer chains. Using the same carbodiimide chemistry, a 10x molar excess of 4-pentenoic acid was added to the reaction with 0.5 equivalents DPTS to the acid and the reaction stirred for 15 minutes until the mixture looked homogenous. DIC (2.7 equivalents to the acid) was added slowly and the reaction allowed to proceed overnight. Workup followed reported procedures using DCM and IPA. One main difference with low molecular weight polymers is the need to chill the solution to prevent clogging during filtration. Polymers were characterized by GPC for reaction completion and absolute molecular weight determination using end-group analysis in ^{1}H NMR. Similar ratios of alcohol to diacid were used to maintain printability from low molecular weight materials. The reaction was allowed to proceed

overnight and then worked up similarly to all other materials. Alkene incorporation was confirmed through ^{1}H NMR.

5.3.5.1 Alkene capped pHTy6.

^{1}H NMR (500 MHz, Chloroform-*d*) δ 7.25 (d, *J* = 8.6 Hz, 51H), 7.15 (d, *J* = 8.6 Hz, 46H), 7.03 (d, *J* = 8.6 Hz, 47H), 6.99 (dd, *J* = 8.6 Hz, 47H), 5.91 (s, 2H), 5.14 (d, *J* = 18.7 Hz, 2H), 5.07 (d, *J* = 10.2 Hz, 2H), 4.28 (t, *J* = 7.0 Hz, 50H), 3.58 (s, 49H), 2.90 (t, *J* = 6.9 Hz, 50H), 2.66 (t, *J* = 7.4 Hz, 5H), 2.57 (t, *J* = 7.5 Hz, 94H), 1.89 – 1.70 (m, 95H), 1.49 (t, *J* = 7.1 Hz, 95H).

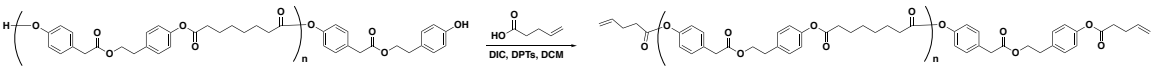

Scheme 5.1. Synthetic schematic of alkene capped pHTy6.

5.3.6 Formulation and UV Curing (Thiol-Ene click chemistry)

Polymer formulations for printing were completed by combining alkene containing polymer, thiol chain extender or crosslinker, and Irgacure 2959 in DCM and solvent casting a film for further processing. This process ensures molecular mixing of the components and improves post printing reactivity. Three variables were explored briefly to establish a proof of concept and processing considerations: (i) chain extension vs. crosslinking from thiol type, (ii) thiol:alkene ratio and (iii) cure time. A linear aliphatic dithiol was used, hexanedithiol, for chain extension and a degradable tetrathiol, pentaerythritol(3-mercaptopropionate), for crosslinking. Ratio of 2:1, 1.5:1, and 1:1 thiol to alkene, were used to ensure reactivity with the polymer. Cure times of 5 minutes, 15 minutes, 30

minutes, and 60 minutes were used to optimize the potential for curing in between print layers.

5.4 Results and Discussions

5.4.1 Polymer Synthesis and Molecular Weight Control

Tyrosol derived poly(ester-arylate)s are synthesized using carbodiimide chemistry between a diphenol and diacid. Specifically, HTy was chosen as the diphenol in printable inks due to their lower melt temperatures. Four diacids: glutaric, suberic, dodecanedioic, and phenylenediacetic acid were used to establish impacts of chemical structure on printability. Additionally, the ability to tune these materials in their degradation and resorption time have been reported previously. A main focus of this project was to establish the impact of molecular weight on the polymer's printability. Often polymers require low molecular weight materials to ensure flow in the melt at processing temperature. These can often have a negative effect on mechanical properties and resorption rates.

$$DP = \frac{1+r}{1+r-2rp} \qquad DP = \frac{1+r}{1-r}\,, when\ p = 1 \qquad \text{(Eq. 1)}$$

Table 5.1. Molecular Weights of Polymeric Inks for Printing Using Carothers Equation.

	pHTy3				pHTy6			
r-value	**0.92**	**0.95**	**0.965**	**0.98**	**0.92**	**0.95**	**0.965**	**0.98**
Mn (kDa)	9.2	13.0	32.0	65.6	11.4	18.5	34.0	64.1
Mw (kDa)	17.3	30.3	56.5	119.9	20.5	35.2	64.6	124.8
PDI	1.9	2.3	1.8	1.8	1.8	1.9	1.9	1.9
DP	24	34	87	170	27	43	83	150
	pHTy10				**pHTyPDA**			
r-value	**0.92**	**0.95**	**0.965**	**0.98**	**0.92**	**0.95**	**0.965**	**0.98**
Mn (kDa)	15.1	19.7	29.8	62.9	7.1	9.9	19.1	32.4
Mw (kDa)	25.5	38.2	57.4	120.5	16.8	28.5	41.3	79.9
PDI	1.7	1.9	1.9	1.9	2.4	2.9	2.2	2.5
DP	28	37	59	116	16	22	44	72

[a]DP values are calculated based on the Mn

Carothers established a correlation between the ratio of diacid and dialcohol in a polymer synthesis in order to predict molecular weight growth. The relationship, known as Carothers equation shows that the degree of polymerization (DP) is related to r, the ratio of diphenol to diacid and p, the conversion factor for the reaction (Equation 1). When assuming the conversion to be 1, indicating complete reactivity, the relationship is easier defined. Four r-values were chosen to represent both low and high molecular weight polymers. For each synthesis, the reactions were allowed to go overnight to ensure complete reactivity. As r values approach 1, the molecular weight grows exponentially.

Resulting polymer molecular weights were reported and indicated increases in DP as r increased (Table 5.1 and Figure 5.2).

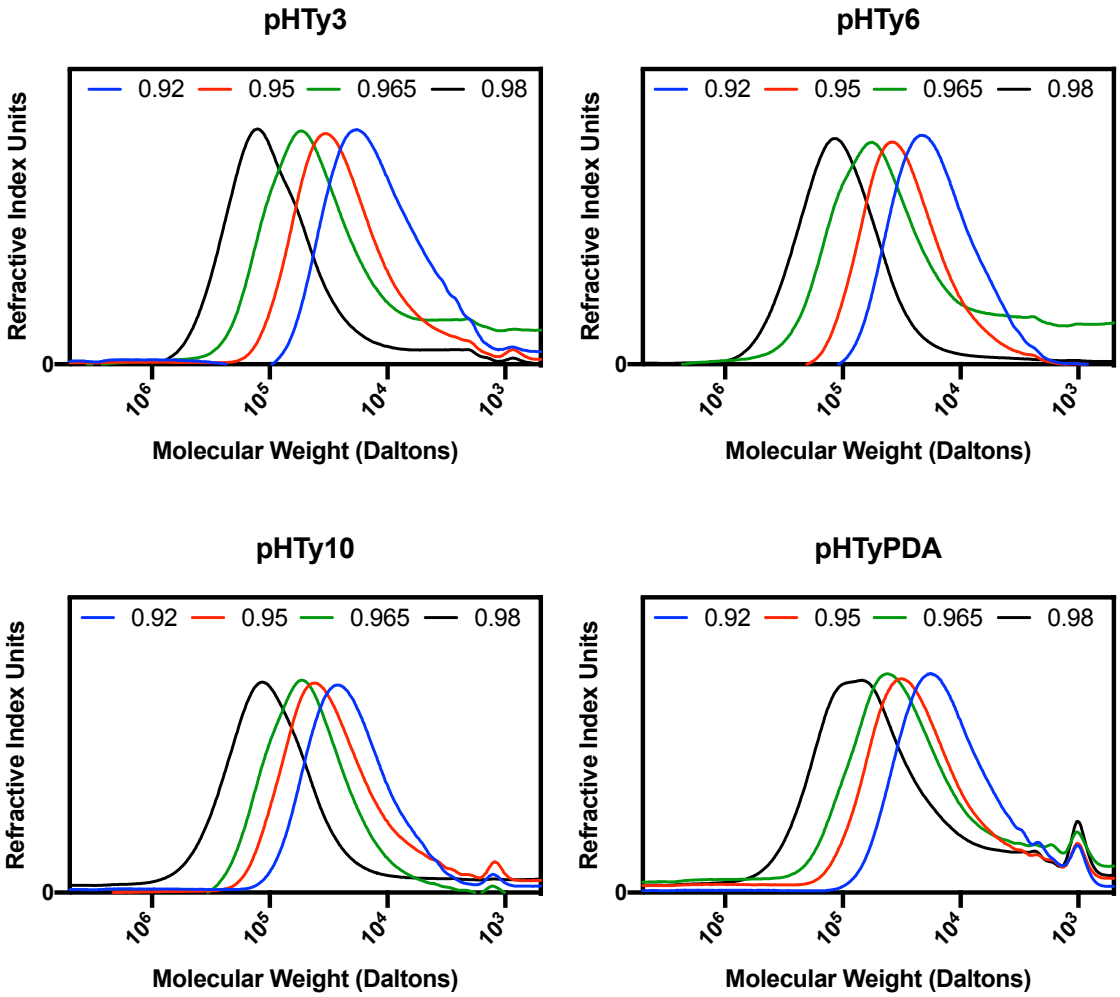

Figure 5.2. GPC curves of 3D printing polymers with varied molecular weights.

5.4.2 Print Optimization

Models created by Sketchup program were transferred as .stl files, converted into g-code using Perfactory software and transferred to Visual Machines software for computer control printing. A high temperature dispense head was used and print temperature was optimized, starting at 20 °C above the melting point until melt flow was appropriate for

printing. The starting temperature for all of the polymers with r= 0.92 value was enough to obtain an adequate extrusion for printing. Fiber diameters and distance between the strands were easily optimized and controlled using built-in program of the Visual Machines software called `Manual parameter tuning`. This program allows to optimize the speed of printing (mm/s) under constant pressure (bar) and vice versa. Optimized conditions were used to print the model created by Sketchup (Figure 5.3). Increase in Mw with r= 0.95 did not affect the print temperature except for HTyPDA where a 10 $^{\circ}$C increase is needed to obtain suitable extrusion for printing. Polymers with an r-value of 0.965 and 0.98 needed a higher printing temperature compared to polymers with an R-value of 0.92 or 0.95, indicating that the viscosity of the polymers increased, affecting extrusion. The melt viscosity of polymers with an R-value of 0.98 was so high that it prevented printing at the highest pressure (8 bar) and lowest speed (0.1 mm/s). Among the polymers, only pHTy10 with r=0.98 was printable, but additional data indicated thermal degradation led to lower viscosity.

The polymers have remarkable phase changing features due to their glass transition temperatures and crystalline properties. For example, scaffolds obtained from pHTy6 print were transparent and sticky upon printing indicating an amorphous form of the polymer. This sticky state remains for approximately 15 min and then the material crystallizes and turns to opaque white. This could allow for macroscale geometric configurations through manual manipulation of the scaffold post printing. pHTy3 is another polymer with remarkable phase changing feature which has a T_g in between room temperature and physiological temperature, making it pliable while handling but not during storage.

All printed scaffolds, regardless of the molecular weight of the polymer, maintained their appearance as a white opaque solid, except for pHTyPDA which appeared yellow and more translucent after printing. This is expected due to increases in conjugation from additional aromatic rings and a glass transition over 10 °C above room temperature, keeping it in the amorphous phase throughout printing. pHTy3 (r = 0.965) and pHTy10 (r = 0.98) appeared slightly yellow which most likely is a result of degradation.

Polymer	r value	Temperature (°C)	Pressure (bar)	Speed (mm/s)	r= 0.92	r= 0.95	r= 0.965	r=0.98
pHTy3	0.92	158	1	7				Not Printable
	0.95	158	4	7				
	0.965	168	4	5				
	0.98	N/A	N/A	N/A				
pHTy6	0.92	108	6	10	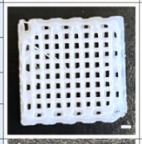			Not Printable
	0.95	108	8	3				
	0.965	138	8	1				
	0.98	188	N/A	N/A				
pHTy10	0.92	120	3.5	9				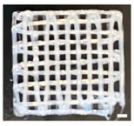
	0.95	120	6.5	5				
	0.965	160	4	4				
	0.98	180	4	5				
pHTyPDA	0.92	163	2	12				Not Printable
	0.95	173	2	4				
	0.965	173	2	6				
	0.98	N/A	N/A	N/A				

Figure 5.3. Printability of the polymers and respective printing parameters. Scale bar is 1 mm.

5.4.3 Printhead Thermal Degradation

One of the main concerns during any prolonged thermal process step is the exposure to heat over long periods of time. Give the degradable nature of these polymers, retention of polymer structure and properties is crucial to their success. Since 3D printing can require

long print times, reproducibility of the print over the entire process time is required. In order to investigate the implications of printing for extended periods of time, polymer was placed in the printhead cartridge, brought to the proper print temperature, and allowed to sit at temperature for up to 4 hours, with the assumption that most prints would be able to finish by then. At 5 predetermined time points, 0.5, 1, 2, 3, and 4 hours, polymer sample was collected and molecular weight was determined (Figure 5.4). Polymers at most molecular weights were printable with little to no degradation observed over 4 hours. The one exception to this was the high molecular weight polymers which were difficult to print until later in the print time. This was characterized by free-flowing polymer at the 3- and 4-hour time points, which data confirms is due to the degradation of the polymer to a lower molecular weight. In all, polymers synthesized at an r value of 0.92 and 0.95 did not have excessive thermal degradation. pHTy6 was able to print at the r value of 0.965 without degradation, while all other polymers experienced slight degrees of degradation. This is most likely a result of low processing temperatures required for this polymer.

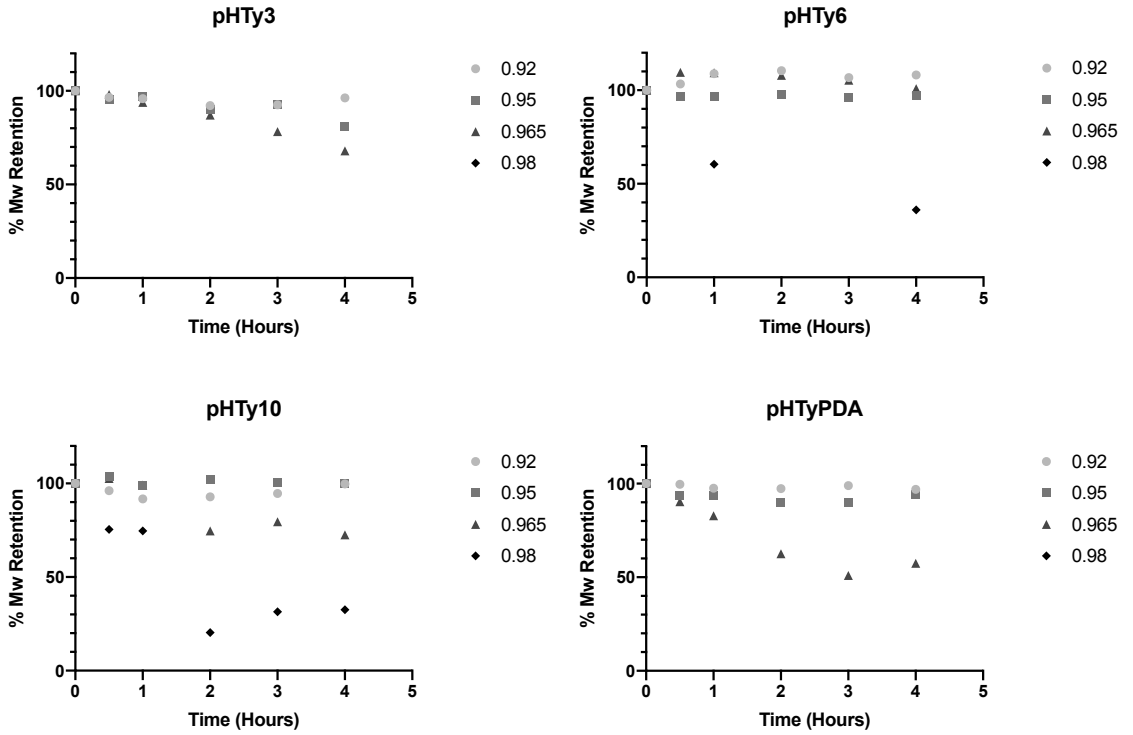

Figure 5.4. Thermal degradation of polymers in the print cartridge. pHTy3 and pHTyPDA do not have data points past T0 due to inability to print.

5.4.4 Polymeric Modifications to Improve Print

Polymers require high enough molecular weights to possess the mechanical properties required for structural integrity. Unfortunately increases in molecular weight result in higher melt viscosities and difficulty in printing, especially when direct ink writing is used. As such, there is a need for polymers that are as printable as low molecular weight polymers with the material properties of higher molecular weight ones. One approach to address this is to cure the polymer post printing resulting in higher molecular weights. Click chemistries provide the ability to perform simple, quantitative chemistries with minimal side reaction potential and non-harsh conditions. Specifically, thiol-alkene click chemistry is radical initiated through UV irradiation to form a thioether bond.[140-143]

Through alkene end-capping of oligomers, multifunctional thiols can be used to either chain extend or crosslink the polymer chains. pHTy6 was chosen at an R-value at 0.92 due to its ease in printing requiring low temperatures and pressures. A second synthetic step was used to introduce the alkene using 4-pentenoic acid. The acid was reacted through the same carbodiimide chemistry used in the polymerization to form an arylate bond. ^{1}H NMR was used to identify the incorporation of alkene peaks (~5-6 ppm) and a slight shift in the end capped phenol functionalities. As evidenced by the peaks at 5.91, 5.14, and 5.07 ppm correlating to the alkene protons, end capping of the polymer was achieved (Figure 5.4). Additionally, no peaks around 6.5 ppm indicates no aromatic protons next to a phenol which would be expected if the polymer was not capped completely.

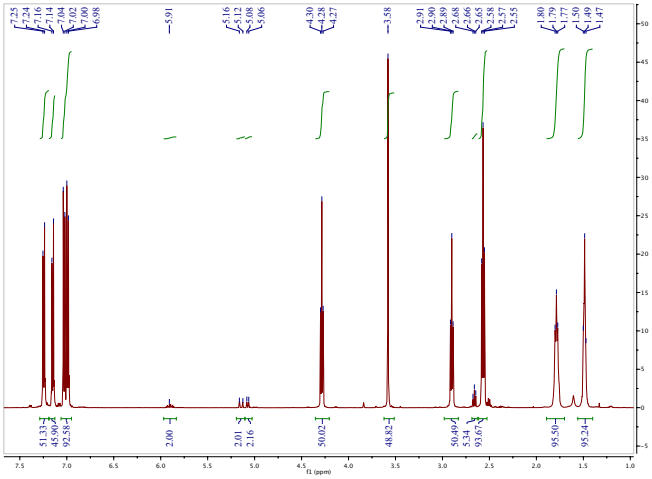

Figure 5.4. Proton NMR of alkene end-capped pHTy6.

5.4.5 UV Curing Printed Constructs

Table 5.2. Formulations for UV curable polymeric inks.

Formulation	Polymer	Thiol	Thiol:Alkene Ratio	Initiator
1	pHTy6 dialkene	hexanedithiol	1:1	Irgacure® 2959
2	pHTy6 dialkene	hexanedithiol	1.5:1	Irgacure® 2959
3	pHTy6 dialkene	hexanedithiol	2:1	Irgacure® 2959
4	pHTy6 dialkene	PETMP	1:1	Irgacure® 2959
5	pHTy6 dialkene	PETMP	1.5:1	Irgacure® 2959
6	pHTy6 dialkene	PETMP	2:1	Irgacure® 2959

Formulations of UV curable polymers for printing include the dialkene capped polymer, a multifunctional thiol, and a radical initiator, in this case Irgacure 2959 which activates at a wavelength of 365 nm (Table 5.2). The formulation allows for curing post print but also introduces a plasticizer into the polymer matrix which facilitates melt flow, improving printability. Two variables in curable polymers: (i) cure time, and (ii) ratio of thiol to alkene can be investigated for each polymer, chain extender pairing. For the purposes of this paper, cure times of 5, 15, and 30 minutes were explored to optimize the ability to either cure between print layers or post entire print. 6 formulations were made looking at two thiols: hexanedithiol for chain extension and PETMP for crosslinking. The PETMP has been explored previously in polymeric constructs by Bowman et al.[144] PETMP specifically contains esters which are hydrolytically labile allowing for degradation of the device despite crosslinking. Additionally, the ratio of thiol to alkene can be used to further

optimize final molecular weight. Three ratios of thiol to alkene, 1:1, 1.5:1, and 2:1 were tested. All polymer formulations were able to print at a lower pressure due to the presence of the crosslinker which acts like a plasticizer.

All polymers were printed in strips for mechanical testing requiring two layers due to the percentage of polymer in the formulation. The main goal of incorporating chain extension or crosslinking into the polymer network was for improved mechanical properties. All polymers were tougher post cross linking (Figure 5.5). Tensile moduli were minimally impacted by cure time but were less stiff overall compared to the low molecular base polymer. The main trend observed was high elongation to break and increased break stress. These correlate to increases in overall toughness of the material. Overall tunability of mechanical properties through changes in thiol:alkene ratio was determined with cure times of 30 min providing the best results.

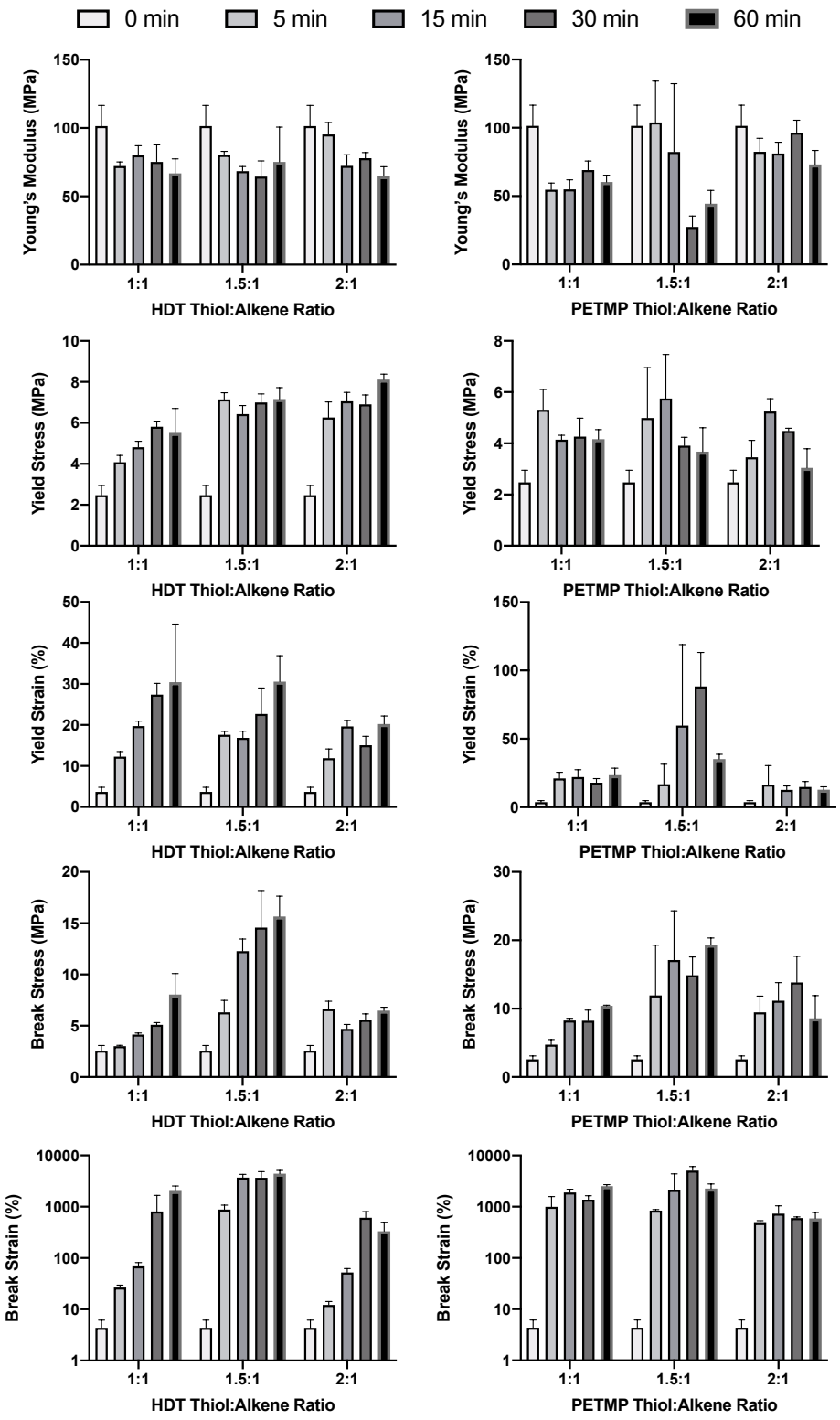

Figure 5.5. Mechanical properties of printed formulations containing HDT (left) or PETMP (right) with varied curing times and thiol:alkene ratios. All samples have an n = 3.

5.5 Conclusion

A library of 3D polymers was established with processing parameters, and tunable properties established. All polymers exhibited levels of printability using direct ink writing. High molecular weight polymers were not printable due to high melt viscosities and therefore required chemical modifications to improve the properties of a printed scaffold. Pressure and print speed were optimized to obtain precise geometries with little to no running of polymer observed. Additionally, thermal degradation in the print head was characterized and showed that high molecular weight polymers, which required higher processing temperatures had higher degrees of thermal degradation, ultimately changing the polymer properties. Chemical modification of the polymer was established by capping oligomers with an alkene to form a curable polymer. When formulated with multifunctional thiols, UV curing resulted in chain extension or crosslinking and in turn, improved mechanical properties. Cure time, while explored, did not have as great of an impact although 60-minute cure times caused degradation of the polymers due to thermal exposure for extended periods of time. Additionally, there were no significant differences found in chain extended or crosslinked polymers but an excess of thiol of 1.5:1 thiol:alkene did greatly improve mechanical properties. 1.5-fold increase in tensile moduli. This established library helps expand on the limited biodegradable polymeric materials available and established processing tunability to attain expansive material properties.

CHAPTER 6: DRUG-POLYMER RELATIONSHIPS TO ENABLE CONTROLLED RELEASE IN IMPLANTABLE DEPOT SYSTEMS

6.1 Abstract

Patient compliance, poor bioavailability, and negative systemic side effects have led to increased attention towards the development of drug-loaded long acting implantables. Developments in bioresorbable polymers have extended to the field of drug delivery, controlling release based on chemical structure. Tyrosol-derived polymers specifically, have shown promise due to their tunable properties and resorbability. Incorporation of hydrophobic domains to induce phase separation and hydrogen bonding sites within the polymer backbone led to advancements in functional materials specially designed for drug delivery applications. Progesterone and acyclovir were chosen as models to represent both hydrophobic and hydrophilic drugs, respectively. As expected, progesterone-loaded devices were more consistent due to better matches in hydrophobicity between the polymer and drug compared to acyclovir. Incorporation of PEG into the polymer backbone also facilitated the release of hydrophobic drugs from the hydrophobic polymer matrix through phase separation when introduced to water. Correlations were also found between processing temperature and release rate due to changes in the drug form. For acyclovir, processing temperatures resided well below the drugs melt and therefore, relied on interactions between the drug and polymer to control release. Hydrogen bonding sites within the polymer backbone reduced burst release at in devices processed at higher temperatures while increased release in devices processed at lower temperatures. Overall polymer structure, processing, and drug hydrophobicity defined the release profiles.

6.2 Introduction

Conventional delivery of drugs has included oral and intravenous applications, but disadvantages in both, including low bioavailability, degradation of the API in harsh acidic environments, and poor patient compliance have led to increased interest into alternative treatment approaches.[145, 146] One potential solution to this is through the use of long acting implantable depot systems. These systems allow for sustained low dosage release over weeks or months, ability to deliver drugs locally to a specific tissue, and bypassing of the harsh environments present through oral administration.[147-151] Another benefit to implantable systems is the ability to remove a device should there be any negative side effects or complications. Long acting implantable systems are mostly used in contraceptives such as Nuvaring® and cancer treatment such as Vantas®.[147] Commonly employed reservoir-based systems use a hollow cavity loaded with a specific API and rely on diffusion across the polymer membrane to sustain release.[152, 153] These systems are mostly made from non-degradable polymers, requiring device removal after their use. Reports of difficulty in device location and extraction after months of use have limited their potential.[154, 155] Polymer drug matrices have aimed to address these problems, controlling release through diffusion of the drug and degradation of the polymer. Specifically, the use of biodegradable polymers that are able to release drug and then degrade and resorb *in vivo* have gained a substantial amount of attention.

While polymers have been used within the pharmaceutical industry for over 50 years, the shift towards biodegradable materials has been more recent. Approaches to control delivery through both chemical modifications and engineering processes have led to a better understanding and design of polymeric drug delivery devices. Poly(lactide-co-

glycolide)s (PLGAs) have been extensively used in drug delivery due to their tunability, processability, and reproducibility.[156, 157] While PLGAs have been effective in systemic drug delivery systems and short acting systems, their use in long acting systems can be problematic due to their acidic degradation products and have been reported to cause late stage acidosis and inflammation in tissue sites. Over the past 20 years, investigation of naturally derived polymers that are tunable with non-acidic degradation products have been completed. Specifically, the Kohn lab's use of amino acid derived poly(ester-arylate)s have exhibited excellent tunability and thermal processability.[97] Prior experience using tyrosine derived biomaterials have been successful for the delivery of hydrophobic and hydrophilic API's loaded in a polymeric coating for hernia meshes and pacemaker pouches. These devices have been commercialized by Medtronic, formally TYRX™, and are attributed to saving thousands of lives. Extensive work looked at compression molded devices loaded with Voclosporin for the treatment of dry eye syndrome by Khan et al.[97] One major disadvantage to these polymers is their limited resorption profile due to a non-hydrolytically labile amide.

Recently, the development of tyrosol-based polyarylates has introduced a bioresorbable polymer library that is thermally processable and has tunable degradation, resorption, and mechanics. Herein, we report the use of tyrosol polyarylates to formulate extrudable implantable depot systems for long acting release of APIs. Tyrosol is a naturally occurring compound found in olive oil and has been proven to have antioxidant and cardioprotective properties.[91] These polymers have been explored and their structure-property relationships defined. With tunable degradative, thermal and mechanical properties, these polymers have utility in a wide range of biomedical applications including

drug delivery. We hypothesize that tunability in the polymer properties, specifically processing temperatures and chemical composition, will impact the release of drug from the polymer matrix. As semi-crystalline polymers, they exhibit melt temperatures which facilitate thermal processing techniques including extrusion and injection molding. Additionally, we investigate the polymer-drug interactions to identify trends in polymer composition, processing parameters, and drug hydrophobicity on release profiles. This work looks to establish design information for future development in implantable depots. Novel materials with unique functionality were designed to facilitate controlled release of APIs. For the release of hydrophobic drugs, phase separation through the incorporation of PEG was used while hydrophilic APIs benefited from hydrogen bonding sites to increase molecular interactions between the drug and polymer.

6.3 Materials and Methods

6.3.1 Materials.

2-(4-hydroxyphenyl)ethanol, 2-(4-hydroxyphenyl)acetic acid, suberic acid, and dodecanedioic acid were purchased from TCI America (Portland, OR). Glutaric acid, glycine, succinic anhydride, and poly(ethylene glycol) were purchased from Sigma Aldrich (St. Louis, MO). Diisopropylcarbodiimide (DIC) was purchased from Oakwood Chemical (Estill, SC), catalysts including p-toluenesulfonic acid, dimethylaminopyridine, and phosphoric acid were purchased from Sigma Aldrich (St. Louis, MO), and solvents were purchased from Fisher Scientific (Houston, TX). APIs were provided by Lubrizol Life Sciences and purchased from Spectrum Chemicals (New Brunswick, NJ). Sodium lauryl

sulfate was purchased from VWR (Radnor, PA) while Dulbecco's PBS packets and hydrochloric acid were purchased from Sigma Aldrich (St. Louis, MO).

6.3.2 Polymer Synthesis and Selection.

Tyrosol-derived polymers were chosen as the base polymer library due to their tunable resorption rates and hydrophobicity. They also contain aromatic rings which can provide a source for π-π interactions with the drug and polymer, favoring drug-polymer miscibility. These polymers are based on a specialized diphenol formed through the esterification of 2-(4-hydroxyphenyl)acetic acid or 2-(4-hydroxyphenyl)propionic acid with tyrosol, denoted as HTy and DTy respectively. Subsequent polymerization with diacids using carbodiimide chemistry including DIC and DPTS was performed and molecular weights monitored by GPC. All polymers chosen for this study had molecular weights larger than 100 kDa as compared to polystyrene standards in chloroform + 0.1% TFA. Polymers comprised of HTy were chosen due to favorable lower melting temperatures, preventing degradation of polymer and drug during the formulation process. Specifically, copolymers with glutaric acid (HGl), suberic acid (HS), and dodecanedioic acid (HD) were compared due to slight variations in the hydrophobicity and logP of the polymers.

For functional polymers, poly(ethylene glycol) or glycine succinamide diacid (GSD) were incorporated into the polymer at 5 mol %. GSD was synthesized through a condensation reaction between glycine and succinic anhydride. The resulting diacid contains an amide bond that acts as a hydrogen bonding site. Subsequent polymerization can proceed through previously described carbodiimide chemistry. One important

synthetic note is that the amide-containing diacid is not able to be incorporated at high percentages using the standard carbodiimide coupling method in dichloromethane due to limited solubility.

6.3.2.1 Poly(HTy glutarate) (HGl).

GPC (Chloroform + 0.1% TFA): M_n = 90.9 kDa, M_w = 157.6 kDa, PDI = 1.73. ^{1}H NMR (500 MHz, Chloroform-*d*) δ 7.25 (d, *J* = 8.5 Hz, 2H), 7.15 (d, *J* = 8.5 Hz, 2H), 7.04 (d, *J* = 8.5 Hz, 2H), 7.00 (d, *J* = 8.5 Hz, 2H), 4.29 (t, *J* = 6.9 Hz, 2H), 3.58 (s, 2H), 2.90 (t, *J* = 6.9 Hz, 2H), 2.71 (t, *J* = 7.3 Hz, 4H), 2.18 (p, *J* = 7.3 Hz, 2H).

Scheme 6.1. Reaction schematic for the synthesis of poly(HTy glutarate).

6.3.2.2 Poly(HTy suberate) (HS).

GPC (Chloroform + 0.1% TFA): M_n = 85.4 kDa, M_w = 152.0 kDa, PDI = 1.78. ^{1}H NMR (500 MHz, Chloroform-*d*) δ 7.25 (d, *J* = 8.6 Hz, 2H), 7.15 (d, *J* = 8.6 Hz, 2H), 7.03 (d, *J* = 8.6 Hz, 2H), 6.99 (d, *J* = 8.5 Hz, 2H), 4.29 (t, *J* = 6.9 Hz, 2H), 3.58 (s, 2H), 2.90 (t, *J* = 6.9 Hz, 2H), 2.57 (t, *J* = 7.4 Hz, 4H), 1.84 – 1.73 (m, 4H), 1.50-1.47 (m, 4H).

Scheme 6.2. Reaction schematic for the synthesis of poly(HTy suberate).

6.3.2.3 Poly(HTy dodecanedioate) (HD).

GPC (Chloroform + 0.1% TFA): M_n = 104.9 kDa, M_w = 191.0 kDa, PDI = 1.82. ^{1}H NMR (500 MHz, Chloroform-*d*) δ 7.24 (d, *J* = 8.5 Hz, 2H), 7.15 (d, *J* = 8.5 Hz, 2H), 7.03 (d, *J* = 8.5 Hz, 2H), 6.99 (d, *J* = 8.5 Hz, 2H), 4.28 (t, *J* = 7.0 Hz, 2H), 3.58 (s, 2H), 2.90 (t, *J* = 7.0 Hz, 2H), 2.54 (t, *J* = 7.5 Hz, 4H), 1.75 (p, *J* = 7.5 Hz, 4H), 1.45 – 1.30 (m, 12H).

Scheme 6.3. Reaction schematic for the synthesis of poly(HTy dodecanedioate).

6.3.2.4 Poly(HTy suberate-co-5% HTy glycinesuccinamidedioate) (HS5HG).

GPC (Chloroform + 0.1% TFA): Mn = 56.6 kDa, Mw = 122.0 kDa, PDI = 2.16. ^{1}H NMR (500 MHz, Chloroform-d) δ 7.39 (d, J = 8.0 Hz, 0.1H), 7.25 (d, J = 8.4 Hz, 2H), 7.15 (d, J = 8.4 Hz, 2H), 7.03 (d, J = 8.4 Hz, 2H), 6.99 (d, J = 8.4 Hz, 2H), 4.29 (t, J = 7.0 Hz, 2H), 3.83 (d, J = 6.4 Hz, 0H), 3.58 (s, 2H), 2.90 (t, J = 6.9 Hz, 2H), 2.66 (s, 0H), 2.57 (t, J = 7.4 Hz, 4H), 1.85 – 1.74 (m, 4H), 1.49 (t, J = 6.8 Hz, 4H). T_g = 11.7 °C, T_m = 54.2 °C, 69.3 °C.

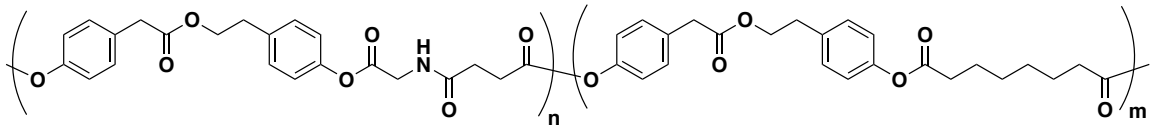

Scheme 6.4 Reaction schematic for the synthesis of poly(HTy suberate-co-5%HTy glycinesuccinamide diaote)

6.3.2.5 Poly(HTy suberate-co-5% PEG_{1K} suberate) (HS5PS).

GPC (Chloroform + 0.1% TFA): Mn = 59.9 kDa, Mw = 187.1 kDa, PDI = 3.12. ^{1}H NMR (500 MHz, Chloroform-d) δ 7.25 (d, J = 8.5 Hz, 2H), 7.15 (d, J = 8.5 Hz, 2H), 7.03 (d, J = 8.5 Hz, 2H), 6.99 (d, J = 8.5 Hz, 2H), 4.28 (t, J = 7.0 Hz, 2H), 3.65 (s, 3H), 3.58 (s, 2H), 2.90 (t, J = 6.9 Hz, 2H), 2.57 (t, J = 7.5 Hz, 4H), 1.84 – 1.74 (m, 5H), 1.49 (t, J = 7.0 Hz, 4H). T_g = -2.6 °C, T_m = 70.3 °C.

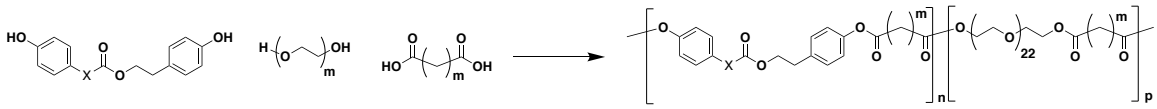

Scheme 6.5 Reaction schematic for the synthesis of poly(HTy suberate-co-5%PEG_{1K} suberate)

For the purposes of this thesis, the nomenclature will follow short names outlined in Table 6.1.

Table 6.1. Polymer nomenclature reference table.

Polymer	Short Name
Poly(HTy glutarate)	HGl
Poly(HTy suberate)	HS
Poly(HTy dodecanedioate)	HD
Poly(HTy suberate-co-5% HTy glycinesuccinamidedioate)	HS5HG
Poly(HTy suberate-co-5% PEG1K suberate)	HS5PS

6.3.3 Model Drug Choices.

Progesterone and Acyclovir were chosen as model drugs for this study (Figure 6.6). Both drugs have utility in long acting implantable formulations, while having significantly different hydrophobicity. Progesterone is an organic steroid lipid molecule and is considered practically insoluble in aqueous media, with a logP of 3.87. It is used for menstrual cycle regulation and hormone replacement therapy among others. Progesterone implants specifically can be used in hormonal contraceptives. Progesterone's chemical structure includes fused rings commonly observed in steroid molecules with two ketones. Conversely, Acyclovir is a nucleoside analogue and antiviral agent that is hydrophilic, with a logP of -1.76, and considered slightly soluble in water. Acyclovir, is commonly used in the treatment of herpes simplex viruses' types 1 and 2 among other viruses within the herpesvirus family. It has also been shown to be effective in treating herpes related eczema and encephalitis. Structurally, Acyclovir is identified by its conjugated fused rings containing amides and amines, along with an ether tail and a free alcohol group.

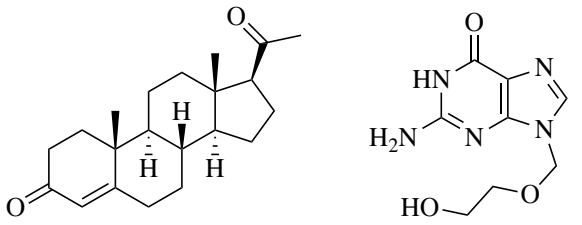

progesterone acyclovir

Figure 6.6 Chemical structures for model APIs: progesterone (left) and acyclovir (right).

6.3.4 Rod Implant Formulation.

Implant devices were made by extrusion of a solid mixture of polymer and drug. First, rheology was carried out on the base polymers to define processing temperatures and to understand polymer flow. Shear viscosity was measured at varying shear rates and increasing temperatures, starting at 20 °C above their melting temperature. Formulations were conducted with admixed polymer and drug powders in the rheometer for scaling purposes and collected through a 3 mm diameter die at different temperatures. This was done to evaluate the effect of processing temperature on drug release. Polymer rods were then kept at ambient conditions overnight to allow for any phase changes that may occur to ensure reproducibility between samples.

Table 6.2. Processing temperatures for various formulations of progesterone loaded rods.

Progesterone (Tm 128 °C) – Loaded Polymeric Implants				
Polymer	**Polymer Glass Transition Temperature**	**Polymer Melting Temperature**	**Low Processing Temperature**	**High Processing Temperature**
HGl	32.5 °C	137.8 °C	125 °C	145 °C
HS	8.5 °C	70.3 °C	90 °C	125 °C
HD	4.1 °C	89.7 °C	100 °C	125 °C
HS5PS	-2.6 °C	70.8 °C	90 °C	110 °C
HS5HG	11.7 °C	69.3 °C	90 °C	125 °C

Table 6.3. Processing temperatures for various formulations of acyclovir loaded rods.

Acyclovir (Tm 265 °C) – Loaded Polymeric Implants				
Polymer	**Polymer Glass Transition Temperature**	**Polymer Melting Temperature**	**Low Processing Temperature**	**High Processing Temperature**
HGl	32.5 °C	137.8 °C	140 °C	160 °C
HS	8.5 °C	70.3 °C	100 °C	140 °C
HD	4.1 °C	89.7 °C	100 °C	140 °C
HS5PS	-2.6 °C	70.8 °C	90 °C	140 °C
HS5HG	11.7 °C	69.3 °C	100 °C	140 °C

6.3.5 Drug-Polymer Miscibility Studies.

Fourier transform infrared spectroscopy (FTIR) and differential scanning calorimetry (DSC) were used to understand drug-polymer interactions. FTIR was conducted, using a Thermo Fisher Scientific Nicolet iS10 with attenuated total resonance and a diamond tip (ATR) and analyzed using OMNIC specta software, on raw polymer and drug and compared to formulations on the surface and core of the rod. Spectra contained 32 scans from 400-4000 cm^{-1} wavenumber and looking at % transmission. Additionally, DSC (Mettler Toledo, DSC2620) was used to evaluate melting temperatures (T_m) and glass transition temperatures (T_g) for drug, polymer, and formulations. Briefly, samples were heated from -20 °C to 160 °C or 275 °C, at a rate of 10 °C/min, for progesterone and acyclovir formulations respectively.

6.3.6 HPLC Methodology for *In Vitro* Analysis.

Samples were run on a Water Alliance 2695 HPLC equipped with a Waters 410 UV absorbance detector and a Waters Atlantis T3 Column 100Å, 5µm, 4.6 mm x 150 mm column. A gradient system composed of Solvent A: Water + 0.05% phosphoric acid, Solvent B: Acetonitrile + 0.05% phosphoric acid, and Solvent C: Methanol + 0.05% phosphoric acid was used with a flow rate of 1.0 mL/min. The column temperature was kept at 35 °C while the autosampler was kept ambient. UV wavelengths and mobile phase gradients are also drug dependent and specified in Table 6.4.

Table 6.4. HPLC Method for Progesterone and Acyclovir.

Parameter	Progesterone (PRO)			Acyclovir (ACV)		
Gradient System	Time (min)	%A	%B	Time (min)	%A	%C
	0	50	50	0	100	0
	6	0	100	1	100	0
	6.01	50	50	6	0	100
	10	50	50	6.01	100	0
				10	100	0
UV Wavelength	240 nm			252 nm		

6.3.7 Drug Solubility and Stability Studies.

Drug solubility and stability was evaluated to ensure sink conditions within the IVE study were maintained. For solubility, a saturated solution of drug in 10 mL of PBS with and without 1 % SLS was tested for both drugs. Samples were then spun down and supernatant collected and diluted 1:10 to ensure quantitative results. Stability studies were run to ensure that drug was stable in solution over longer periods of time. This allows time points to be stretched out assuming sink conditions are met.

6.3.8 Drug Loading Efficiency.

Drug loading efficiency was determined for each polymeric rod sample. Generally, rod samples approximately 5-10 mg in mass were collected and the drug extracted. The extraction was analyzed on HPLC to determine the appropriate loading efficiency. For progesterone, samples were dissolved in extraction media at a concentration of 1 mg/mL. The media consisted of a 1:1:18 DCM:DMSO:ACN mixture. The solvents were added individually in the order presented to the sample with at least 30 minutes of mixing between additions. The resulting mixture was then diluted 1:10 using the same mixture of solvents into the theoretical working range drug concentration of 50 µg/mL. For acyclovir containing devices, the same procedure was carried out with the one major change being a switch from ACN to MeOH due to the HPLC mobile phases used. When using HPLC to evaluate the loading efficiency, a separate calibration curve was made in the identical extraction media with 10 samples serially diluted 2-fold from 1 mg/mL. Drug loading efficiency was characterized by Equation 6.1:

$$loading\ efficiency\ (\%) = \frac{mass\ of\ drug\ in\ device}{mass\ of\ device} \quad \text{(Eq. 6.1)}$$

6.3.9 *In-Vitro* Elution Studies.

Samples of formulated rod were placed in a 20 mL vial and numbered for reference. Rods were cut approximately 1 cm in length and weighed to normalize data in later calculations. 5 mL phosphate buffered saline (PBS) solution with 1% w/v sodium lauryl sulfate (SLS) at a pH 6.8 was used. At each time point, media was removed and diluted 1:10 or 1:1 with fresh media for HPLC to ensure values fell within the working range of the calibration

curve. Fresh media was placed in the vial and the samples incubated at 37 °C. On weekends, media volume was doubled or tripled to maintain sink conditions. Daily release and cumulative release were calculated as raw amount and percent release for each polymer sample.

6.4 Results and Discussions

6.4.1 Polymer Selection and Modification

Polymers with minor chemical changes were used to investigate the effect of polymer properties on the release kinetics of a drug. Polymers based on HTy were chosen due to the lower processing temperatures. Diacid chain length impact was investigated due to tunability in degradation/resorption, thermal properties, and hydrophobicity. Increasing carbon chain length in the diacid from glutarate (3), to suberate (6), to dodecanedioate (10), resulted in increased hydrophobicity (Figure 6.7A). The increase in chain length led to slower degradation and resorption rates (Figure 6.7C-D). HS was determined to be the lead candidate due to it having the lowest melt temperature (Figure 6.7B).

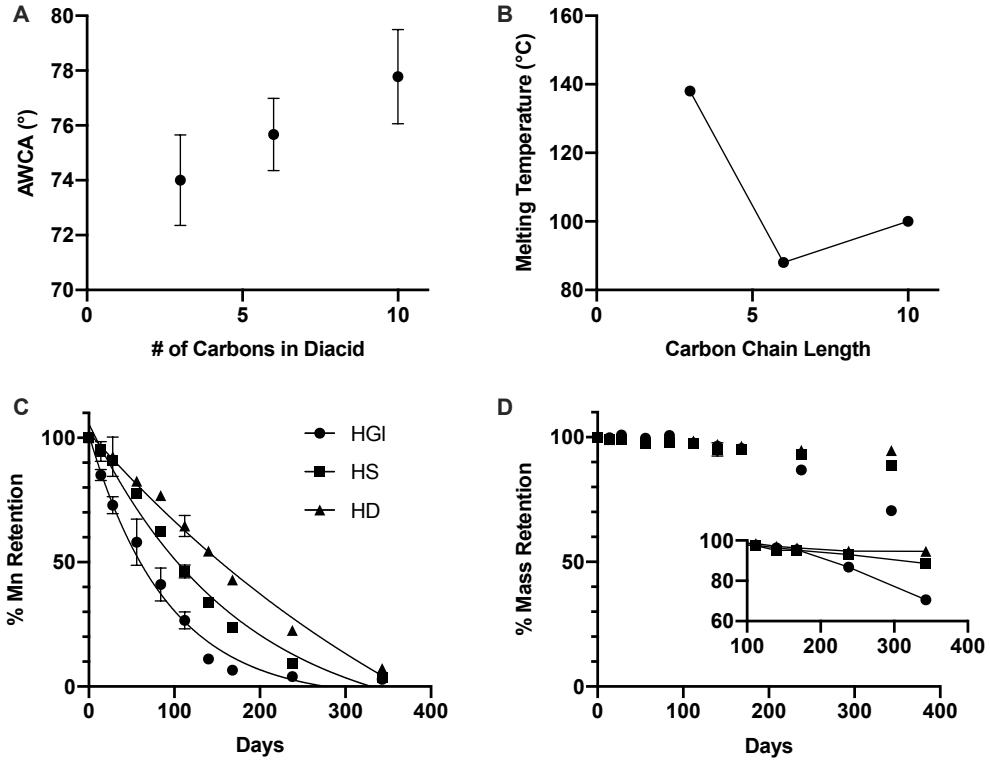

Figure 6.7. HTy based poly(ester-arylate)s with tunable properties including (A) hydrophobicity, (B) melting temperature, (C) degradation, and (D) resorption.

Another trend to investigate was the incorporation of PEG into the polymer backbone. Incorporating a hydrophilic block into the backbone of a hydrophobic polymer induces phase separation which can facilitate the release of a hydrophobic drug. PEG incorporation plays a role in the thermal properties along with the chemical properties of the polymers. Several amounts of PEG incorporation were investigated including 1%, 5%, and 10%. Addition of larger percentages of PEG resulted in lower amounts of the HTy component. This is expected to decrease crystallinity in addition to the other material properties. One initial synthetic observation was the change in molecular weight growth kinetics. Larger amounts of PEG resulted in lower molecular weights. This is most likely

a result of more water present in the reaction, quenching catalyst. Overall increasing PEG incorporation led to a more hydrophilic material and lower glass transition and melt temperatures (Figure 6.8). For the purpose of this work, modifications to HS were used and 5% PEG addition was explored as a balance between synthetic complexity and hydrophobicity.

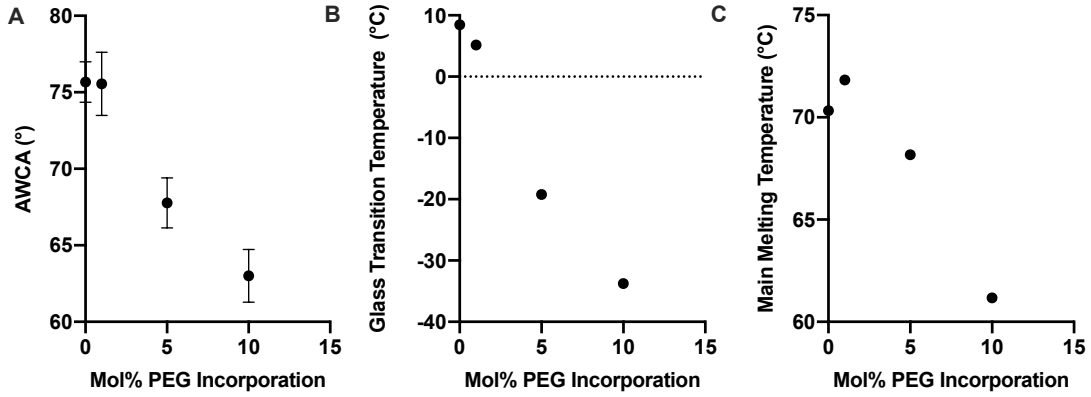

Figure 6.8. Impact of PEG incorporation in HS on material properties including (A) hydrophobicity and (B-C) thermal properties.

Finally, incorporation of hydrophilic drugs into hydrophobic polymers leads to burst release or "dumping" of drug due to poor polymer-drug interaction. One way to limit this is through hydrogen bonding sites in the polymer. Incorporation of amides into the polymer backbone provides a perfect functionality to promote hydrogen bonding between the polymer and the API. In order to minimize the thermal processability of the polymer, the diacid needed to be modified while maintaining levels of crystallinity so the polymer still exhibited a melt feature. The combination of an amino acid with a cyclic anhydride to afford a diacid component has been used as an additive in topical formulations for

dermatological purposes.[158] That being said, it is to the best of our knowledge that no one has used these functionalities in polyesters. To maintain crystallinity, it was decided to design a diacid that did not have any pendant chain. Based off of glycine and succinic anhydride, the diacid was similar in length to suberic acid with an incorporation of the amide. Synthetically, incorporation of the amide-containing diacid was limited to 5 mol% due to poor molecular weight growth at higher amounts. As expected, the incorporation of the amide into the polymer backbone, resulted in an increase in the glass transition temperature from 8.5 °C to 11.7 °C due to hydrogen bonding and the melting point increased from ~70 °C to 80 °C (Figure 6.9).

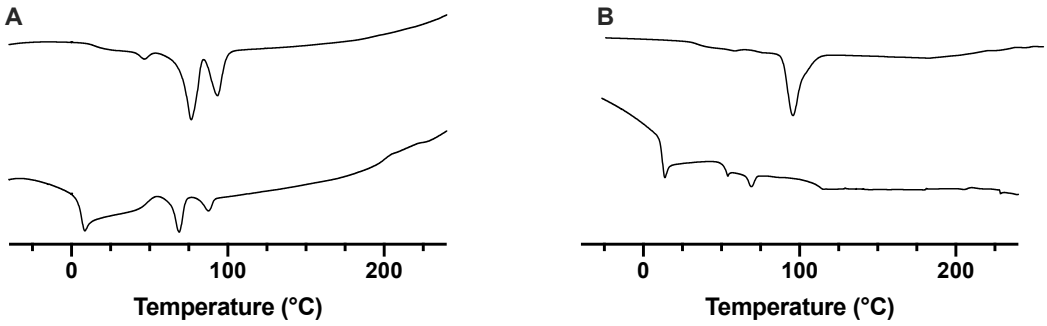

Figure 6.9. DSC of HS (left) and HS5HG (right) with both the initial heat (top) and reheat (bottom) show a slight shift in glass transition temperature.

6.4.2 Melt Processability of Polymers

Implantable rods are fabricated using extrusion techniques. In order to determine the potential for extrusion of the polymers, capillary rheometry was completed. At a minimum of three temperatures, starting at ~20 °C above the polymer's melting temperature, shear viscosities were measured at 5 stages of shear rate from 10 to 1000 s^{-1}

(Figure 6.6). All polymers were processable at temperatures well below their decomposition temperatures, which are above 300 °C. HS5PS was processable at the lowest temperature of 90 °C. HGl on the other hand had the highest temperature to process which was expected due to its higher melting point. Additionally, the incorporation of amide in the polymer backbone did not inhibit the processability of the polymer which can be a concern due to hydrogen bonding. It is expected that processing temperatures may be slightly lower than rheometry suggests due to plasticization from the API, especially at 50 % w/w loading.

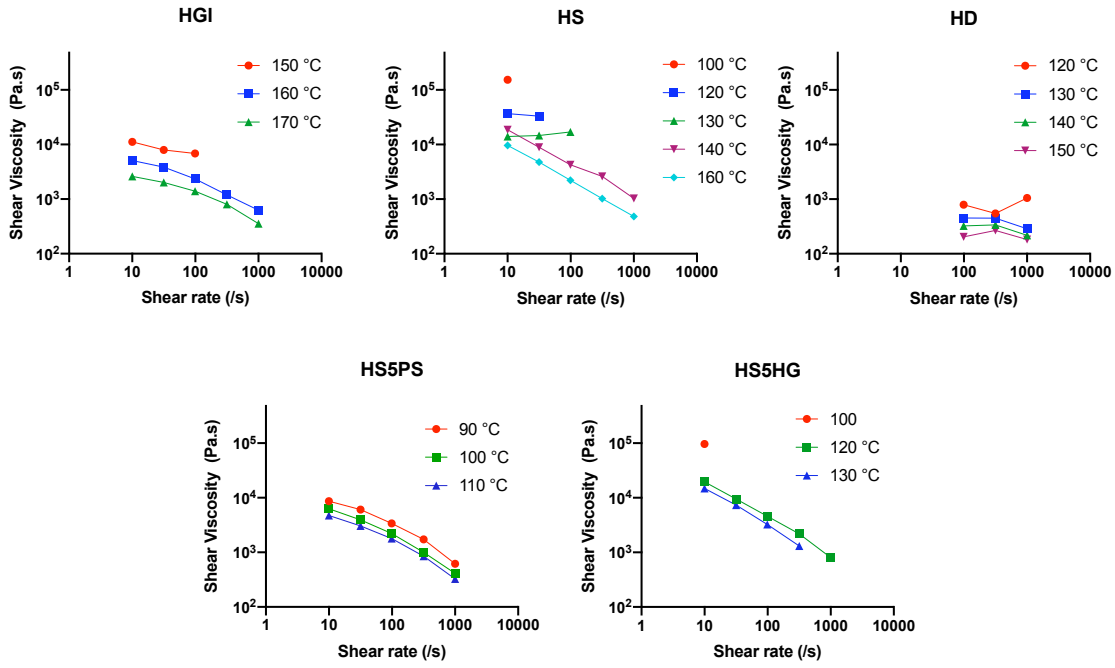

Figure 6.6. Melt capillary rheometry of polymers at various temepratures.

6.4.3 Formulation and Drug Loading Efficiency

Implantable rods with a defined diameter of 3 mm long were formulated at 50% w/w drug loading. These implants can be used for subcutaneous implant for the treatment

of diseases like HIV and contraceptives for birth control. Two model drugs were chosen to represent hydrophobic and hydrophilic APIs as a way to identify interactions between hydrophobic polymers and various drug types. A capillary rheometer was used to extrude rods, using a die to define the diameter of the rod. One important note is the ability for the drug to act as a plasticizer during melt processing, enabling lower temperatures to formulate the device. Two processing temperatures were tested for each polymer to identify implications in processing temperature.

Table 6.5. Drug loading of progesterone in extruded polymeric rods.

Polymer	Processing Temperature (°C)	Attempted Loading (%)	Loading Content (%)	Loading Efficiency (%)
HGl	125	50	45 ± 2	89 ± 4
	145	50	47 ± 1	93 ± 2
HS	90	50	45 ± 1	91 ± 2
	125	50	49 ± 2	97 ± 3
HD	100	50	41 ± 3	82 ± 6
	125	50	44 ± 2	87 ± 6
HS5PS	90	50	48 ± 3	97 ± 6
	110	50	48 ± 2	96 ± 5
HS5HG	90	50	44 ± 0.1	88 ± 0.1
	125	50	43 ± 2	87 ± 4

For progesterone loaded rods, all of them had high loading efficiencies (Table 6.5). This is expected as the both the drug and polymer are considered hydrophobic. The most hydrophilic polymer, which was PEG containing, had the lowest loading efficiency of the batch. Overall, all polymers were able to load drug at over 40 % w/w out of an attempted 50 % w/w loading and efficiencies were all above 80 %, most over 90 %. It is important to note for progesterone-loaded rods that the melting temperature of the drug itself is 125 -

130 °C. This means that drug was partially melted for samples processed above 125 °C while ones below were not. For those where the polymer and drug melted, the rods were clear with a slightly yellow tinge. All polymers were tacky upon extrusion, most likely due to melted drug. One exception to this was HS, which exhibited stickiness from the polymer itself. Despite translucency during processing, after 24 hours at ambient conditions, the polymer and drug crystalized and an opaque white rod was formed (Figure 6.7).

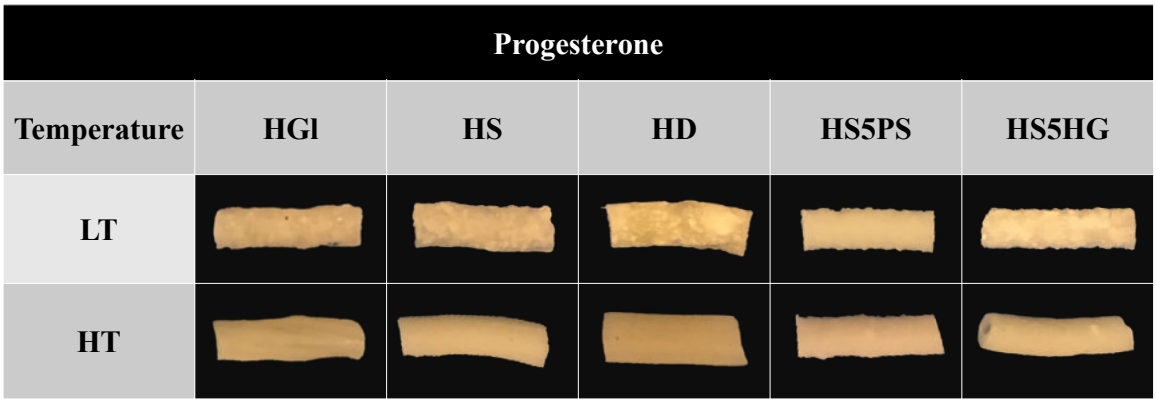

Figure 6.7. Images of progesterone-loaded polymeric rods post extrusion.

Table 6.6. Drug loading of acyclovir in extruded polymeric rods.

Polymer	Processing Temperature (°C)	Attempted Loading (%)	Loading Content (%)	Loading Efficiency (%)
HGl	125	50	39 ± 6	78 ± 12
	140	50	37 ± 3	74 ± 6
HS	100	50	32 ± 2	64 ± 4
	140	50	38 ± 4	76 ± 7
HD	100	50	35 ± 2	69 ± 5
	140	50	34 ± 6	68 ± 12
HS5PS	140	50	44 ± 7	88 ± 15
HS5HG	100	50	39 ± 1	77 ± 3
	140	50	42 ± 4	83 ± 7

As expected, the acyclovir-loaded rods were less successful with loading efficiencies (Table 6.6). This is most likely due to inherent phase separation from a hydrophilic drug contrasting with the hydrophobic polymer. PEG-containing polymers and amide-containing polymers had better drug loading then pure HS which is most likely due to the functionalities facilitating the drug-polymer interactions. The most hydrophobic polymer, HD, was also the least efficient in loading, with only ~ 35 % w/w loading out of the 50 % attempted, a 69 % loading efficiency. Processing temperature also played a role in the sample appearance. For all polymers, higher processing temperatures resulted in a barbed like appearance for the rods (Figure 6.8). This is most likely the outcome of phase separation and the drug coming to the surface of the polymeric rod. While the drug stayed within the polymer matrix, it is expected that higher processing temperatures will exhibit a higher burst release *in vitro*. This adds another handle to control drug release, which is affected by the processing temperature of the rod.

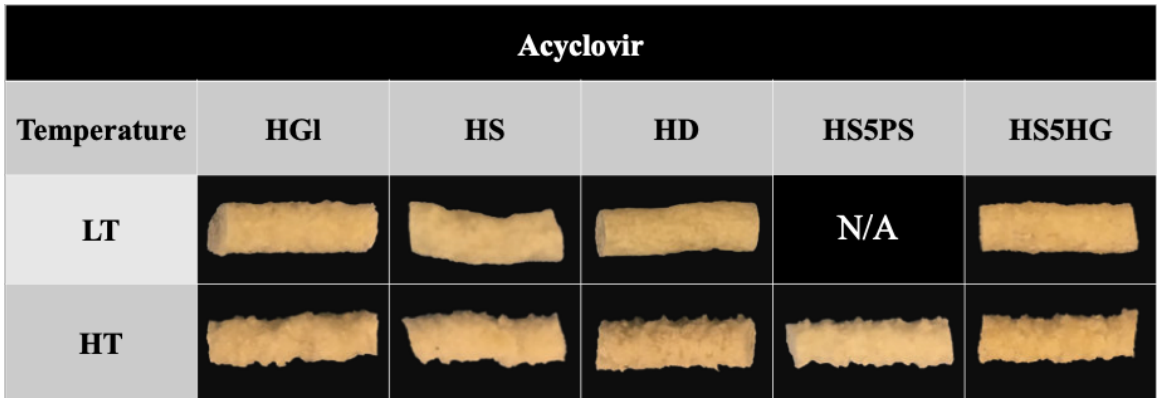

Figure 6.8. Images of acyclovir-loaded polymeric rods post extrusion.

6.4.4 Device Characterization

Formulations were characterized by FTIR for polymer drug interactions and DSC for thermal analysis. Both were used to qualitatively confirm the presence of drug. FTIR provided a spatial and qualitative look at where drug resides in the rod. Using a micro-ATR tip for the FTIR enabled us to look at the difference in spectra for the surface of the rod versus the core of the rod. Micro-ATR has a depth of penetration around 0.5-3 μm so differences can be expected based on portions of the rod that are exposed to the laser. Qualitatively, all samples including both core and side of the rod contained polymer and drug peaks.

For progesterone-loaded rods (Figure 6.9 and 6.10), processing temperatures lower than 125 °C resulted in higher amounts of drug on the surface relative to the polymer. The exception to this was HS5HG which showed similar spectra regardless of location. At higher processing temperatures, differences in the spectra were minimal. Comparatively, greater discrepancies were noticed in the acyclovir-loaded rods (Figure 6.11 and 6.12). This was expected due to a larger mismatch between the polymer and drug hydrophobicity. Higher processing temperatures had more prominent drug-related peaks on the surface of the rods compared to lower processing temperatures. This is hypothesized to be due to phase separation during processing, “pushing” drug to the surface. HS5PS had the most spectral consistency at a higher processing temperature, which would be expected given the hydrophilic oligomers.

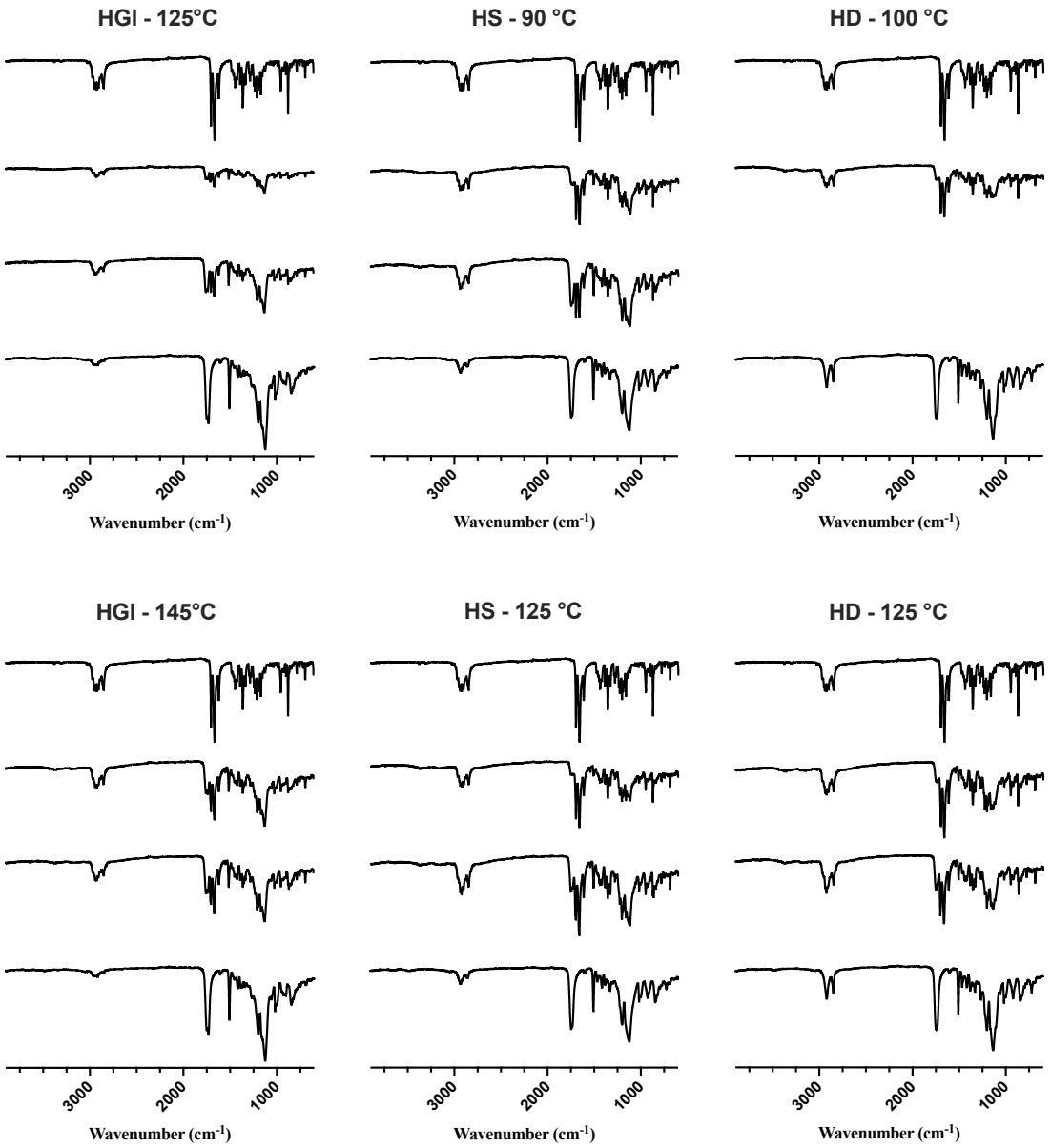

Figure 6.9. FTIR spectra investigating diacid length trends of polymer only, polymer-progesterone formulation core, polymer-progesterone formulation side, progesterone only (bottom to top) at different processing temperatures.

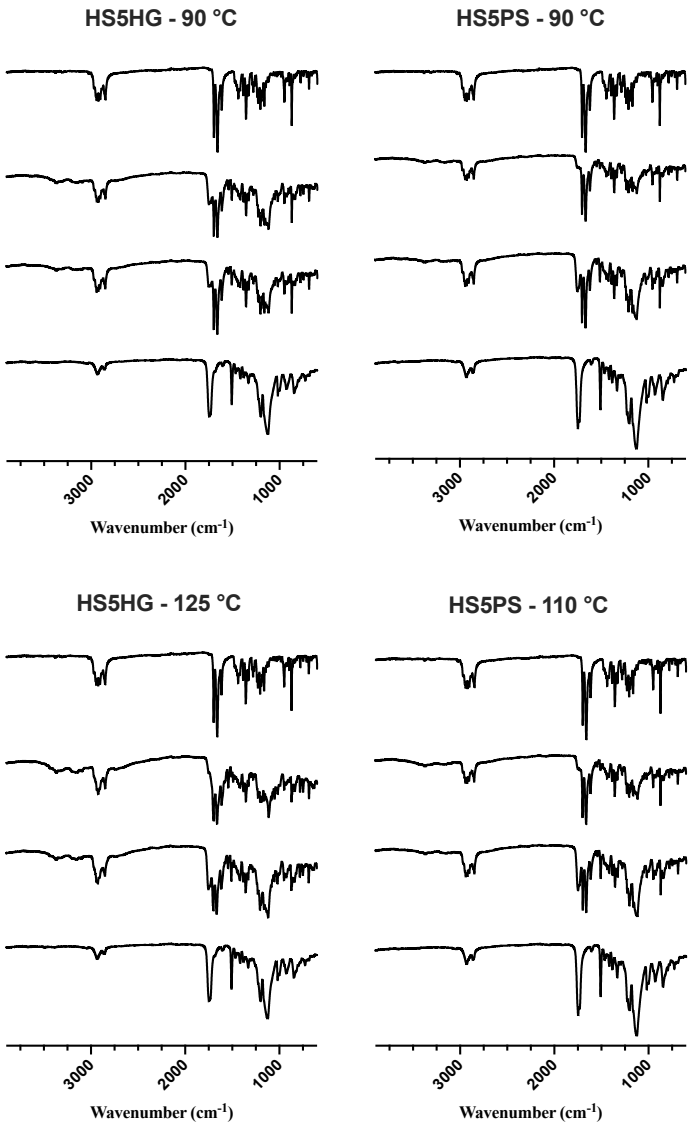

Figure 6.10. FTIR spectra investigating functionality trends of polymer only, polymer-progesterone formulation core, polymer-progesterone formulation side, progesterone only (bottom to top) at different processing temperatures.

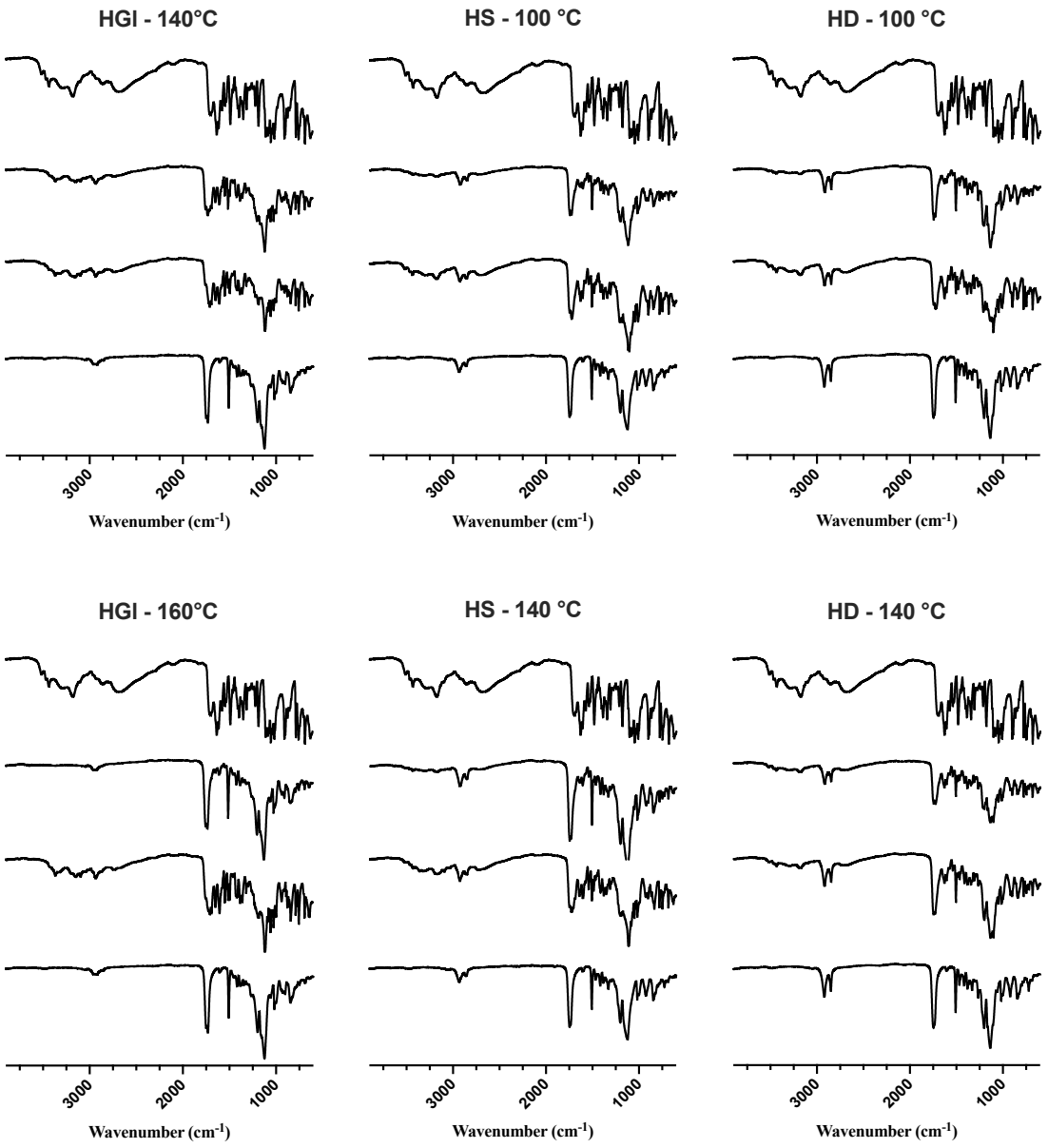

Figure 6.11. FTIR spectra investigating diacid length trends of polymer only, polymer-acyclovir formulation core, polymer-acyclovir formulation side, acyclovir only (bottom to top) at different processing temperatures.

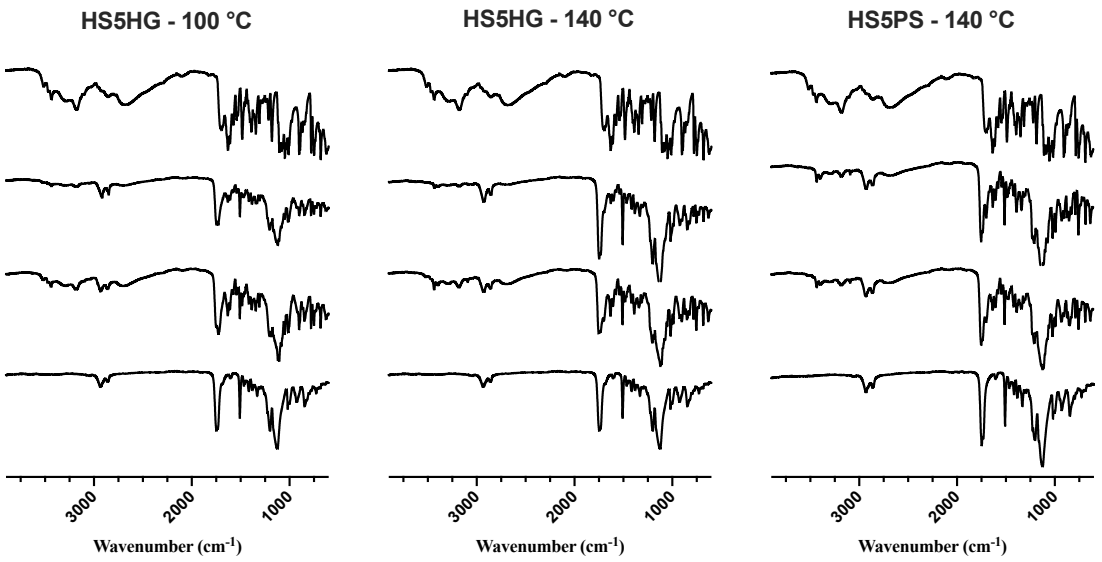

Figure 6.12. FTIR spectra investigating functionality trends of polymer only, polymer-acyclovir formulation core, polymer-acyclovir formulation side, acyclovir only (bottom to top) at different processing temperatures.

Additionally, DSC was used to understand the impact thermal processing had on the thermal properties of the drug and polymer. For progesterone, there were two crystalline forms of the drug present in most formulations (Figure 6.13). This is due to the proximity of the processing temperature to the drug's melting temperature (125 – 130 °C). Form I of progesterone has a melting temperature of ~ 128 °C while form II has a melting point of ~ 122 °C. These have implications on solubility, with form II exhibiting greater solubility in PBS.[159] All formulations containing progesterone, had broadening of the drug's melting endotherm due to disruption in the crystal packing from polymer-drug interactions. Additionally, formulations processed at 125 °C and above showed either exclusively form II of the drug or a mixture of both forms. The exception to this was the PEG-containing polymers which even at lower processing temperatures of 90 °C, had

extreme broadening of the drug's melting endotherm. This indicates polymer-drug interactions that can facilitate release during implantation. Overall, all progesterone-containing formulations showed drug incorporation into the polymer matrix.

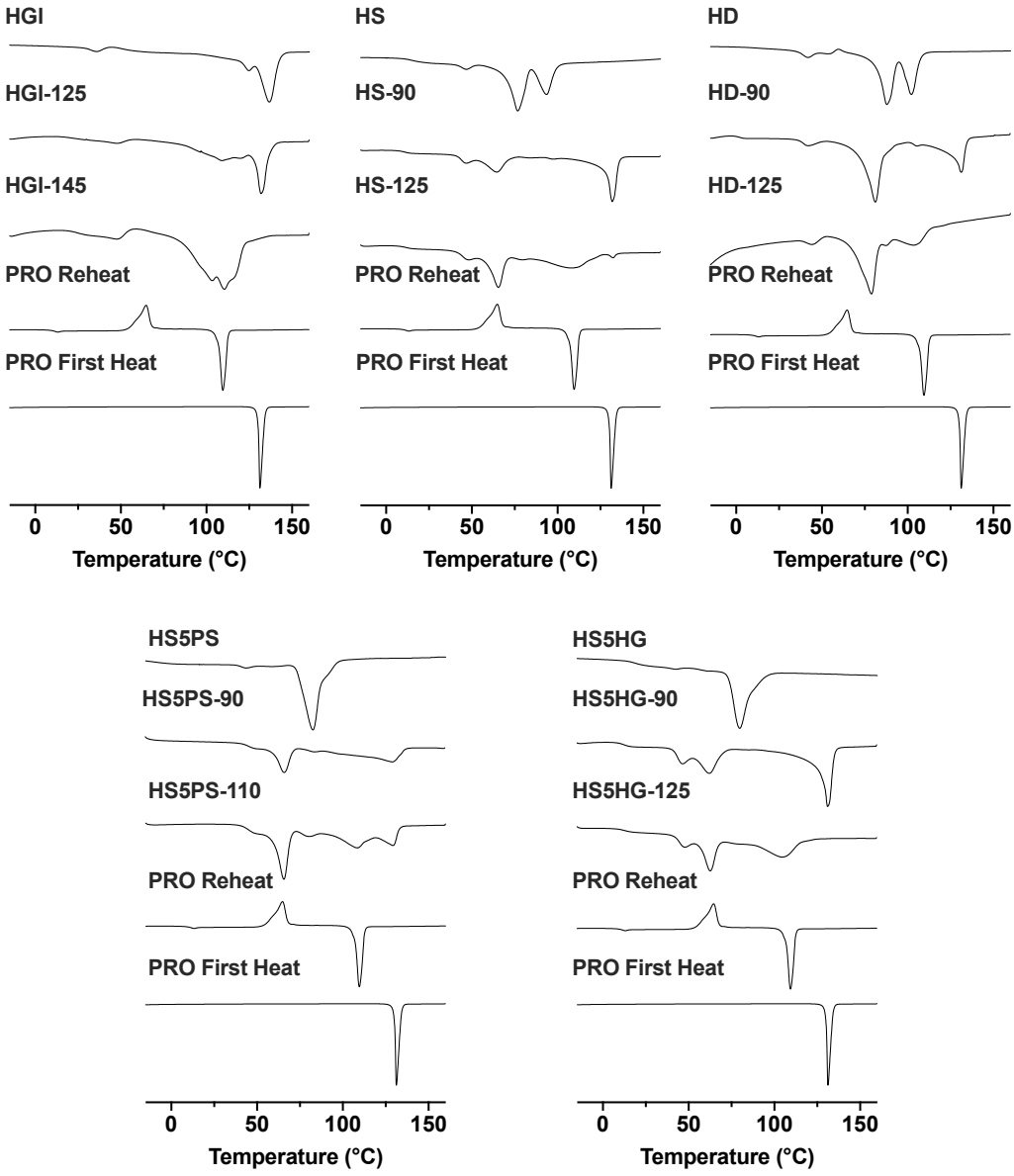

Figure 6.13. DSC curves for formulations of progesterone with various polymers. All curves shown are the first heat only with the exception of the drug reheat, denoted PRO reheat.

Comparatively, all acyclovir-containing formulations were processed below the drug melt temperature, which is reported at ~ 255 - 260 °C. Acyclovir is unique in its ability to hydrogen bond at multiple domains within the molecule (Figure 6.14). In the presence of polymers, acyclovir has been reported to reside in forms I or VI. Polymers including PET, PVC, PVS, PP produced form VI while nylon 6,12 produced a mixture of forms VI and II.[160] The one distinction is form VI of acyclovir, which has reportedly formed in the presence of nylon 6,12, a polyamide, and contains a melting point that is sharp and in between form I's broad melting point and form II's sharp melting point. When heated to the drug melting point, all formulations exhibited broadening of the melting endotherm for the drug, switching from form V to form I. (Figure 6.15). This confirms polymer-drug interactions and incorporation in the polymer matrix. While all melting endotherms looked the same, the one exception to this was HS5HG formulated at 140 °C. The melting point for the drug in this curve showed two overlapping peaks. This could be due to hydrogen bonding between the polymer and drug resulting in a slight increase in melting temperature, albeit lower than the melting temperature of the drug with no polymer interaction.

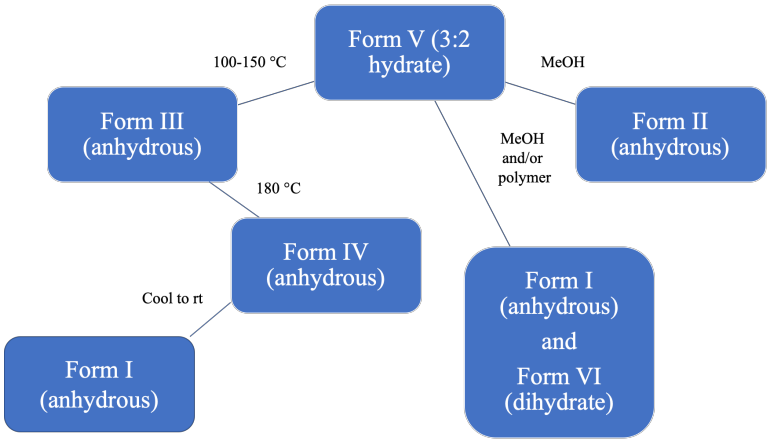

Figure 6.14. Polymorphs of acyclovir.[160]

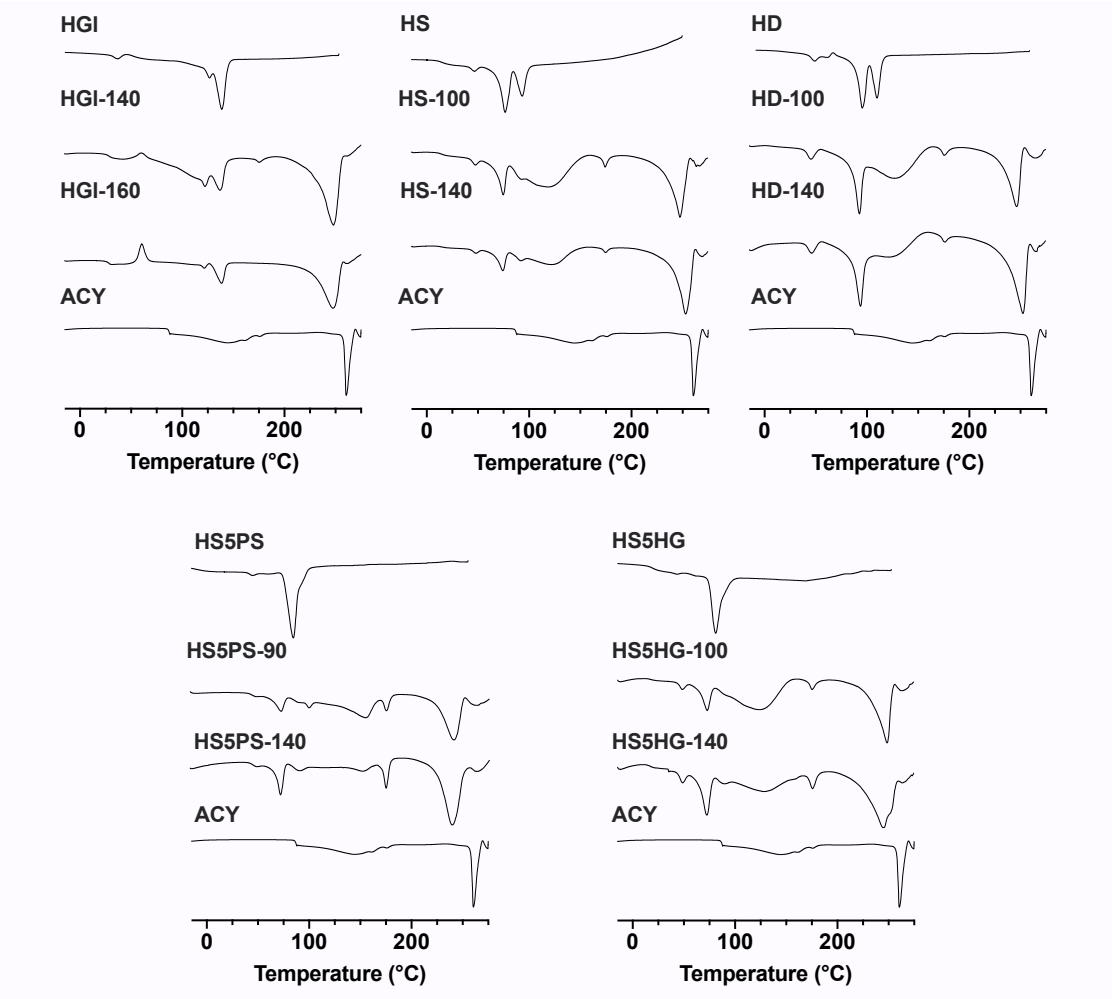

Figure 6.15. DSC curves for formulations of acyclovir with various polymers. All curves shown are the first heat only.

When investigating the hydrogen bonding potential of HS5HG with acyclovir during melt processing, we compared mixed drug and polymer to thermally processed ones. HS5HG is the only formulation that shows the presence of form VI when heated to the higher processing temperature (Figure 6.16). Additionally, FTIR was used to investigate drug form. Unfortunately form VI, which was most interesting due to its polymer interactions was not identified due to its poor stability without polymer. By

spectral comparison, acyclovir as is resides in Form V. Thermal processing and polymer drug interactions cause changes in form, mostly to form I or II depending on the polymer. This confirms that incorporation of amides into the polymer backbone can facilitate hydrogen bonding between the drug and polymer matrix.

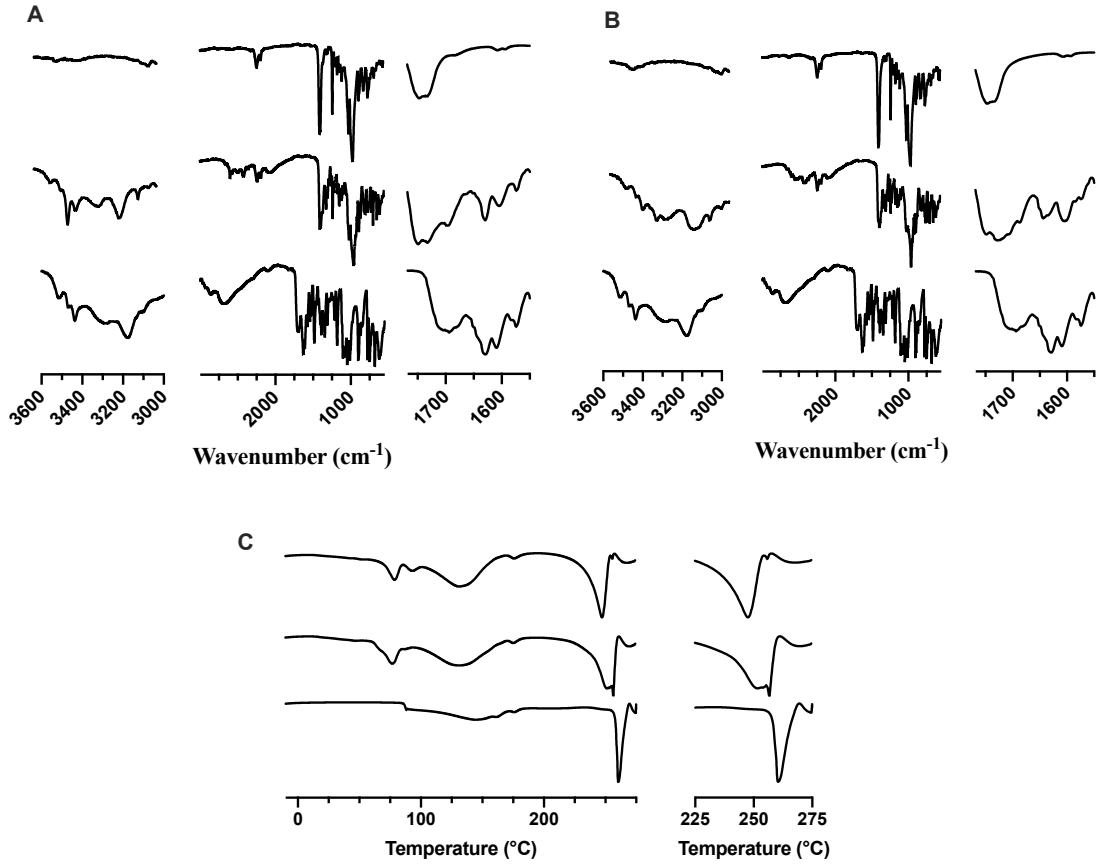

Figure 6.16. FTIR of (A) HS5HG and (B) HS formulations comparing polymer (top), polymer-drug (middle), and drug (bottom) with focuses on the amine/alcohol region and carbonyl/alkene region. (C) DSC of HS + acyclovir, HS5HG + acyclovir, and acyclovir alone (top to bottom), with a focus on the melting point at 260 °C.

Overall both hydrophobic and hydrophilic model drugs showed interactions with the polymer matrix, regardless of the diacid present with the most notable differences being progesterone's interaction with PEG-containing polymer and acyclovir's interaction with GSD-containing polymer. Characterization confirmed the presence of multiple forms of acyclovir in the formulation, primarily forms I, II, and VI depending on the polymer. Progesterone also had multiple forms, I and II. Polymer choice and processing temperature played a role in the forms of drug present. These are expected to impact release profiles.

6.4.5 *In Vitro* Elution Studies

Release of drug from a polymeric device is controlled by a combination of diffusion of water into the polymer matrix and degradation of the polymer device. *In-vitro* elution was tested for 19 different samples in triplicate, varying 5 polymer, 2 processing temperatures per polymer, and 2 drugs. Extruded rods 3 mm in diameter and 1 cm long were used for this study. PBS at a pH of 6.8 with 1% w/w SDS was used as the elution media to increase progesterone's solubility from 0.1 mg/mL in water to 2.45 mg/mL in the chosen media. It was important to keep the pH neutral to prevent any acid catalyzed degradation of the polymer. Acyclovir was less of a concern given its hydrophilicity. All samples were weighed and placed in 20 mL glass vials and 5 mL of media was used daily with the exception of weekends and one-week time points later in the study which used 10-15 mL each. Aliquots were taken for HPLC at each time point to measure release and the entire media was exchanged. This ensured sink conditions throughout the study. For all samples, daily release curves and cumulative release curves were calculated. All samples

were plotted as both mass and percentage release. Samples were analyzed up to 46 days, at which point a linear release rate was established.

Rods loaded with progesterone released in two phases (Figure 6.17). Both polymer composition and processing temperature resulted in changes in the release. Progesterone release was largely dictated by processing temperature. As mentioned, processing the implant by melting both the polymer and drug increased the release rate most likely as a result of increasing the drug's solubility. Additionally, functional polymers played a role through increasing water uptake to the polymer. Phase separation is hypothesized to enable release of drug from an otherwise hydrophobic polymer. PEG can cause phase separation, promoting the release of even hydrophobic drugs.[50] Increasing the diacid chain length, and as a result, the polymer hydrophobicity, had minimal effect on the release rates of the drug. Other than HS processed at 90 °C, all release rates had similar results.

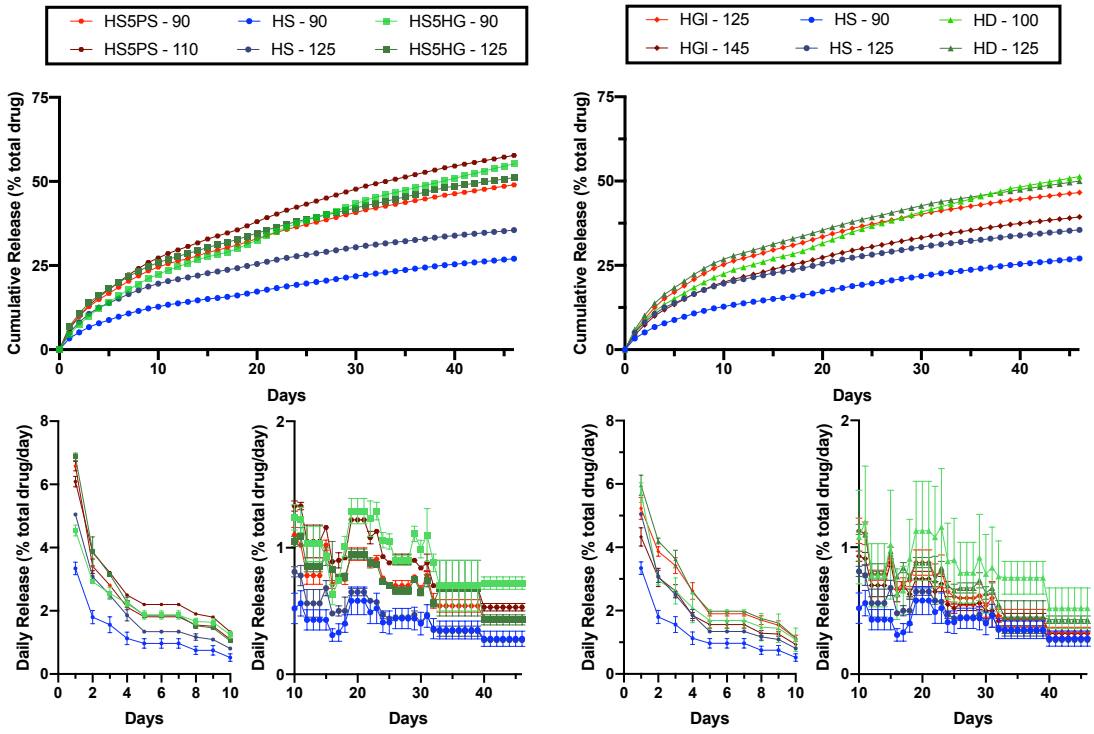

Figure 6.17. Progesterone release rates for functional polymers (left) and tunable diacid length polymers (right). Data is plotted as cumulative release (top) and daily release (bottom).

For acyclovir loaded rods, one clear impact on the release rates was the processing temperature (Figure 6.18). Regardless of diacid or functionality, higher processing temperatures, at 140 °C and above, resulted in a higher release of drug. This is most likely due to the change in form the drug had. As hypothesized, incorporating the amide into the backbone, slowed down the burst release from the polymer matrix compared to the addition of PEG. At lower temperatures, larger error bars were observed due to poor mixing of drug with polymer. Diacid chain length played less of a role in the release of acyclovir at higher temperatures but at the lower temperatures, the more hydrophobic polymer, HD, had the slowest release. This is most likely a result of the slower diffusion rate of water into the

polymer controlling the release of drug. Daily release rates at early time points had a dependence on the polymer chain length and processing temperature. Overall, this indicates that processing temperature plays a role on release rates, as expected due to changes in the drug form.

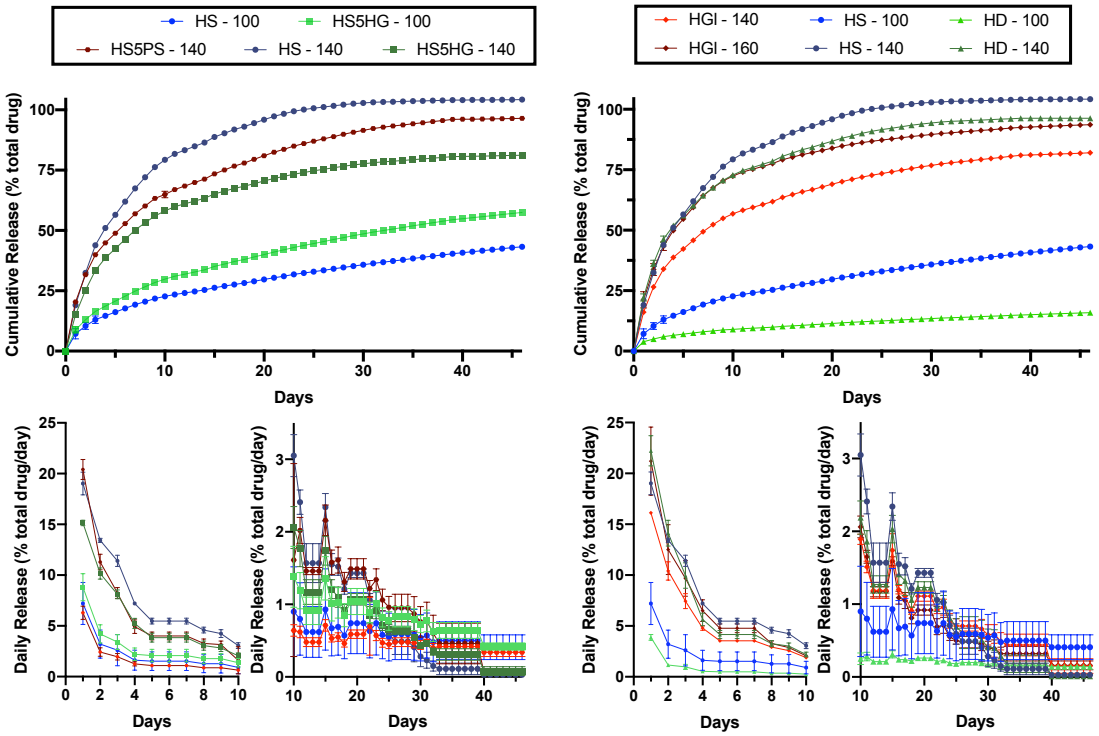

Figure 6.18. Acyclovir release rates for functional polymers (left) and tunable diacid length polymers (right). Data is plotted as cumulative release (top) and daily release (bottom).

6.5 Conclusion

Drug release tunability was demonstrated by altering polymer composition, processing temperatures, and drug-polymer hydrophobicity. Polymer composition played a larger role in processability and drug form post loading than it did on the release rates. For progesterone, diacid length was not a factor in the loading efficiency or release rate. Polymers processed at 125 °C resulted in form II of the drug while lower processing temperatures maintained form I. Higher release was exhibited in the higher processing temperature samples and the addition of PEG to the polymer backbone further increased the release rate. For acyclovir, there was less polymer-drug interactions due to the hydrophilic nature of the drug. Similarly, to progesterone, the drug form played a large role on the release. Higher temperature processing resulted in faster release while lower temperatures slowed the release but introduced more variability most likely as a result of poor mixing. In all, functional materials with indications towards controlling release by device design were established and application focused research can benefit from this fundamental study.

CHAPTER 7: CONCLUSIONS AND FUTURE WORK

"All our dreams can come true, if we have the courage to pursue them."

-Walt Disney

In this thesis, we took a wholistic approach to new biomaterial design, starting from the design phase through to the application. Throughout the work, we optimized synthetic protocols, characterized polymer properties, established structure-property relationships, and used those to select lead polymers for use in applications. This fundamental work can continue with more applications over the next several decades, exploring both fundamental science and application specific research.

Synthetically, the design of a polymer library that is based on the concept of resorbable diphenols was achieved. Tyrosol-based polymers exhibited faster resorption rates than their tyrosine counterparts. This is in large part to the compositional switch from amide to ester in the diphenol unit. Subsequent polymers investigated symmetry in the diphenol and carbon chain length or bond rigidity in the diacid. Collectively over 30 polymers were explored across multiple disciplines of science but the work translates to over 100 polymers as part of this library.

Chemical, physical, thermal, mechanical, and biological properties were all explored. Diphenols played a large role in melting points, resorption, and processing. HTy-containing polymers were lower melting and easier to thermally process. They also had increased solubility and therefore resorbed faster. Diacids played a much larger role in all polymer properties. Carbon chain length in the diacid was fundamental in the polymer

hydrophobicity and as a result degradation of the polymers. Short chain diacids showed significant mass loss in a solid polymer disc in less than a year. This is expected to further increase with increasing porosity and surface area.

Bond rigidity in the diacid has some unique properties associated with them. Double bond-containing polymers had the lowest cell adhesion of any polymer and were the faster resorbing, despite not being more hydrophilic. Aromatic rings were printable and maintained their amorphous nature due to glass transition temperatures above physiological temperatures. They also required some of the highest processing temperatures. The semicrystalline polymers were capable of improving mechanical properties through drawing and annealing fibers. All polymers had increases in mechanical properties with some of the films matching reported PLA mechanical properties. The versatility of this polymer library is expected to contribute significantly to the biomaterials field.

Moving towards translation of a material to a device, application focus research was carried out. Nerve regeneration, additive manufacturing, and drug delivery were all explored and modifications made to the polymer library to improve their efficacy. Two lead candidates for nerve guidance braided conduits were chosen from over 100 polymers through structure-property analysis focusing on mechanical strength, biocompatibility, and resorption profiles. Those two materials were fundamental in securing funding for in vivo studies which are planning to be carried out as a follow up to this work.

3D printing is a fast-growing area of biomaterials research and there is a clear need for new materials with tunable properties. Printability was established in HTy-containing polymers due to their low processing temperatures. Minor chemical modifications through

end capping of low molecular weight polymer chains with alkenes allowed for post printing thiol-ene chemistry to chain extend or crosslink the material. This increase polymer properties while still maintaining degradability and biocompatibility. This work also has potential to incorporate bioactive molecules into the polymer matrix. The presence of thiols in bioactive molecules such as peptides and protein allow for similar conjugation techniques which can further enhance the bioactivity of the polymers.

Lastly drug delivery was explored as a result of previous success with tyrosine derived polymers. Long acting implantables require strong polymer-drug interactions with tunable degradation to control release of the drug. Tyrosol polymers, being more hydrophobic, were capable of loading high amounts of progesterone, a hydrophobic drug, while maintaining controlled release. Incorporating PEG into the polymer backbone improved the release of drug from the polymer. Likewise, hydrogen bonding was used to reduce burst release of hydrophilic drug in the polymer matrix. Through structural investigations, the polymers showed interactions with acyclovir, a hydrophilic drug, that has also been reported in the literature. This work has the ability to transform drug delivery in the market similarly to previous tyrosine derived polymers that impacted drug release as coatings a decade ago.

While this concludes the work presented in this thesis, many additional research activities are being carried out past my thesis. Specifically, polymer-peptide conjugates for controlled degradation and resorption is continuing to be explored within the lab in an effort to make more cell-selective materials. Additionally, unique biological properties of these polymers will be further explored for potential cues into polymer design moving forward. Drug delivery also has other potential aside from the previously mentioned work.

Self-assembled nanospheres and microparticles have shown preliminary promise using these materials and further research is anticipated from this. In all this work didn't just complete a degree but it provided a foundation for years of research to come. Establishing a new polymer library and characterizing it across the field is daunting but necessary to accelerate research on new materials for the future. It is my hope that my legacy within this research is not just in the data presented today but also the data and research to come over the next decade.

Appendix 1. Biological Evaluation of Tyrosol-Derived Poly(ester-arylate)s.

In this section, preliminary *in vitro* cell culture work was completed to evaluate the effect of polymer composition on cell adhesion and proliferation. These effects can be impacted by scaffold architecture and other external factors that were not explored in this work. It is the hope that this fundamental work will lead to the identification of unique biological properties in this polymer library that can advance specific areas of regenerative medicine. A prominent application for biodegradable materials is to support tissue regeneration. In this process, a degradable and resorbable polymeric scaffold replaces damaged or diseased tissue until newly formed tissue can form. This process involves many cell types, growth factors, and proteins. In order to better understand how the body will respond to a new material, cell-material interactions need to be evaluated.

Different cells may sense and respond to their surrounding environment differently. In order to explore if chemical properties of polymers can influence cellular behaviors, the basic cellular behaviors such as adhesion and proliferation of multiple human primary cells on polymer surfaces were assessed in vitro. Fibroblasts and stem cells are the common cell types at any wound environment including at the site of material implantation. The responses of fibroblasts and stem cells on different polymer surfaces were compared in vitro. For potential bone regeneration and nerve repair applications, the adhesion and proliferation of human osteoblasts was also evaluated on various polymer surfaces.

A1. 1 Materials and Methods

A1.1.1 Materials

Human dermal fibroblasts (HDF, #PCS-201-012) were purchased from ATCC. Human mesenchymal stem cells (hMSC, #PT-2501) were purchased from Lonza. Human Schwann cells (HSC #1700) and culture medium were purchased from ScienCell Research Laboratory. Human osteoblasts-femoral (HO-f, #4610) and culture medium were purchased from ScienCell Research Laboratory. DMEM medium for HDF, MEM-alpha medium for hMSC and fetal bovine serum were purchased from Gibco.

A1.1.2 Cell Adhesion Assay

Cells (HDF, hMSC, HO-f or HSC) were cultured and maintained following the manufactures' instructions. 10 mm/disc of polymer films were sterilized under UV for 1 h. Polymer films were placed in the wells of non-tissue culture treated 48-well plate and held in place by O-rings. Cells were trypsinized from an 80% confluent culture and counted. $2x10^4$ cells were added to each well containing polymer film and incubated at 37°C with 5% CO_2 and 95% humidity. After 24 h, medium was removed from each well and cells were washed once with PBS. 0.2 mL of medium containing 10% alamarBlue was added to each well. After incubated at 37°C for 45 min, the fluorescent intensity was read using TECAN Spark plate reader with Ex/Em=540nm/590nm.

A1.1.3 Cell proliferation Assay

Polymer films were placed in the wells of non-tissue culture treated 48-well plate and held in place by O-rings. $2x10^4$ cells were seeded onto each polymer film and incubated

at 37°C with 5% CO_2 and 95% humidity for 24 h (Day 1). The viability of cells at Day 1 was monitored using alamarBlue assay. After the assay, cells were washed with PBS twice and continued to culture for 3 days. On Day 4, the viability of cells in each well was measured using alamarBlue assay. Repeat the viability measurement on Day 7. The proliferation of cells on Day 4 or Day 7 on each polymer surface was normalized to that of Day 1.

A1.2 Fibroblasts

One of the most abundant cell types found in the body are fibroblasts. These cells are found in connective tissue and are found in wound healing applications.[161] When characterizing the cell-material interactions between tyrosol-based poly(ester-arylate)s and human dermal fibroblasts (HDF), the attachment (adhesion) of cells to different polymer surfaces were compared after 24 h. All polymer surfaces supported cell adhesion, with most comparable to tissue culture treated polystyrene (Figure A1.1A). The exceptions to this were pHTyPDA and pHTy10 which supported less adhesion. Additionally, no significant differences were found between HTy and DTy polymers except for ones containing PDA in which HTy is more adherent. Another important cellular behavior may be influenced by material is proliferation. After the adhesion, the ability of adhered cells to proliferate over 7 days on different polymer surfaces was monitored using viability assays. As shown in Figure A1.1B-C, after initial attachment, adhered cells proliferate at similar rates on different polymer surfaces. This result suggested that HDF adhered to all

polymer surfaces with certain preference. On the other hand, all polymer surfaces supported the proliferation of HDF similarly.

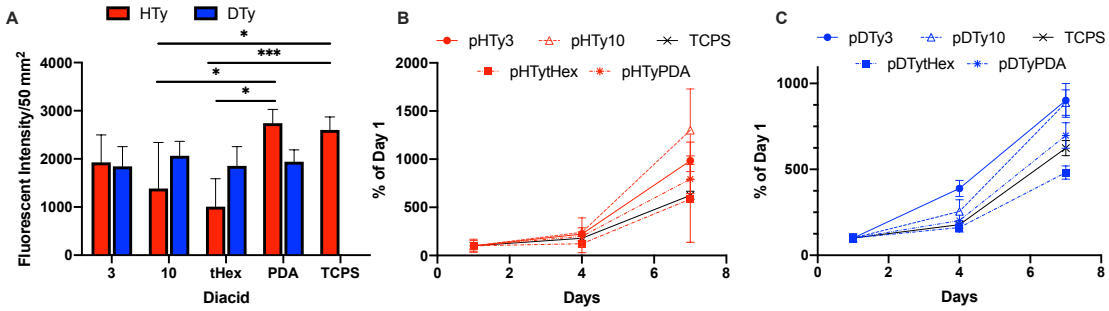

Figure A1.1. HDF adhesion (A) and proliferation rates for HTy (B) and DTy (C) polymers. All samples had an n = 4 and two-way ANOVA tests were run with post-hoc Tukey test where * = $p<0.05$ and *** = $p<0.005$.

A1.3 Human Mesenchymal Stem Cells

Human mesenchymal stem cells (hMSC) are another common cell type biomaterials encounter *in vivo*. hMSCs can differentiate into myocytes (muscle), adipocytes (fat), osteoblasts (bone), neurons (nerve), or chondrocyte (cartilage) depending on the environment they are in.[162-164] Through gene expression analysis, we can gain insight into a material's ability to promote specific tissue regeneration *in vivo*. hMSCs adhere to all polymers with the exception of the tHex polymers which were non-adherent and did not support proliferation (Figure A1.2A). Another trend that was observed is that HTy polymers had higher proliferation rates compared to DTy ones (Figure A1.2B-C).

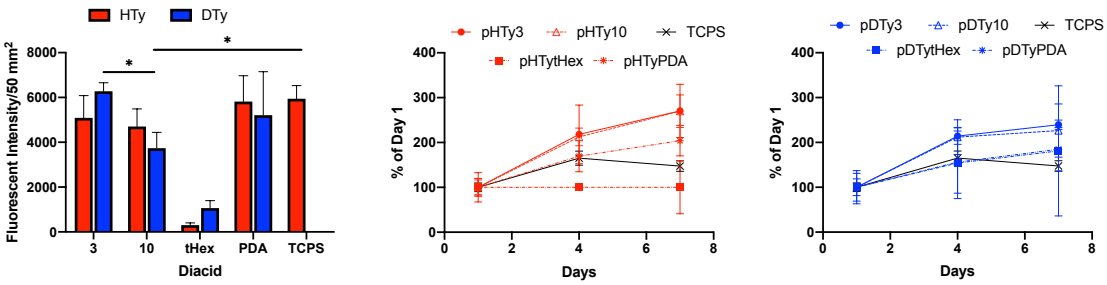

Figure A1.2. hMSC adhesion (A) and proliferation (B-C) on tyrosol polymers. Two-way ANOVA tests were run with post-hoc Tukey test where * = $p < 0.05$.

A1.4 Osteoblasts

Given the hydrophobic and rigid nature of these polymers, one of the potential applications of this library of polymers is to support bone regeneration. Previous work in our lab investigating tyrosine-derived polymers have shown great promise in the regeneration of bone.[165-169] With a similar structure, it was hypothesized tyrosol polymers would also be good candidates. The interaction between osteoblasts and tyrosol polymers was also explored in this study. Human Osteoblasts (femoral) (HO-f) adhered to all polymers but seemed to be more responsive to distinct chemical composition compared with that of HDFs (Figure A1.3A-C). More hydrophobic materials tended to be better substrates with pHTy10 and pDTy10 being comparable to TCPS. Surprisingly, pDTy6 was a poor substrate for osteoblasts. This observation warrants further investigation. There is no clear reason as to why this would happen but it can be the source of further studies. Proliferation was evident in all polymers and ALP expression for all samples was similar. pDTy6 was the only polymer to have significantly lower DNA content compared to other

polymers. In all, it is evident that tyrosol polymers are a potential candidate for bone regenerative applications pending additional characterization.

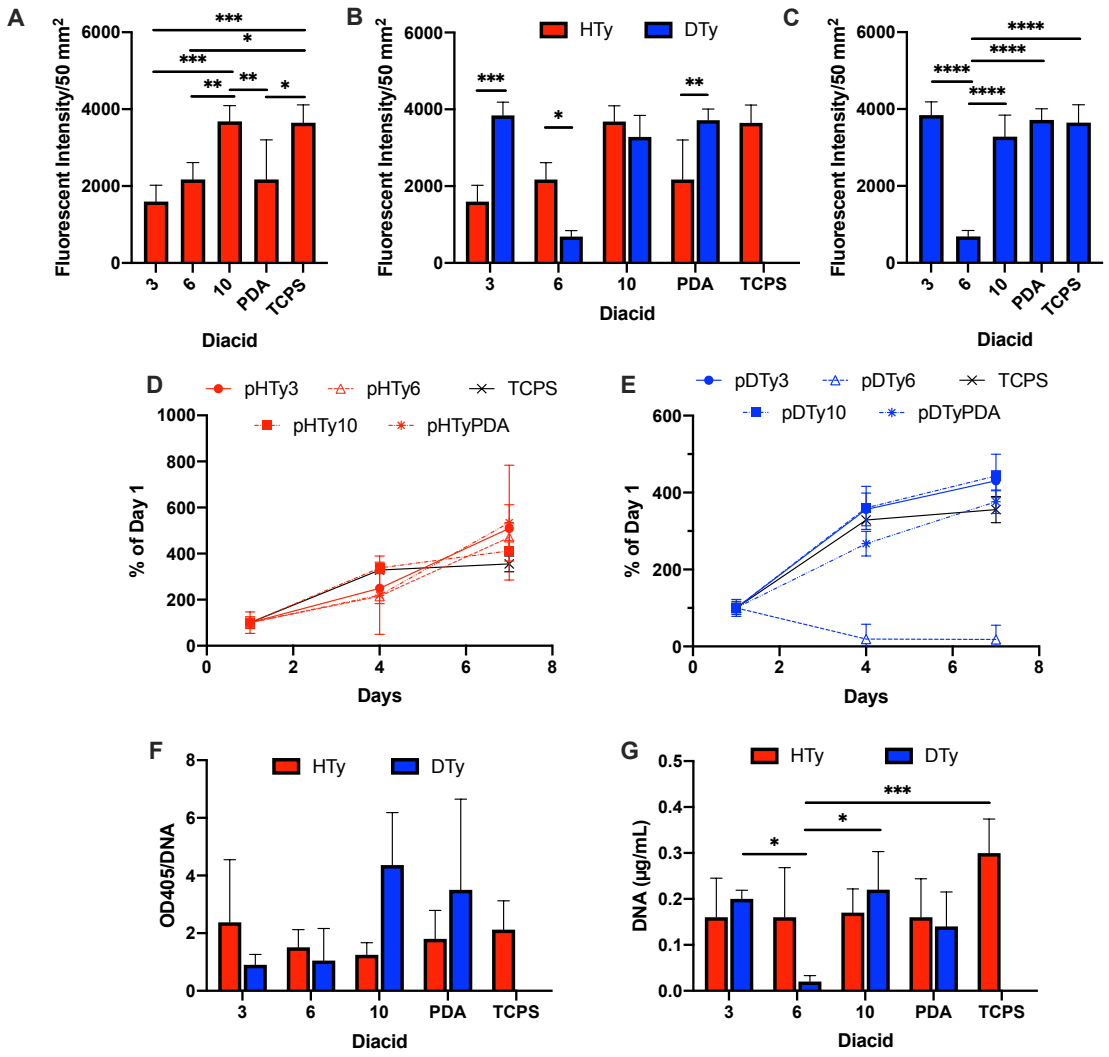

Figure A1.3. Adhesion (A-C), proliferation (D-E), for HO-f on tyrosol derived polymers. All samples had an n = 4 and two-way ANOVA tests were run with post-hoc Tukey test where * = $p<0.05$, ** = $p< 0.01$, *** = $p<0.005$, **** = $p<0.0001$.

A1.5 Conclusion

Results from these preliminary *in vitro* cell-material interaction assessments indicate that most tyrosol polymers, with the exception of tHex containing polymers, are good cell substrates and support adhesion and proliferation of various cell types participating in tissue regeneration. More interestingly, some cells such as osteoblasts seemed to be more responsive to chemical properties than other cells such as HDFs and HSCs. These observations serve as a start pointing for a more focused and detailed study for biologists in the lab in a near future.

References

1. In *Clinical Applications of Biomaterials*, NIH Consens Statement Online, Nov 1-3, 1982; Online, 1982; pp 1-19.

2. Woolf, S. H.; Schoomaker, H. Life Expectancy and Mortality Rates in the United States, 1959-2017. *JAMA* **2019,** 322 (20), 1996-2016 DOI: 10.1001/jama.2019.16932.

3. Brown, G. C. Living too long: the current focus of medical research on increasing the quantity, rather than the quality, of life is damaging our health and harming the economy. *EMBO Rep* **2015,** 16 (2), 137-41 DOI: 10.15252/embr.201439518.

4. *Biomaterials Market Size, Share & Trends Analysis Report By Product (Natural, Metallic, Polymer), By Application (Cardiovascular, Orthopedics, Plastic Surgery), By Region, And Segment Forecasts, 2020 - 2027*; 2020.

5. Huebsch, N.; Mooney, D. J. Inspiration and application in the evolution of biomaterials. *Nature* **2009,** 462 (7272), 426-32 DOI: 10.1038/nature08601.

6. Yaqub, K. M.; Min-Hua, C. A Review on role of biomaterials in biomedical field. *Int. J. Bio-Pharma Res.* **2019,** 8 (9), 2788-2793.

7. Patel, N. R.; Gohil, P. P. A Review on Biomaterials: Scope, Applications & Human Anatomy Significance. *Int. J. Emerging Tech. Adv. Eng.* **2012,** 2 (4), 91-101.

8. Langer, R. S.; Peppas, N. A. Present and future applications of biomaterials in controlled drug delivery systems. *Biomaterials* **1981,** 2 (4), 201-14 DOI: 10.1016/0142-9612(81)90059-4.

9. Kohane, D. S.; Langer, R. Polymeric biomaterials in tissue engineering. *Pediatr Res* **2008,** 63 (5), 487-91 DOI: 10.1203/01.pdr.0000305937.26105.e7.

10. Navarro, M.; Michiardi, A.; Castano, O.; Planell, J. A. Biomaterials in orthopaedics. *J R Soc Interface* **2008,** 5 (27), 1137-58 DOI: 10.1098/rsif.2008.0151.

11. Yang, Y.; Zhang, Y.; Chai, R.; Gu, Z. Designs of Biomaterials and Microenvironments for Neuroengineering. *Neural Plast* **2018,** 2018, 1021969 DOI: 10.1155/2018/1021969.

12. Huang, Y. C.; Huang, Y. Y. Biomaterials and strategies for nerve regeneration. *Artif Organs* **2006,** 30 (7), 514-22 DOI: 10.1111/j.1525-1594.2006.00253.x.

13. Allan, B. Closer to nature: new biomaterials and tissue engineering in ophthalmology. *Br J Ophthalmol* **1999,** 83 (11), 1235-40 DOI: 10.1136/bjo.83.11.1235.

14. Tuna, E. B.; Oshida, Y.; Ozen, B.; Gjorgievska, E.; Tuzuner, T. Biomaterials for Dental Applications. *Biomed Res Int* **2017,** 2017, 2520536 DOI: 10.1155/2017/2520536.

15. Langer, R. Biomaterials and biotechnology: from the discovery of the first angiogenesis inhibitors to the development of controlled drug delivery systems and the foundation of tissue engineering. *J Biomed Mater Res A* **2013,** 101 (9), 2449-55 DOI: 10.1002/jbm.a.34811.

16. Buckles, R. G. Biomaterials for drug delivery systems. *J Biomed Mater Res* **1983,** 17 (1), 109-28 DOI: 10.1002/jbm.820170110.

17. Parida, P.; Behera, A.; Mishra, S. C. Classification of Biomaterials used in Medicine. *Int. J. Adv. Appl. Sci.* **2012,** 1 (3), 125-129.

18. Pal, S., *Mechanical Properties of Biological Materials. In: Design of Artificial Human Joints & Organs*. Springer: Boston, MA, 2014.

19. Stroncek, J. D.; Reichert, W. M., Overview of Wound Healing in Different Tissue Types. In *Indwelling Neural Implants: Strategies for Contending with the In Vivo Environment*, Reichert, W. M., Ed. Boca Raton (FL), 2008.

20. Prasad, K.; Bazaka, O.; Chua, M.; Rochford, M.; Fedrick, L.; Spoor, J.; Symes, R.; Tieppo, M.; Collins, C.; Cao, A.; Markwell, D.; Ostrikov, K. K.; Bazaka, K. Metallic Biomaterials: Current Challenges and Opportunities. *Materials (Basel)* **2017,** 10 (8), DOI: 10.3390/ma10080884.

21. Niinomi, M.; Nakai, M. Titanium-Based Biomaterials for Preventing Stress Shielding between Implant Devices and Bone. *Int J Biomater* **2011,** 2011, 836587 DOI: 10.1155/2011/836587.

22. Chen, Q.; Zhu, C.; Thouas, G. A. Progress and challenges in biomaterials used for bone tissue engineering: bioactive glasses and elastomeric composites. *Prog Biomater* **2012,** 1 (1), 2 DOI: 10.1186/2194-0517-1-2.

23. Eliaz, N. Corrosion of Metallic Biomaterials: A Review. *Materials (Basel)* **2019,** 12 (3), DOI: 10.3390/ma12030407.

24. Ananth, H.; Kundapur, V.; Mohammed, H. S.; Anand, M.; Amarnath, G. S.; Mankar, S. A Review on Biomaterials in Dental Implantology. *Int J Biomed Sci* **2015,** 11 (3), 113-20.

25. Baino, F.; Novajra, G.; Vitale-Brovarone, C. Bioceramics and Scaffolds: A Winning Combination for Tissue Engineering. *Front Bioeng Biotechnol* **2015,** 3, 202 DOI: 10.3389/fbioe.2015.00202.

26. Gao, C.; Deng, Y.; Feng, P.; Mao, Z.; Li, P.; Yang, B.; Deng, J.; Cao, Y.; Shuai, C.; Peng, S. Current Progress in Bioactive Ceramic Scaffolds for Bone Repair and Regeneration. *Int. J. Mol. Sci* **2014,** 15 (3), 4714-4732.

27. Sohail, M.; Mudassir; Minhas, M. U.; Khan, S.; Hussain, Z.; de Matas, M.; Shah, S. A.; Khan, S.; Kousar, M.; Ullah, K. Natural and synthetic polymer-based smart biomaterials for management of ulcerative colitis: a review of recent developments and future prospects. *Drug Deliv Transl Res* **2019,** 9 (2), 595-614 DOI: 10.1007/s13346-018-0512-x.

28. Ige, O. O.; Umoru, L. E.; Aribo, S. Natural Products: A Minefield of Biomaterials. *ISRN Mater. Sci.* **2012,** 2012, 20.

29. Williams, D. F. Challenges With the Development of Biomaterials for Sustainable Tissue Engineering. *Front Bioeng Biotechnol* **2019,** 7, 127 DOI: 10.3389/fbioe.2019.00127.

30. Yadav, S.; Gangwar, S. An Overview on Recent progresses and future perspective of biomaterials. *Iop Conf Ser-Mat Sci* **2018,** 404, DOI: Artn 012013 10.1088/1757-899x/404/1/012013.

31. Ulery, B. D.; Nair, L. S.; Laurencin, C. T. Biomedical Applications of Biodegradable Polymers. *J Polym Sci B Polym Phys* **2011,** 49 (12), 832-864 DOI: 10.1002/polb.22259.

32. Kohn, J. New approaches to biomaterials design. *Nat Mater* **2004,** 3 (11), 745-7 DOI: 10.1038/nmat1249.

33. BaoLin, G.; Ma, P. X. Synthetic biodegradable functional polymers for tissue engineering: a brief review. *Sci China Chem* **2014,** 57 (4), 490-500 DOI: 10.1007/s11426-014-5086-y.

34. Austin, M. J.; Rosales, A. M. Tunable biomaterials from synthetic, sequence-controlled polymers. *Biomater Sci* **2019,** 7 (2), 490-505 DOI: 10.1039/c8bm01215f.

35. Babaie, E.; Bhaduri, S. B. Fabrication Aspects of Porous Biomaterials in Orthopedic Applications: A Review. *ACS Biomater. Sci. Eng.* **2018,** 4 (1), 1-39.

36. Zhu, L.; Luo, D.; Liu, Y. Effect of the nano/microscale structure of biomaterial scaffolds on bone regeneration. *Int J Oral Sci* **2020,** 12 (1), 6 DOI: 10.1038/s41368-020-0073-y.

37. Falentin-Daudre, C. Functionalization of Biomaterials and Applications. *Biomaterials* **2014**, 119-133 DOI: Book_Doi 10.1002/9781119043553.

38. Bienek, D. R.; Tutak, W.; Skrtic, D. Bioactive Polymeric Materials for Tissue Repair. *J Funct Biomater* **2017,** 8 (1), DOI: 10.3390/jfb8010004.

39. Shu, J. Y.; Panganiban, B.; Xu, T. Peptide-polymer conjugates: from fundamental science to application. *Annu Rev Phys Chem* **2013,** 64, 631-57 DOI: 10.1146/annurev-physchem-040412-110108.

40. Song, R.; Murphy, M.; Li, C.; Ting, K.; Soo, C.; Zheng, Z. Current development of biodegradable polymeric materials for biomedical applications. *Drug Des Devel Ther* **2018,** 12, 3117-3145 DOI: 10.2147/DDDT.S165440.

41. Nair, L. S.; Laurencin, C. T. Biodegradable polymers as biomaterials. *Prog Polym Sci* **2007,** 32 (8-9), 762-798 DOI: 10.1016/j.progpolymsci.2007.05.017.

42. Anderson, J. M.; Rodriguez, A.; Chang, D. T. Foreign body reaction to biomaterials. *Semin Immunol* **2008,** 20 (2), 86-100 DOI: 10.1016/j.smim.2007.11.004.

43. Mariani, E.; Lisignoli, G.; Borzi, R. M.; Pulsatelli, L. Biomaterials: Foreign Bodies or Tuners for the Immune Response? *Int J Mol Sci* **2019,** 20 (3), DOI: 10.3390/ijms20030636.

44. Brannigan, R. P.; Dove, A. P. Synthesis, properties and biomedical applications of hydrolytically degradable materials based on aliphatic polyesters and polycarbonates. *Biomater Sci* **2016,** 5 (1), 9-21 DOI: 10.1039/c6bm00584e.

45. Velasco, M. A.; Narvaez-Tovar, C. A.; Garzon-Alvarado, D. A. Design, materials, and mechanobiology of biodegradable scaffolds for bone tissue engineering. *Biomed Res Int* **2015,** 2015, 729076 DOI: 10.1155/2015/729076.

46. Gentile, P.; Chiono, V.; Carmagnola, I.; Hatton, P. V. An overview of poly(lactic-co-glycolic) acid (PLGA)-based biomaterials for bone tissue engineering. *Int J Mol Sci* **2014,** 15 (3), 3640-59 DOI: 10.3390/ijms15033640.

47. Woodard, L. N.; Grunlan, M. A. Hydrolytic Degradation and Erosion of Polyester Biomaterials. *ACS Macro Lett* **2018,** 7 (8), 976-982 DOI: 10.1021/acsmacrolett.8b00424.

48. Meechaisue, C.; Dubin, R.; Supaphol, P.; Hoven, V. P.; Kohn, J. Electrospun mat of tyrosine-derived polycarbonate fibers for potential use as tissue scaffolding material. *J Biomat Sci-Polym E* **2006,** 17 (9), 1039-1056 DOI: Doi 10.1163/156856206778365988.

49. Ertel, S. I.; Kohn, J.; Zimmerman, M. C.; Parsons, J. R. Evaluation of Poly(Dth Carbonate), a Tyrosine-Derived Degradable Polymer, for Orthopedic Applications. *J Biomed Mater Res* **1995,** 29 (11), 1337-1348 DOI: DOI 10.1002/jbm.820291105.

50. Khan, I. J.; Murthy, N. S.; Kohn, J. Hydration-induced phase separation in amphiphilic polymer matrices and its influence on voclosporin release. *J Funct Biomater* **2012,** 3 (4), 745-59 DOI: 10.3390/jfb3040745.

51. Magno, M. H. R.; Kim, J.; Srinivasan, A.; McBride, S.; Bolikal, D.; Darr, A.; Hollinger, J. O.; Kohn, J. Synthesis, degradation and biocompatibility of tyrosine-derived polycarbonate scaffolds. *J Mater Chem* **2010,** 20 (40), 8885-8893 DOI: 10.1039/c0jm00868k.

52. Bourke, S. L.; Kohn, J. Polymers derived from the amino acid L-tyrosine: polycarbonates, polyarylates and copolymers with poly(ethylene glycol). *Adv Drug Deliver Rev* **2003,** 55 (4), 447-466 DOI: 10.1016/S0169-409x(03)00038-3.

53. Jaffe, M.; Pai, V.; Ophir, Z.; Wu, J.; Kohn, J. Process-structure-property relationships of erodable polymeric biomaterials, I: Poly (desaminotyrosyl arylates). *Polym Advan Technol* **2002,** 13 (10-12), 926-937 DOI: 10.1002/pat.278.

54. Tangpasuthadol, V.; Shefer, A.; Yu, C.; Zhou, J.; Kohn, J. Thermal properties and enthalpy relaxation of tyrosine-derived polyarylates. *J Appl Polym Sci* **1997,** 63 (11), 1441-1448.

55. Chen, S. S.; Ortiz, O.; Pastino, A. K.; Wu, X. H.; Hu, B.; Hollinger, J. O.; Bromage, T. G.; Kohn, J. Hybrid Bone Scaffold Induces Bone Bridging in Goat Calvarial Critical Size Defects Without Growth Factor Augmentation. *Regen Eng Transl Med* **2020**, DOI: 10.1007/s40883-019-00144-z.

56. Kim, J.; Magno, M. H. R.; Ortiz, O.; McBride, S.; Darr, A.; Kohn, J.; Hollinger, J. O. Next-generation resorbable polymer scaffolds with surface-precipitated calcium phosphate coatings. *Regen Biomater* **2015,** 2 (1), 1-8 DOI: 10.1093/rb/rbu019.

57. Macri, L. K.; Sheihet, L.; Singer, A. J.; Kohn, J.; Clark, R. A. F. Ultrafast and fast bioerodible electrospun fiber mats for topical delivery of a hydrophilic peptide. *J Control Release* **2012,** 161 (3), 813-820 DOI: 10.1016/j.jconrel.2012.04.035.

58. Gubskaya, A. V.; Khan, I. J.; Valenzuela, L. M.; Lisnyak, Y. V.; Kohn, J. Investigating the Release of a Hydrophobic Peptide from Matrices of Biodegradable Polymers: An Integrated Method Approach. *Polymer (Guildf)* **2013,** 54 (15), 3806-3820 DOI: 10.1016/j.polymer.2013.05.038.

59. Ezra, M.; Bushman, J.; Shreiber, D.; Schachner, M.; Kohn, J. Porous and Nonporous Nerve Conduits: The Effects of a Hydrogel Luminal Filler With and Without a Neurite-Promoting Moiety. *Tissue Eng Pt A* **2016,** 22 (9-10), 818-826 DOI: 10.1089/ten.tea.2015.0354.

60. Bhatnagar, D.; Bushman, J. S.; Murthy, N. S.; Merolli, A.; Kaplan, H. M.; Kohn, J. Fibrin glue as a stabilization strategy in peripheral nerve repair when using porous nerve guidance conduits. *J Mater Sci-Mater M* **2017,** 28 (5), DOI: ARTN 79 10.1007/s10856-017-5889-4.

61. Clements, B. A.; Bushman, J.; Murthy, N. S.; Ezra, M.; Pastore, C. M.; Kohn, J. Design of barrier coatings on kink-resistant peripheral nerve conduits. *J Tissue Eng* **2016,** 7, DOI: Unsp 2041731416629471 10.1177/2041731416629471.

62. Domb, A. A. Biodegradable polymers derived from fatty acids, saccharides and amino acids. *Abstr Pap Am Chem S* **2016,** 251.

63. Khan, W.; Muthupandian, S.; Farah, S.; Kumar, N.; Domb, A. J. Biodegradable Polymers Derived From Amino Acids. *Macromol Biosci* **2011,** 11 (12), 1625-1636 DOI: 10.1002/mabi.201100324.

64. Bentolila, A.; Vlodavsky, I.; Haloun, C.; Domb, A. J. Synthesis and heparin-like biological activity of amino acid-based polymers. *Polym Advan Technol* **2000,** 11 (8-12), 377-387 DOI: Doi 10.1002/1099-1581(200008/12)11:8/12<377::Aid-Pat985>3.0.Co;2-D.

65. Khan, W.; Muthupandian, S.; Farah, S.; Kumar, N.; Domb, A. J. Biodegradable polymers derived from amino acids. *Macromol Biosci* **2011,** 11 (12), 1625-36 DOI: 10.1002/mabi.201100324.

66. Yu, J. Y.; Lin, F.; Lin, P. P.; Gao, Y. H.; Becker, M. L. Phenylalanine-Based Poly(ester urea): Synthesis, Characterization, and in vitro Degradation. *Macromolecules* **2014,** 47 (1), 121-129 DOI: 10.1021/ma401752b.

67. Chen, K.; Dreger, N. Z.; Peng, F.; Vogt, B. D.; Becker, M. L.; Cakrnak, M. Nonlinear Mechano-Optical Behavior and Strain-Induced Structural Changes of L-Valine-Based Poly(ester urea)s. *Macromolecules* **2018,** 51 (20), 8114-8126 DOI: 10.1021/acs.macromol.8b01176.

68. Dreger, N. Z.; Fan, Z. B.; Zander, Z. K.; Tantisuwanno, C.; Haines, M. C.; Waggoner, M.; Parsell, T.; Sondergaard, C. S.; Hiles, M.; Premanandan, C.; Becker, M. L. Amino acid-based Poly(ester urea) copolymer films for hernia-repair applications. *Biomaterials* **2018,** 182, 44-57 DOI: 10.1016/j.biomaterials.2018.08.003.

69. Abel, A. K.; Dreger, N. Z.; Nettleton, K.; Gustafson, T. P.; Forster, S. P.; Becker, M. L. Amino Acid-Based Poly(ester urea)s as a Matrix for Extended Release of Entecavir. *Biomacromolecules* **2020,** 21 (2), 946-954 DOI: 10.1021/acs.biomac.9b01586.

70. Dreger, N. Z.; Zander, Z. K.; Hsu, Y. H.; Luong, D.; Chen, P.; Le, N.; Parsell, T.; Sondergaard, C.; Dunbar, M. L.; Koewler, N. J.; Suckow, M. A.; Becker, M. L. Zwitterionic amino acid-based Poly(ester urea)s suppress adhesion formation in a rat intra-abdominal cecal abrasion model. *Biomaterials* **2019,** 221, 119399 DOI: 10.1016/j.biomaterials.2019.119399.

71. Dreger, N. Z.; Fan, Z.; Zander, Z. K.; Tantisuwanno, C.; Haines, M. C.; Waggoner, M.; Parsell, T.; Sondergaard, C. S.; Hiles, M.; Premanandan, C.; Becker, M. L. Amino acid-based Poly(ester urea) copolymer films for hernia-repair applications. *Biomaterials* **2018,** 182, 44-57 DOI: 10.1016/j.biomaterials.2018.08.003.

72. Zhou, J.; Defante, A. P.; Lin, F.; Xu, Y.; Yu, J.; Gao, Y.; Childers, E.; Dhinojwala, A.; Becker, M. L. Adhesion properties of catechol-based biodegradable amino acid-based poly(ester urea) copolymers inspired from mussel proteins. *Biomacromolecules* **2015,** 16 (1), 266-74 DOI: 10.1021/bm501456g.

73. Stakleff, K. S.; Lin, F.; Smith Callahan, L. A.; Wade, M. B.; Esterle, A.; Miller, J.; Graham, M.; Becker, M. L. Resorbable, amino acid-based poly(ester urea)s crosslinked with osteogenic growth peptide with enhanced mechanical properties and bioactivity. *Acta Biomater* **2013,** 9 (2), 5132-42 DOI: 10.1016/j.actbio.2012.08.035.

74. Gopferich, A. Mechanisms of polymer degradation and erosion. *Biomaterials* **1996,** 17 (2), 103-14 DOI: 10.1016/0142-9612(96)85755-3.

75. Gopferich, A. Mechanisms of polymer degradation and erosion. *Biomaterials* **1996,** 17 (2), 103-114 DOI: Doi 10.1016/0142-9612(96)85755-3.

76. Valenzuela, L. M.; Michniak, B.; Kohn, J. Variability of Water Uptake Studies of Biomedical Polymers. *J. Appl. Polym. Sci.* **2010**.

77. Tangpasuthadol, V.; Pendharkar, S. M.; Peterson, R. C.; Kohn, J. Hydrolytic degradation of tyrosine-derived polycarbonates, a class of new biomaterials. Part II: 3-yr study of polymeric devices. *Biomaterials* **2000,** 21 (23), 2379-87 DOI: 10.1016/s0142-9612(00)00105-8.

78. Sommerfeld, S. D.; Zhang, Z.; Costache, M. C.; Vega, S. L.; Kohn, J. Enzymatic Surface Erosion of High Tensile Strength Polycarbonates Based on Natural Phenols. *Biomacromolecules* **2014,** 15 (3), 830-836 DOI: 10.1021/bm4016539.

79. Tangpasuthadol, V.; Pendharkar, S. M.; Kohn, J. Hydrolytic degradation of tyrosine-derived polycarbonates, a class of new biomaterials. Part I: study of model compounds. *Biomaterials* **2000,** 21 (23), 2371-8 DOI: 10.1016/s0142-9612(00)00104-6.

80. Gopferich, A.; Tessmar, J. Polyanhydride degradation and erosion. *Adv Drug Deliv Rev* **2002,** 54 (7), 911-31 DOI: 10.1016/s0169-409x(02)00051-0.

81. Andrews, E. H. Structure-Property Relationships in a Polymer. *Angew Chem Int Edit* **1974,** 13 (2), 113-121 DOI: DOI 10.1002/anie.197401131.

82. Gotz, C.; Lim, G. T.; Puskas, J. E.; Altstadt, V. Investigation of structure-property relationships of polyisobutylene-based biomaterials: Morphology, thermal, quasi-static tensile and long-term dynamic fatigue behavior. *J Mech Behav Biomed Mater* **2012,** 10, 206-15 DOI: 10.1016/j.jmbbm.2012.02.016.

83. Brocchini, S.; James, K.; Tangpasuthadol, V.; Kohn, J. Structure-property correlations in a combinatorial library of degradable biomaterials. *J Biomed Mater Res* **1998,** 42 (1), 66-75 DOI: Doi 10.1002/(Sici)1097-4636(199810)42:1<66::Aid-Jbm9>3.0.Co;2-M.

84. Kay, G.; Eby, E. L.; Brown, B.; Lyon, J.; Eggington, S.; Kumar, G.; Fenwick, E.; Sohail, M. R.; Wright, D. J. Cost-effectiveness of TYRX absorbable antibacterial envelope for prevention of cardiovascular implantable electronic device infection. *J Med Econ* **2018,** 21 (3), 294-300 DOI: 10.1080/13696998.2017.1409227.

85. Pollman, M. J. Engineering a bioresorbable stent: REVA programme update. *EuroIntervention* **2009,** 5 Suppl F, F54-7 DOI: 10.4244/EIJV5IFA9.

86. Moses, J. E.; Moorhouse, A. D. The growing applications of click chemistry. *Chem Soc Rev* **2007,** 36 (8), 1249-1262 DOI: 10.1039/b613014n.

87. Lowe, A. B. Thiol-ene "click" reactions and recent applications in polymer and materials synthesis: a first update. *Polym Chem-Uk* **2014,** 5 (17), 4820-4870 DOI: 10.1039/c4py00339j.

88. Diaz, D. D.; Punna, S.; Holzer, P.; Mcpherson, A. K.; Sharpless, K. B.; Fokin, V. V.; Finn, M. G. Click chemistry in materials synthesis. 1. Adhesive polymers from copper-catalyzed azide-alkyne cycloaddition. *J Polym Sci Pol Chem* **2004,** 42 (17), 4392-4403 DOI: 10.1002/pola.20330.

89. Kim, E.; Koo, H. Biomedical applications of copper-free click chemistry: in vitro, in vivo, and ex vivo. *Chem Sci* **2019,** 10 (34), 7835-7851 DOI: 10.1039/c9sc03368h.

90. Li, Z. H.; Kosuri, S.; Foster, H.; Cohen, J.; Jumeaux, C.; Stevens, M. M.; Chapman, R.; Gormley, A. J. A Dual Wavelength Polymerization and Bioconjugation Strategy for High Throughput Synthesis of Multivalent Ligands. *J Am Chem Soc* **2019,** 141 (50), 19823-19830 DOI: 10.1021/jacs.9b09899.

91. Karkovic Markovic, A.; Toric, J.; Barbaric, M.; Jakobusic Brala, C. Hydroxytyrosol, Tyrosol and Derivatives and Their Potential Effects on Human Health. *Molecules* **2019,** 24 (10), DOI: 10.3390/molecules24102001.

92. Ulery, B. D.; Nair, L. S.; Laurencin, C. T. Biomedical Applications of Biodegradable Polymers. *J Polym Sci Pol Phys* **2011,** 49 (12), 832-864 DOI: 10.1002/polb.22259.

93. Lyu, S.; Untereker, D. Degradability of polymers for implantable biomedical devices. *Int J Mol Sci* **2009,** 10 (9), 4033-65 DOI: 10.3390/ijms10094033.

94. von Burkersroda, F.; Schedl, L.; Gopferich, A. Why degradable polymers undergo surface erosion or bulk erosion. *Biomaterials* **2002,** 23 (21), 4221-4231 DOI: Pii S0142-9612(02)00170-9

Doi 10.1016/S0142-9612(02)00170-9.

95. Fukushima, K. Poly(trimethylene carbonate)-based polymers engineered for biodegradable functional biomaterials. *Biomater Sci-Uk* **2016,** 4 (1), 9-24 DOI: 10.1039/c5bm00123d.

96. Jinnouchi, H.; Torii, S.; Sakamoto, A.; Kolodgie, F. D.; Virmani, R.; Finn, A. V. Fully bioresorbable vascular scaffolds: lessons learned and future directions. *Nat Rev Cardiol* **2019,** 16 (5), 286-304 DOI: 10.1038/s41569-018-0124-7.

97. Bourke, S. L.; Kohn, J. Polymers derived from the amino acid L-tyrosine: polycarbonates, polyarylates and copolymers with poly(ethylene glycol). *Adv Drug Deliv Rev* **2003,** 55 (4), 447-66 DOI: 10.1016/s0169-409x(03)00038-3.

98. Ji, S.; Dube, K.; Chesterman, J. P.; Fung, S. L.; Liaw, C. Y.; Kohn, J.; Guvendiren, M. Polyester-based ink platform with tunable bioactivity for 3D printing of tissue engineering scaffolds. *Biomater Sci-Uk* **2019,** 7 (2), 560-570 DOI: 10.1039/c8bm01269e.

99. Zhang, H.; Xie, C.; Liu, Z.; Gong, J.; Bao, Y.; Zhang, M.; Hao, H.; Hou, B.; Yin, Q. Identification and Molecular Understanding of the Odd–Even Effect of Dicarboxylic Acids Aqueous Solubility. *Ind. Eng. Chem. Res.* **2013,** 52 (51), 18458-18465.

100. Bertron, A.; Duchesne, J.; Escadeillas, G. Attack of cement pastes exposed to organic acids in manure. *Cem. Concr. Compos.* **2005,** 27, 898-909.

101. Ma, X.; Chakraborty, P.; Henz, B. J.; Zachariah, M. R. Molecular dynamic simulation of dicarboxylic acid coated aqueous aerosol: structure and processing of water vapor. *Phys Chem Chem Phys* **2011,** 13 (20), 9374-84 DOI: 10.1039/c0cp01923b.

102. Bretti, C.; Crea, F.; Foti, C.; Sammartano, S. Solubility and Activity Coefficients of Acidic and Basic Nonelectrolytes in Aqueous Salt Solutions. 2. Solubility and Activity Coefficients of Suberic, Azelaic, and Sebacic Acids in NaCl(aq), (CH3)4NCl(aq), and (C2H5)4NI(aq) at Different Ionic Strengths and at t = 25 °C. *J. Chem. Eng. Data* **2006,** 51 (5), 1660-1667.

103. Sebok, A.; Vasanits-Zsigrai, A.; Helenkar, A.; Zaray, G.; Molnar-Perl, I. Multiresidue analysis of pollutants as their trimethylsilyl derivatives, by gas chromatography-mass spectrometry. *J Chromatogr A* **2009,** 1216 (12), 2288-301 DOI: 10.1016/j.chroma.2009.01.056.

104. Queimada, A. J.; Mota, F. L.; Pinho, S. P.; Macedo, E. A. Solubilities of biologically active phenolic compounds: measurements and modeling. *J Phys Chem B* **2009,** 113 (11), 3469-76 DOI: 10.1021/jp808683y.

105. Murano, G. FDA perspective on specifications for biotechnology products--from IND to PLA. *Dev Biol Stand* **1997,** 91, 3-13.

106. Lassalle, V.; Ferreira, M. L. PLA nano- and microparticles for drug delivery: an overview of the methods of preparation. *Macromol Biosci* **2007,** 7 (6), 767-83 DOI: 10.1002/mabi.200700022.

107. You, Y.; Min, B. M.; Lee, S. J.; Lee, T. S.; Park, W. H. In vitro degradation behavior of electrospun polyglycolide, polylactide, and poly(lactide-co-glycolide). *J Appl Polym Sci* **2005,** 95 (2), 193-200 DOI: 10.1002/app.21116.

108. de Castro, P.; Salmoria, G.; de Mello Roesler, C.; da Rosa, E.; Fancello, E. A study on the response of PLGA 85/15 under compression and heat-treatment testing cycles. *Mech. Time-Depend. Mater.* **2020**.

109. Diaz, E.; Puerto, I.; Ribeiro, S.; Lanceros-Mendez, S.; Barandiaran, J. M. The Influence of Copolymer Composition on PLGA/nHA Scaffolds' Cytotoxicity and In Vitro Degradation. *Nanomaterials (Basel)* **2017,** 7 (7), DOI: 10.3390/nano7070173.

110. Singh, V.; Tiwari, M. Structure-Processing-Property Relationship of Poly(Glycolic Acid) for Drug Delivery Systems 1: Synthesis and Catalysis. *Int J Polym Sci* **2010**, DOI: Artn 652719

10.1155/2010/652719.

111. Soccio, M.; Lotti, N.; Finelli, L.; Munari, A. Thermal characterization of novel aliphatic polyesters with ether and thioether linkages. *e-Polym.* **2011,** 35.

112. Zhang, H.; Xie, C.; Liu, Z.; Gong, J.; Bao, Y.; Zhang, M.; Hao, H.; Hou, B.; Yin, Q. Identification and Molecular Understanding of the Odd–Even Effect of Dicarboxylic Acids Aqueous Solubility. *Ind. Eng. Chem. Res.* **2013,** 52 (51), 18458-18465.

113. Schut, J.; Bolikal, D.; Khan, I.; Pesnell, A.; Rege, A.; Rojas, R.; Sheihet, L.; Murthy, N.; Kohn, J. Glass transition temperature prediction of polymers through the mass-per-flexible-bond principle. *Polymer (Guildf)* **2007,** 48 (20), 6115-6124 DOI: 10.1016/j.polymer.2007.07.048.

114. Carvalho, C. R.; Oliveira, J. M.; Reis, R. L. Modern Trends for Peripheral Nerve Repair and Regeneration: Beyond the Hollow Nerve Guidance Conduit. *Front Bioeng Biotechnol* **2019,** 7, 337 DOI: 10.3389/fbioe.2019.00337.

115. Arslantunali, D.; Dursun, T.; Yucel, D.; Hasirci, N.; Hasirci, V. Peripheral nerve conduits: technology update. *Med Devices (Auckl)* **2014,** 7, 405-24 DOI: 10.2147/MDER.S59124.

116. Muheremu, A.; Ao, Q. Past, Present, and Future of Nerve Conduits in the Treatment of Peripheral Nerve Injury. *Biomed Res Int* **2015,** 2015, 237507 DOI: 10.1155/2015/237507.

117. Stang, F.; Keilhoff, G.; Fansa, H. Biocompatibility of Different Nerve Tubes. *Materials (Basel)* **2009,** 2 (4), 1480-1507.

118. Burrell, J. C.; Bhatnagar, D.; Brown, D. P.; Murthy, N. S.; Dutton, J.; Browne, K. D.; Laimo, F. A.; Ali, Z. S.; Rosen, J. M.; Kaplan, H. M.; Kohn, J.; Cullen, D. K. Tyrosine-derived polycarbonate nerve guidance tubes elicit proregenerative extracellular matrix deposition when used to bridge segmental nerve defects in swine. *J Biomed Mater Res A* **2020**, DOI: 10.1002/jbm.a.37110.

119. Nectow, A. R.; Marra, K. G.; Kaplan, D. L. Biomaterials for the development of peripheral nerve guidance conduits. *Tissue Eng Part B Rev* **2012,** 18 (1), 40-50 DOI: 10.1089/ten.TEB.2011.0240.

120. Schuh, C. M. A. P.; Sandval-Castellanos, A. M.; De Gregorio, C.; Contreras-Kallens, P.; Haycock, J. W., The Role of Schwann Cells in Peripheral Nerve Function, Injury, and Repair. In *Cell Engineering and Regeneration*, J., G., D., M. P., R., O., H., R., S., W., Eds. Springer: 2020; pp 1-22.

121. Farah, S.; Anderson, D. G.; Langer, R. Physical and mechanical properties of PLA, and their functions in widespread applications - A comprehensive review. *Adv Drug Deliv Rev* **2016,** 107, 367-392 DOI: 10.1016/j.addr.2016.06.012.

122. Jessen, K. R.; Mirsky, R. The Success and Failure of the Schwann Cell Response to Nerve Injury. *Front Cell Neurosci* **2019,** 13, 33 DOI: 10.3389/fncel.2019.00033.

123. Tamay, D. G.; Dursun Usal, T.; Alagoz, A. S.; Yucel, D.; Hasirci, N.; Hasirci, V. 3D and 4D Printing of Polymers for Tissue Engineering Applications. *Front Bioeng Biotechnol* **2019,** 7, 164 DOI: 10.3389/fbioe.2019.00164.

124. Derakhshanfar, S.; Mbeleck, R.; Xu, K.; Zhang, X.; Zhong, W.; Xing, M. 3D bioprinting for biomedical devices and tissue engineering: A review of recent trends and advances. *Bioact Mater* **2018,** 3 (2), 144-156 DOI: 10.1016/j.bioactmat.2017.11.008.

125. Richards, D. J.; Tan, Y.; Jia, J.; Yao, H.; Mei, Y. 3D Printing for Tissue Engineering. *Isr J Chem* **2013,** 53 (9-10), 805-814.

126. Nesic, D.; Schaefer, B. M.; Sun, Y.; Saulacic, N.; Sailer, I. 3D Printing Approach in Dentistry: The Future for Personalized Oral Soft Tissue Regeneration. *J Clin Med* **2020,** 9 (7), DOI: 10.3390/jcm9072238.

127. Kessler, A.; Hickel, R.; Reymus, M. 3D Printing in Dentistry-State of the Art. *Oper Dent* **2020,** 45 (1), 30-40 DOI: 10.2341/18-229-L.

128. Oberoi, G.; Nitsch, S.; Edelmayer, M.; Janjic, K.; Muller, A. S.; Agis, H. 3D Printing-Encompassing the Facets of Dentistry. *Front Bioeng Biotechnol* **2018,** 6, 172 DOI: 10.3389/fbioe.2018.00172.

129. Dawood, A.; Marti Marti, B.; Sauret-Jackson, V.; Darwood, A. 3D printing in dentistry. *Br Dent J* **2015,** 219 (11), 521-9 DOI: 10.1038/sj.bdj.2015.914.

130. Kotta, S.; Nair, A.; Alsabeelah, N. 3D Printing Technology in Drug Delivery: Recent Progress and Application. *Curr Pharm Des* **2018,** 24 (42), 5039-5048 DOI: 10.2174/1381612825666181206123828.

131. Mathew, E.; Pitzanti, G.; Larraneta, E.; Lamprou, D. A. 3D Printing of Pharmaceuticals and Drug Delivery Devices. *Pharmaceutics* **2020,** 12 (3), DOI: 10.3390/pharmaceutics12030266.

132. Beg, S.; Almalki, W. H.; Malik, A.; Farhan, M.; Aatif, M.; Rahman, Z.; Alruwaili, N. K.; Alrobaian, M.; Tarique, M.; Rahman, M. 3D printing for drug delivery and biomedical applications. *Drug Discov Today* **2020,** 25 (9), 1668-1681 DOI: 10.1016/j.drudis.2020.07.007.

133. Sun, Z.; Lau, I.; Wong, Y. H.; Yeong, C. H. Personalized Three-Dimensional Printed Models in Congenital Heart Disease. *J Clin Med* **2019,** 8 (4), DOI: 10.3390/jcm8040522.

134. Bucking, T. M.; Hill, E. R.; Robertson, J. L.; Maneas, E.; Plumb, A. A.; Nikitichev, D. I. From medical imaging data to 3D printed anatomical models. *PLoS One* **2017,** 12 (5), e0178540 DOI: 10.1371/journal.pone.0178540.

135. Guvendiren, M.; Molde, J.; Soares, R. M.; Kohn, J. Designing Biomaterials for 3D Printing. *ACS Biomater Sci Eng* **2016,** 2 (10), 1679-1693 DOI: 10.1021/acsbiomaterials.6b00121.

136. Yang, E.; Miao, S.; Zhong, J.; Zhang, Z.; Mills, D. K.; Zhang, L. G. Bio-Based Polymers for 3D Printing of Bioscaffolds. *Polym Rev (Phila Pa)* **2018,** 58 (4), 668-687 DOI: 10.1080/15583724.2018.1484761.

137. Serra, T.; Planell, J. A.; Navarro, M. High-resolution PLA-based composite scaffolds via 3-D printing technology. *Acta Biomater* **2013,** 9 (3), 5521-30 DOI: 10.1016/j.actbio.2012.10.041.

138. Hassanajili, S.; Karami-Pour, A.; Oryan, A.; Talaei-Khozani, T. Preparation and characterization of PLA/PCL/HA composite scaffolds using indirect 3D printing for bone tissue engineering. *Mater Sci Eng C Mater Biol Appl* **2019,** 104, 109960 DOI: 10.1016/j.msec.2019.109960.

139. Ji, S.; Dube, K.; Chesterman, J. P.; Fung, S. L.; Liaw, C. Y.; Kohn, J.; Guvendiren, M. Polyester-based ink platform with tunable bioactivity for 3D printing of tissue engineering scaffolds. *Biomater Sci* **2019,** 7 (2), 560-570 DOI: 10.1039/c8bm01269e.

140. Lowe, A. Thiol–ene "click" reactions and recent applications in polymer and materials synthesis: a first update. *Polym. Chem.* **2014,** 5 (17), 4820 - 4870.

141. Hoyle, C. E.; Lowe, A. B.; Bowman, C. N. Thiol-click chemistry: a multifaceted toolbox for small molecule and polymer synthesis. *Chem Soc Rev* **2010,** 39 (4), 1355-87 DOI: 10.1039/b901979k.

142. Liu, Y.; Hou, W.; Sun, H.; Cui, C.; Zhang, L.; Jiang, Y.; Wu, Y.; Wang, Y.; Li, J.; Sumerlin, B. S.; Liu, Q.; Tan, W. Thiol-ene click chemistry: a biocompatible way for

orthogonal bioconjugation of colloidal nanoparticles. *Chem Sci* **2017,** 8 (9), 6182-6187 DOI: 10.1039/c7sc01447c.

143. Northrop, B. H.; Coffey, R. N. Thiol-ene click chemistry: computational and kinetic analysis of the influence of alkene functionality. *J Am Chem Soc* **2012,** 134 (33), 13804-17 DOI: 10.1021/ja305441d.

144. Podgorski, M.; Becka, E.; Chatani, S.; Claudino, M.; Bowman, C. N. Ester-free Thiol-X Resins: New Materials with Enhanced Mechanical Behavior and Solvent Resistance. *Polym Chem* **2015,** 6 (12), 2234-2240 DOI: 10.1039/C4PY01552E.

145. Homayun, B.; Lin, X.; Choi, H. J. Challenges and Recent Progress in Oral Drug Delivery Systems for Biopharmaceuticals. *Pharmaceutics* **2019,** 11 (3), DOI: 10.3390/pharmaceutics11030129.

146. Kumar, M. N.; Kumar, N. Polymeric controlled drug-delivery systems: perspective issues and opportunities. *Drug Dev Ind Pharm* **2001,** 27 (1), 1-30 DOI: 10.1081/ddc-100000124.

147. Stewart, S. A.; Dominguez-Robles, J.; Donnelly, R. F.; Larraneta, E. Implantable Polymeric Drug Delivery Devices: Classification, Manufacture, Materials, and Clinical Applications. *Polymers (Basel)* **2018,** 10 (12), DOI: 10.3390/polym10121379.

148. Benhabbour, S. R.; Kovarova, M.; Jones, C.; Copeland, D. J.; Shrivastava, R.; Swanson, M. D.; Sykes, C.; Ho, P. T.; Cottrell, M. L.; Sridharan, A.; Fix, S. M.; Thayer, O.; Long, J. M.; Hazuda, D. J.; Dayton, P. A.; Mumper, R. J.; Kashuba, A. D. M.; Victor Garcia, J. Ultra-long-acting tunable biodegradable and removable controlled release implants for drug delivery. *Nat Commun* **2019,** 10 (1), 4324 DOI: 10.1038/s41467-019-12141-5.

149. Langer, R. Implantable controlled release systems. *Pharmacol Ther* **1983,** 21 (1), 35-51 DOI: 10.1016/0163-7258(83)90066-9.

150. Meng, E.; Hoang, T. Micro- and nano-fabricated implantable drug-delivery systems. *Ther Deliv* **2012,** 3 (12), 1457-67 DOI: 10.4155/tde.12.132.

151. Fialho, S. L.; da Silva Cunha, A. Manufacturing techniques of biodegradable implants intended for intraocular application. *Drug Deliv* **2005,** 12 (2), 109-16 DOI: 10.1080/10717540590921432.

152. Stevenson, C. L.; Santini, J. T., Jr.; Langer, R. Reservoir-based drug delivery systems utilizing microtechnology. *Adv Drug Deliv Rev* **2012,** 64 (14), 1590-602 DOI: 10.1016/j.addr.2012.02.005.

153. Yang, W. W.; Pierstorff, E. Reservoir-based polymer drug delivery systems. *J Lab Autom* **2012,** 17 (1), 50-8 DOI: 10.1177/2211068211428189.

154. Pons-Faudoa, F. P.; Ballerini, A.; Sakamoto, J.; Grattoni, A. Advanced implantable drug delivery technologies: transforming the clinical landscape of therapeutics for chronic diseases. *Biomed Microdevices* **2019,** 21 (2), 47 DOI: 10.1007/s10544-019-0389-6.

155. Manickavasagam, D.; Oyewumi, M. O. Critical assessment of implantable drug delivery devices in glaucoma management. *J Drug Deliv* **2013,** 2013, 895013 DOI: 10.1155/2013/895013.

156. Makadia, H. K.; Siegel, S. J. Poly Lactic-co-Glycolic Acid (PLGA) as Biodegradable Controlled Drug Delivery Carrier. *Polymers (Basel)* **2011,** 3 (3), 1377-1397 DOI: 10.3390/polym3031377.

157. Mir, M.; Ahmed, N.; Rehman, A. U. Recent applications of PLGA based nanostructures in drug delivery. *Colloids Surf B Biointerfaces* **2017,** 159, 217-231 DOI: 10.1016/j.colsurfb.2017.07.038.

158. Harbhajan, P. Compositions and Methods for Treating Dermatological Conditions 5 May 2011, 2011.

159. Tripathi, R.; Biradar, S. V.; Mishra, B.; Paradkar, A. R. Study of polymorphs of progesterone by novel melt sonocrystallization technique: a technical note. *AAPS PharmSciTech* **2010,** 11 (3), 1493-8 DOI: 10.1208/s12249-010-9508-7.

160. Lutker, K. M.; Quinones, R.; Xu, J.; Ramamoorthy, A.; Matzger, A. J. Polymorphs and hydrates of acyclovir. *J Pharm Sci* **2011,** 100 (3), 949-63 DOI: 10.1002/jps.22336.

161. Hannan, R. T.; Peirce, S. M.; Barker, T. H. Fibroblasts: Diverse Cells Critical to Biomaterials Integration. *ACS Biomater Sci Eng* **2018,** 4 (4), 1223-1232 DOI: 10.1021/acsbiomaterials.7b00244.

162. Willerth, S. M.; Sakiyama-Elbert, S. E., Combining stem cells and biomaterial scaffolds for constructing tissues and cell delivery. In *StemBook*, Cambridge (MA), 2008.

163. Hwang, N. S.; Varghese, S.; Elisseeff, J. Controlled differentiation of stem cells. *Adv Drug Deliv Rev* **2008,** 60 (2), 199-214 DOI: 10.1016/j.addr.2007.08.036.

164. Clause, K. C.; Liu, L. J.; Tobita, K. Directed stem cell differentiation: the role of physical forces. *Cell Commun Adhes* **2010,** 17 (2), 48-54 DOI: 10.3109/15419061.2010.492535.

165. James, K.; Levene, H.; Parsons, J. R.; Kohn, J. Small changes in polymer chemistry have a large effect on the bone-implant interface: evaluation of a series of degradable

tyrosine-derived polycarbonates in bone defects. *Biomaterials* **1999,** 20 (23-24), 2203-12 DOI: 10.1016/s0142-9612(99)00151-9.

166. Kim, J.; Magno, M. H.; Waters, H.; Doll, B. A.; McBride, S.; Alvarez, P.; Darr, A.; Vasanji, A.; Kohn, J.; Hollinger, J. O. Bone regeneration in a rabbit critical-sized calvarial model using tyrosine-derived polycarbonate scaffolds. *Tissue Eng Part A* **2012,** 18 (11-12), 1132-9 DOI: 10.1089/ten.TEA.2011.0582.

167. Choueka, J.; Charvet, J. L.; Koval, K. J.; Alexander, H.; James, K. S.; Hooper, K. A.; Kohn, J. Canine bone response to tyrosine-derived polycarbonates and poly(L-lactic acid). *J Biomed Mater Res* **1996,** 31 (1), 35-41 DOI: 10.1002/(SICI)1097-4636(199605)31:1<35::AID-JBM5>3.0.CO;2-R.

168. Zhang, W.; Zhang, Z.; Chen, S.; Macri, L.; Kohn, J.; Yelick, P. C. Mandibular Jaw Bone Regeneration Using Human Dental Cell-Seeded Tyrosine-Derived Polycarbonate Scaffolds. *Tissue Eng Part A* **2016,** 22 (13-14), 985-93 DOI: 10.1089/ten.TEA.2016.0166.

169. Chen, S. S.; Ortiz, O.; Pastino, A. K.; Wu, X.; Hu, B.; Hollinger, J. O.; Bromage, T. G.; Kohn, J. Hybrid Bone Scaffold Induces Bone Bridging in Goat Calvarial Critical Size Defects Without Growth Factor Augmentation. *Regener. Eng. Transl. Med.* **2020,** 6, 189-200.